UNIVERSITY OF BELGRADE

FACULTY OF TECHNOLOGY AND METALLURGY

Ahmad Hakky Mohammad

OPTIMIZATION OF THE ADSORPTION PROCESS OF POLLUTANTS FROM AQUEOUS SOLUTIONS USING *PONTEDERIA CRASSIPES* BIOMASS

Doctoral Dissertation

Belgrade, 2023.

УНИВЕРЗИТЕТ У БЕОГРАДУ

ТЕХНОЛОШКО - МЕТАЛУШКИ ФАКУЛТЕТ

Ahmad Hakky Mohammad

ОПТИМИЗАЦИЈА ПРОЦЕСА АДСОРПЦИЈЕ ЗАГАЂУЈУЋИХ МАТЕРИЈА ИЗ ВОДЕНИХ РАСТВОРА ПРИМЕНОМ БИОМАСЕ *PONTEDERIA CRASSIPES*

докторска дисертација

Београд, 2023.

ADVISOR:

_____
Dr. Mirjana Kijevčanin, professor
University of Belgrade, Faculty of Technology and Metallurgy

COMMITTEE:

_____
1. Dr. Ivona Radović, professor
University of Belgrade, Faculty of Technology and Metallurgy

_____
2. Dr. Tatjana Kaluđerović Radoičić, professor
University of Belgrade, Faculty of Technology and Metallurgy

_____
3. Dr. Gorica Ivaniš, senior research associate
University of Belgrade, Faculty of Technology and Metallurgy

_____
 4. Dr. Zorica Lopičić, senior research associate
Institute for Technology of Nuclear and Other Mineral Raw Materials

DATE:

_____

OPTIMIZATION OF THE ADSORPTION PROCESS OF POLLUTANTS FROM AQUEOUS SOLUTIONS USING *PONTEDERIA CRASSIPES* BIOMASS

Abstract

The object of the present doctoral dissertation was to perform a detailed fundamental study of water hyacinth utilization as a precursor material for activated carbons synthesis and their application in the process of the removal of pesticide glyphosate and pharmaceutic metformin. The activated carbons were synthesized by the process of chemical activation of raw water hyacinth, by $ZnCl_2$ and H_3PO_4 prior to controlled carbonization. The dissertation investigated the effect of various impregnation weight mass ratios of $ZnCl_2$ or H_3PO_4 and dry water hyacinth (0.5 – 3.0)(wt/wt), as well as different carbonization temperatures in the range from 400 ⁰C – 800 ⁰C. The study summarized the impact of the impregnation ratio and carbonization temperatures on the textural properties of the activated carbons, i.e. specific surface area and pore volumes. The highest values of the S_{BET} were obtained for activated carbons synthesized under optimal conditions of impregnation ratio and carbonization temperature. The sample impregnated in ratio 2.0 wt/wt in the presence of the $ZnCl_2$ and at a carbonization temperature of 500 ⁰C ($2.0ZC_{500}$) showed S_{BET} of 1314 m^2g^{-1} and 78% of its porosity belonging to the mesopores. Activated carbon obtained by impregnation of raw water hyacinth by H_3PO_4 using the impregnation ratio of 1.5 and a carbonization temperature of 600 ⁰C ($1.5PC_{600}$) showed the highest values of the specific surface area of 1421 m^2g^{-1} with 60.2% of porosity in the area of mesopore, with a certain amount of micropore. The selected samples were characterized in detail by elemental analysis, adsorption–desorption physisorption of nitrogen at −196 ⁰C, by FTIR spectroscopy, SEM analysis, and point of zero charge (pH_{PZC}).

Detail adsorption study of glyphosate and metformin was performed on samples $2.0ZC_{500}$ and $1.5PC_{600}$ in order to test the adsorption properties of activated carbons and their potential ability to be used in real systems for wastewater treatment. The effect of the adsorbent mass (concentration), adsorbate (pollutant) initial concentration, pH of initial adsorbate solution, and temperature were investigated. Appropriate isotherms, kinetics, and thermodynamics models were applied to adsorption data to describe the adsorption processes. It was found that $2.0ZC_{500}$ and $1.5PC_{600}$ showed an adsorption capacity of 146.05 mg g^{-1} and 122.47 mg g^{-1} toward metformin, respectively, while maximal adsorption capacities of $2.0ZC_{500}$ and $1.5PC_{600}$ toward glyphosate were 240.80 mg g^{-1} and 246.91 mg g^{-1}, respectively. The Langmuir isotherm model described well adsorption metformin on both adsorbents. However, the adsorption of glyphosate on 1.5PC600 was also fitted with the Langmuir isotherm model, while glyphosate adsorption on 2.0ZC500 was better fitted with the Redlich-Peterson model. All the investigated adsorption systems followed the pattern of the pseudo-second-order kinetic model. The thermodynamic study revealed that all investigated processes were endothermic and spontaneous. The desorption and study of reusability confirmed that samples can be successfully recovered and reused in five consecutive cycles.

Based on the presented results, water hyacinth can be turned from waste and dangerous material to useful starting material for the production of activated carbons, materials efficient in wastewater treatment.

Key words: *pontederia crassipes* biomass; activated carbons synthesis; pyrolysis; pesticide removal; adsorption; thermodynamic modeling.

ОПТИМИЗАЦИЈА ПРОЦЕСА АДСОРПЦИЈЕ ЗАГАЂУЈУЋИХ МАТЕРИЈА ИЗ ВОДЕНИХ РАСТВОРА ПРИМЕНОМ БИОМАСЕ PONTEDERIA CRASSIPES

Сажетак

Циљ ове докторске дисертације био је да се изврши детаљно испитивање коришћења биомасе *Pontederia crassipes* као сировине за синтезу активног угља, као и њене примене у процесу уклањања пестицида глифосата и метформина из фармацеутског отпада. Активни угаљ је синтетисан процесом контролисане карбонизације биомасе *Pontederia crassipes*, којој је претходила њена хемијска активација помоћу $ZnCl_2$ и H_3PO_4. У дисертацији је испитиван утицај различитих односа импрегнације $ZnCl_2$ или H_3PO_4 и суве биомасе (0,5 – 3,0 мас/мас), као и различитих температура карбонизације у опсегу од 400 – 800 ºC. Током истраживања испитиван је утицај односа импрегнације и температуре карбонизације на текстурна својства активног угља, односно специфичну површину и запремине пора. Највеће вредности S_{BET} добијене су за активни угаљ синтетизован у оптималним условима односа импрегнације и температуре карбонизације. Узорак импрегниран у односу 2,0 мас/мас у присуству $ZnCl_2$ и на температури карбонизације од 500 ºC ($2.0ZC_{500}$) показао је S_{BET} од $1314 m^2 g^{-1}$ и 78% његове порозности припада мезопорама. Активни угаљ добијен импрегнацијом сирове биомасе *Pontederia crassipes* са H_3PO_4 применом односа импрегнације 1,5 мас/мас и температуре карбонизације од 600 ºC ($1.5PC_{600}$) показао је највеће вредности специфичне површине од $1421 m^2 g^{-1}$ са 60,2% порозности у области мезопора и са одређеном количином микропора. Одабрани узорци су детаљно окарактерисани елементарном анализом, фиизичком адсорпциом / десорпциом азота на −196 ºC, FTIR спектроскопијом, SEM анализом и тачком нултог наелектрисања (pH_{PZC}).

Детаљна анализа адсорпције глифосата и метформина урађена је на узорцима $2.0ZC_{500}$ и $1.5PC_{600}$ у циљу испитивања адсорпционих својстава активног угља и могућности његове употребе у реалним системима за пречишћавање отпадних вода. Испитиван је утицај масе (концентрације) адсорбента, почетне концентрације адсорбата (загађивача), pH почетног раствора адсорбата и температуре. Одговарајући модели изотерми, кинетике и термодинамике примењени су на податке о адсорпцији да би се описали процеси адсорпције. Утврђено је да су $2.0ZC_{500}$ и $1.5PC_{600}$ показали адсорпциони капацитет од 146,05 mgg^{-1} и 122,47 mgg^{-1} према метформину, док је максимални адсорпциони капацитет $2.0ZC_{500}$ и $1.5PC_{600}$ према глифосату био 240,80 mgg^{-1}, односно 246,91 mgg^{-1}. Модел Лангмуирове изотерме је добро описао адсорпцију метформина на оба адсорбента. С друге стране, адсорпција глифосата на $1.5PC_{600}$ је, такође, била описана моделом Лангмуирове изотерме, док је за адсорпцији глифосата на $2.0ZC_{500}$ Редлих-Петерсонов модел дао боље слагање. Сви испитивани адсорпциони системи су пратили образац кинетичког модела псеудодругог реда. Термодинамичка анализа је показала да су сви испитивани процеси ендотермни и спонтани. Испитивање десорпција и поновне употребе адсорбента потврдили су да се испитивани узорци могу успешно повратити и поново употребити у пет узастопних циклуса адсорпције / десорпције.

На основу приказаних резултата, биомаса *Pontederia crassipes* се може претворити од отпада и опасног материјала у користан полазни материјал за производњу активног угља, материјала ефикасног у третману отпадних вода.

Кључне речи: биомаса *Pontederia crassipes*; синтеза активног угља; пироліза; уклањање пестицида; адсорпција; термодинамичко моделовање.

Contents

1. INTRODUCTION

One of the leading environmental problems in Africa and Asia is the presence of water hyacinth (*Eichhornia crassipes*) in natural waters (mostly rivers and lakes) – Figure 1.

Figure 1. The water hyacinth – *Eichhornia crassipes* plant

Water hyacinth is a perennial aquatic plant that originates from South America, brought in the early 20th century to the Asian countries as an ornamental plant. Over the years, due to the pronounced ability of both vegetative and sexual reproduction, this plant starts to be observed as a weed due to rapid growth of $1m^2$ for less than a month. The water hyacinth can also be reproduced by the seeds. One plant can produce up to 5000 thousand seeds and after sinking to the water body bottom, it can remain viable for up to 20 years (Awashti et al., 2013). Very fast the water hyacinth has reached a distribution of tens of hectares of water surface, where it can be maintained as a perennial plant for up to ten years. Water hyacinth forms dense and impenetrable floating mats on water surfaces, causing many problems in aquatic ecosystems – Figure 2.

This plant has shown a strong negative impact on the biodiversity of the aquatic system in many ways: its presence leads to a significant reduction in the amount of light in the water, and prevents access to wildlife (birds in particular) thereby disrupting the normal functioning of fauna and representing a suitable environment for mosquitoes breeding (Awashti et al., 2013; Bote et al., 2020).

Figure 2. Dense and impenetrable floating mats on water surfaces formed by water hyacinth (Bhankok Post)

The water hyacinth has direct effects on the chemistry of water. The enormous amount of organics originates from plant decomposition and leads to oxygen deficiency and the production of anaerobic conditions. The anaerobic conditions have been responsible for the death of fish and other aquatic organisms. The conditions created by water hyacinth presence led to the development of several human diseases, i.e. intermediate snail hosts of bilharzia, and those produced with mosquito transmission (malaria and encephalitis) (Honlah et al., 2019).

The additional problem is related to irrigation and fishing wherethe presence of water hyacinth often completely prevents water traffic. A huge amount of floating plants weeds also cause damage to numerous infrastructures on rivers and lakes (Bote et al., 2020).

In the last few years, due to the caused environmental problem as well as due to the enormous amount of water hyacinth weed in the rivers and lakes, the attention of scientists has been focused on its use and application. Since water hyacinth contains approx. 60 % lignocellulose, 20% hemicellulose and l0% lignin with high carbon-nitrogen ratio can be considered as the source of alternative renewable energy (Abdel-Fattah and Abdel-Naby, 2012).

Water hyacinth can be used as raw materials for various purposes: for bioethanol production (Awasthi et al., 2013), biogas production under microbiological decomposition in the presence of bacteria, funguses, and yeasts (Adegunloye et al., 2013), etc. Raja and Lee (2012) investigated the possibility of biogas production and described the pre-treatment process of water hyacinth. The group studied different factors (temperature, pH, carbon/ nitrogen ratio and water content) on biogas production (Raja and Lee, 2012). Sankar et al. (2005) extracted the fatty acids from water hyacinth and used it as the feed for biogas digester (Sankar et al., 2005). Also, Girisuta and co-authors (2008) investigated acid catalysed hydrolysis of the water hyacinth plant to Levulinic acid, which can be used for synthesis of organic compounds in flavouring and fragrance industry (Girisuta et al., 2008). Priya and Selvan (2014) have used water hyacinth as a biosorbent for the textile effluent treatment (Priya and Selivan, 2014), while Lay with co-workers (2013) has evaluated hydrogen production from water hyacinth and beverage wastewater using method of dark fermentative production (Lay et al, 2013).

Utilization of water hyacinth biomass as source of lignocellulose for activated carbon production can be one of the strategies in water pollution control. Using activated carbon obtained from lignocellulose waste biomass instead of fossil coal might reduce the production of greenhouse gasses,

representing a green approach in the synthesis of materials that can be further used in the process of pollutant removal. Water hyacinth biomass as abundant agricultural waste has been used as raw material for converting into activated carbon in several studies found in literature (Tarapitakcheevin et al., 2013; Boonpoke, 2015; Riyanto and Prabalaras, 2019; González-García et al., 2019).

Tarapitakcheevin *et al.*, (2013) investigated water hyacinth as starting material for activated carbon production using NaCl as low-cost and non-toxic chemical activator. The authors investigated only one mass ratio between water hyacinth and NaCl and produced activated carbon further used in the process of textile dye adsorption. Thailand water hyacinth from Phayao Lake was used for activated carbon production in process of chemical activation with $ZnCl_2$ in study performed by Bonpoke (2015). The author used equal amounts of chemical activator and raw water hyacinth material performing carbonization in temperature range from 400⁰C to 600⁰C. The activated carbons were further tested for adsorption of wastewater of paper production industry. Riyanto and Prabalarias (2019) used water hyacinth as raw material for production activated carbon. The raw starting material was submitted to the pre-carbonization process at 400⁰C, activated by 30% phosphoric acid in applied impregnation ratio of 1:4 (wt/wt), and finally carbonized at 600⁰C. The obtained material was further applied as adsorbent of cobalt ions. González-García et al. (2019) used water hyacinth for activated carbons synthesis in process of chemical activation by potassium-carbonate varying activation time (1 or 2 hours) and carbonization temperature (450⁰C and 550⁰C). The authors applied double higher mass of potassium-carbonate to mass of water hyacinth. The activated carbons from the study were tested as adsorbents of pharmaceutic naproxen. Based on the presented literature regarding the utilization of water hyacinth as a precursor in activated carbon production, can be noticed the amount of applied activation agent is not sufficiently investigated. Further, there is no comprehensive study based on the detailed investigation of the effect of the applied amount of activation agent through a wider range of carbonization temperatures on surface characteristics of activated carbons produced by water hyacinth biowaste.

2. THEORETICAL SECTION

2.1. Waste biomass as a precursor for active carbon producing

Today, lignocellulose from different types of biomasses is widely investigated as a precursor for activated carbon production, especially due to its availability and low price. The active carbon has been produced from numerous agricultural wastes, such as coconut shells, rubber shells, hazelnut shells, palm kernel shells, almond shells, plum stones, cotton stalks, rice husk, etc. (Nor et al., 2013).

Ozdemir et al., (2014) produced a low-cost activated carbon from the grape stalk by the process of chemical activation. The obtained activated carbons showed very high values for textural properties: BET surface area, and total pore volume of 1411 m^2g^{-1}, and 0.723 cm^3g^{-1}, respectively. The surface analysis revealed the presence of acidic surface functional groups and highly porous surfaces with cracks, channels and large holes (Ozdemir et al., 2014).

An agricultural waste – nuts of *Terminalia Arjuna*, were used to prepare activated carbons by chemical activation process using $ZnCl_2$ as activator under four different activation temperatures in range of 300ºC-600ºC. s. The biomass precursor and applied synthesis conditions enabled the production of the activated carbons with good surface properties, with values of surface area and micropore volumes of 1260 m^2g^{-1} and 0.522 $cm^3 g^{-1}$, respectively. The obtained activated carbon was tested for phenol removal (Mohanty et al, 2005).

Cardoso et al, (2008) recognized the cork powder potential as biowaste material for the preparation of activated carbons, for the the atmospheric pollution control. The authors prepared a series of activated carbons by chemical activation of cork powder to obtain materials with S_{BET} higher than 1300 $m^2 g^{-1}$. Due to suitable precursor and well-tailored synthesis parameters, the activated carbon shown developed microporosity, with value of microporous volumes higher than 0.5 $cm^3 g^{-1}$. The cork powder derived activated carbons shown good adsorption properties and selective adsorption toward volatile organic compounds (Cardoso et al, 2008).

Yorgun et. al (2009) shown that woods and forest wastes represent a significant source of lignocellulose materials for preparing activated carbons. Paulownia represents a large number of species of adaptable and fast-growing trees. The Paulownia originated in China, although today is widely spread in Japan, Brazil, Turkey and Europe. Chemically activated Paulownia (P. Tomentose) was subjected to the carbonization process, which resulted by production of the activated carbons with extremely high values of the specific surface area of even 2736 $m^2 g^{-1}$.

Based on the described utilization of lignocellulose precursors, many companies recognized the potential value of different lignocellulose materials and applied innovative approaches and produced activated carbons from waste biomass. For example, one of the many companies is Eleven Carbon[TM], which markets and sells activated carbons produced from coconut shell across continents. The simplified scheme of activated carbon production by company Eleven Carbon[TM] is given in Figure 4.
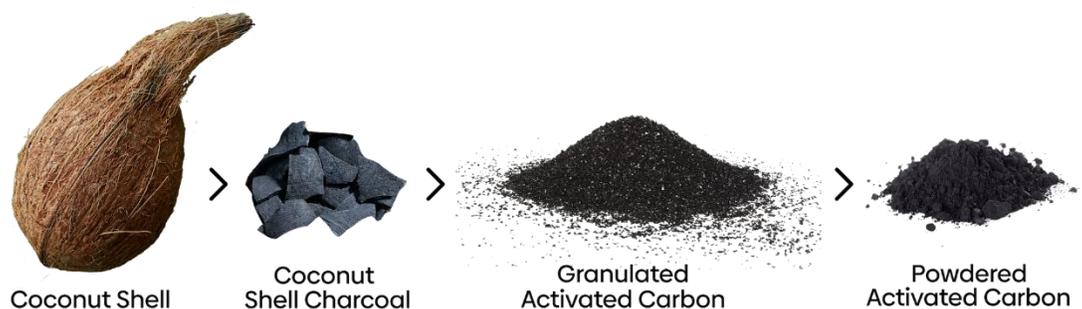
Figure 3. The simplified scheme of powdered activated carbon production by Eleven Carbon[TM]

Therefore, the materials with appropriate lignocellulosic component content could be considered as alternative precursor for activated carbon production. Among many lignocellulose materials characterized as biowaste, scientific attention has been directed to the utilization of water hyacinth weed as a precursor of functional carbon materials or value-added chemicals (Boonpoke, 2015; Riyanto and Prabalaras, 2019; Saning et al. 2019). Bonpoke (2015) used water hyacinth as a raw material to produce activated carbon in a chemical activation process. The obtained carbons showed a large surface area in the range of $912 – 1066 \ m^2 \ g^{-1}$, with pronounced microporosity. The resulting carbons were successfully used for the purification of wastewater in the production of mulberry pulp and paper, loaded with a high content of chemical and organic substances. Riyanto and Prabalaras (2019) used activated carbons obtained from water hyacinth leaves through a two-stage carbonization process for heavy metal adsorption. The study determines the adsorption system in both terms: adsorption kinetic and dynamic.

2.2. Lignocellulose biomass structure

Lignocellulose biomass derived from agricultural by-products was proven to be a promising type of raw material for producing activated carbon. Lignocellulose biomass contains two carbohydrate components: cellulose and hemicellulose, as well as lignin, a heterogeneous polymeric compound of phenolic nature. Content of cellulose, hemicellulose and lignin varies and significantly depending on plant species, climate, soil fertility, fertilization, etc. Among these three components, lignin has been the recognized as main precursor for producing activated carbon, since its high carbon content (González-García et al., 2019; Saning et al.2019,).

Cinnamyl alcohols (p-coumaroyl, coniferyl and sinapyl alcohol) polymerize via a phenolic and ethylene group into a three-dimensional lignin network. Despite relatively simple and few monomers, the lignin has been characterized by a very complex chemical structure (Figure 1).
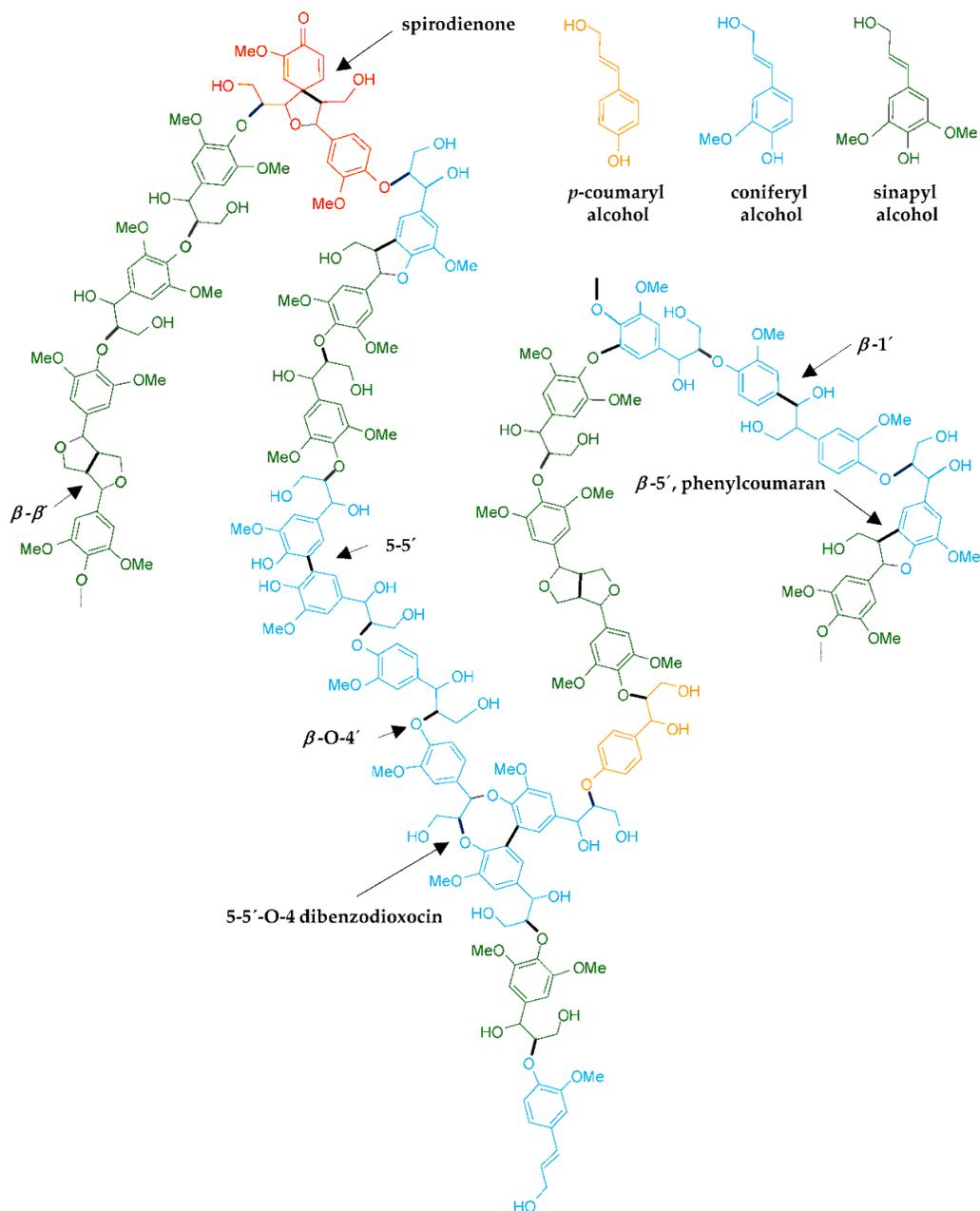
Figure 4. Lignin structure (Fillat et al. 2017)

Although the lignin has be recognized as the major contributor of activated carbons, each component (cellulose, hemicellulose, lignin) contributes to the evolution of the mean pore size and specific porous volume of activated carbons, whatever is its weight contribution (Cagnon et al., 2009). The structure and organization in cellulose fibres is presented in Figure 5.
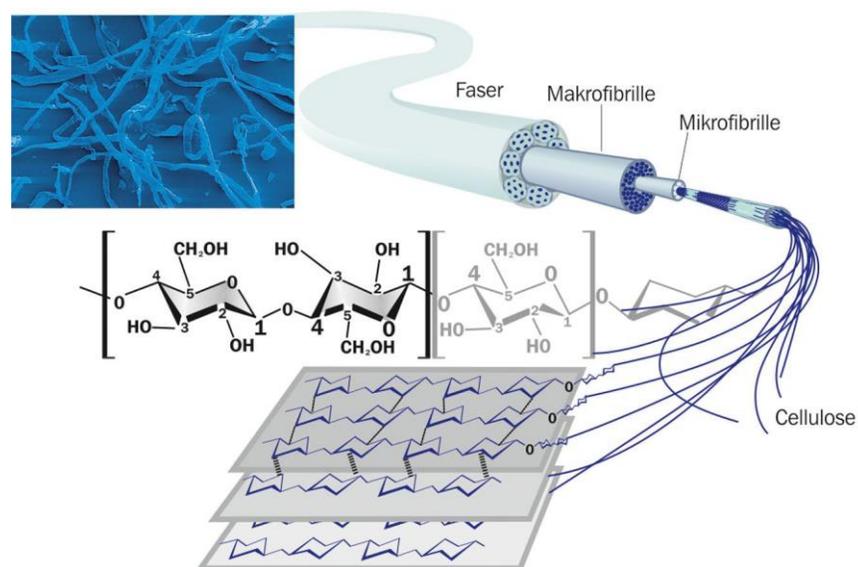
Figure 5. Structure of cellulose fibres (Mohammad, 2017).

Activated carbon is a porous carbonaceous material with high degree of porosity and high developed surface area. The active carbons contain many functional groups such as carbonyl, carboxyl, phenol, lactone, etc. that are capable to interact with many pollutants in adsorption process (Gao et al., 2018). Besides carbon, oxygen and hydrogen, sulfur and nitrogen can be also present as constituent of different functional groups. The amount and type of functional groups present on activated carbon surfaces depends on lignocellulose precursor materials, as well as applied carbonization and activation process (Gao et al., 2018; Ioannidou and Zabaniotou, 2007).

The water hyacinth is characterized by a high content of lignocellulosic biomass, including 48% hemicellulose as the major component, along with 20 % hemicellulose and with 4.8% of average lignin content (Zhang *et al.*, 2018), so it can potentially be employed as a proper carbon source. Along with the lignocellulosic constituents, the phytochemical composition of water hyacinth also includes polyphenols compounds, different flavonoids, fatty acids with different carbon length, alkaloids and sterols (Bakrim et al., 2022).

2.3. Methods for preparation and activation of activated carbon from lignocellulose biomass

There are two main directions in activated carbon synthesis, which will be discussed and explained in this subsection.

2.3.1. Carbonization followed by physical activation

Carbonization followed by physical activation is a two-step procedure: pyrolysis or carbonization under an inert atmosphere, followed by controlled gasification (activation) of the char under mildly oxidizing agents such as steam or carbon dioxide. The process of physical activation is commonly applied in the industrial production of activated carbons since this process enables the low price of the production. However, it seems that the drawbacks of the process are related to limited development of surface and low activation yield. The activation time and temperature are the major process parameters that affect the low activation yield. The extended time of carbonization and increasing the carbonization

temperatures decreased the yield of activated carbons mainly due to the production of a higher amount of volatile organic compound. These problems can be partially overcome by introducing of different physical agents, steam, CO_2 and air (Ioannidou and Zabaniotou, 2007).

Carbonization process is a phase to enrich carbon content in carbonaceous material by eliminating non-carbon species using thermal decomposition. The further activation develops porosity, creates some ordering of the structure, and generates a highly porous solid as the final product. One of the most important parameters of carbonization process is the temperature. High carbonization temperature would result in a higher amount of volatile substances released from the raw lignocellulose material. In practice, the carbonization temperature is in range of 500⁰C to 900⁰C, and the quality of produced activated carbon also depends on the starting material. Higher temperature will also increase amount of ash, as well as fixed carbon content. Thus, higher temperatures result in better quality of the carbon, but also decrease the yield, due to the primary decomposition of biomass at higher temperatures and also secondary decomposition of char residue. The other important carbonization parameters are: heating rate, nitrogen flow rate, and finally, residence time (Lua et al., 2006; Ioannidou and Zabaniotou, 2007).

The objective of physical activation process is to enhance the pore volume, to enlarge the diameter of the pores and to increase the porosity of an activated carbon. Activation process can be performed by steam or CO_2 (Cagnon et al., 2009; Mak et al., 2009). The steam is more effective than CO_2, because activated carbon with a relatively higher surface area can be produced. The smaller molecule size of water is responsible to facilitate diffusion within the char's porous structure effectively i.e. water molecules can easily penetrate into the carbon porous structure, which improve porosity of material (Mak et al, 2009). Also, Nowiciki et al. (2010) reported that activation by steam is significantly faster process that activation by other physical agents, which is unbelievably valuable with industrial aspect (Nowicki et al., 2010). Recently, Yi et al., (2021) produced activated carbon by process of physical activation proposing a novel pressuring method instead of usually application of activating agents under atmosphere pressure. The suggested procedure led to dramatically increase in textural properties of carbons, especially in specific surface area and total pore volume, and developing of micropore structure with the average pore diameter of 1.6 nm. This group of authors prepared activated carbons with specific surface area higher than 2600 m^2 g^{-1} and with well distribution of pore size.

2.3.2. Carbonization followed by chemical activation

The chemical activation of raw lignocellulose precursor material is usually one step method for activated carbons preparation. Different chemical agents have been used for this purpose: hydroxides and carbonates of alkali and alkaline earth metals (NaOH, KOH, K_2CO_3, and Na_2CO_3), chlorides of aluminum or zinc ($AlCl_3$, $ZnCl_2$) and different mineral acids (H_3PO_4, H_2SO_4, HCl). These chemical agents have been used as dehydrating agents that caused pyrolytic decomposition and do not allow the formation of tar (Kumar and Jena, 2016).

The main advantage of chemical activation in comparison with physical activation is better development of porous structure of activated carbons. Also, chemical activation needs lower temperature and shorter time than those used in physical activation, and the carbon yield is usually higher since formation of tar and the production of other volatile substances are very low (Kumar and Jena, 2016; Yorgun and Yildiz, 2015).

2.3.2.1. Activation by ZnCl2

Among many chemical agents, the $ZnCl_2$ is one of the most effective chemicals used for producing activated carbons with highly developed porosity (Hu et al., 2001; Yue and Economy, 2006). This activation agent has high activating capability, and it is relatively low-cost. In process of chemical activation with $ZnCl_2$, the starting lignocellulose materials are impregnated with concentrate $ZnCl_2$ solution (in defined ratio to raw starting material). This first step is followed by pyrolytic process at temperature range from 500ºC – 800ºC. The excess of $ZnCl_2$ contribute to the pore development since $ZnCl_2$ contributes to the decomposition of organic components, slow down the tar production and contributes the carbon yield (Hu et al., 2001; Yue and Economy, 2006).

Ozdemir et al., (2014) used agro-waste of grape stalk for production of activated carbons and used zinc chloride as activator in the CO_2 atmosphere. The authors varied a mass ratio between raw grape stalk and $ZnCl_2$ in optimization of synthesis process. The synthesis enabled production of activated carbon with high value of specific surface area of 1411 m^2 g^{-1} and with the value of total pore volume of 0.723 cm^3 g^{-1}.

Mohanty et al., (2005) shown that high surface area activated carbons can be produced from *Terminalia Arjuna* nuts in the presence of $ZnCl_2$ as chemical activator. This groups of authors reported that $ZnCl_2$ plays important role in activated carbon fabrication because slowing down the escape of tar during carbonization process. Besides that, the authors emphasized significance of appropriate mass ratio of starting lignocellulose materials and $ZnCl_2$, as well as important role of washing process that follow the carbonization and its influence on the surface development. The activated carbons produced in this study shown the specific surface area and micropore volume of 1260 m^2g^{-1} and 0.560 cm^3 g^{-1}, respectively.

Chen et al, 2017, reported study regarding fabrication of activated carbons based on tobacco stem via process of carbonization and chemical activation in the presence of $ZnCl_2$. The obtained activated carbon has shown high specific surface and great thermal stability. Besides that, the authors observed that $ZnCl_2$ has better activation behaviour in comparison with other chemical agents applied in this study. Also, the authors pointed out the significance of the portion of the applied chemical agent and found that small differences in the amount of $ZnCl_2$ can affect on the formation of pores and their widening.

The interesting study regarding fabrication of activated carbons from forest lignocellulose materials., i.e., Paulownia wood (P. Tomentose) presented Yorgun et.al., 2009. The authors prepared activated carbons from Paulownia wood by process of carbonization followed by chemical activation with $ZnCl_2$. The $ZnCl_2$ was applied in different mass ratios in respect to mass of lignocellulose material and optimal ratio was determined. The activated carbons have shown microporous properties with specific surface area and total pore volume of 2736 m^2 g^{-1} and 1.387 cm^3 g^{-1}, respectively. These authors found that impact of the impregnation ratio between activating agent and raw material is stronger than impact of the carbonization temperature on the textural development.

Sometimes, the combination of more chemical agents has been used. Hu and Srinivasan (2001) synthetized porous activated carbons from coconut shells and palm seeds used both $ZnCl_2$ and CO_2 for chemical activation. They found that using a different amount of $ZnCl_2$ influenced different porosity of the products, from micro – to mesoporous (Hu and Srinivasan, 2001).

Based on the literature survey dealing with the application of $ZnCl_2$ as a chemical activator of raw lignocellulose material in the proceeding of activated carbons fabrication by the carbonization process, it can be summarized that $ZnCl_2$ has significant role in several aspects. This activator strongly induces the porosity of the starting material and, in the same time, acts on the decomposition of the organic matter present in lignocellulose matrix. The fabricated activated carbons have high values of the

specific surface area and the total pore volume, and most of them are successfully used in adsorption process.

2.3.2.2. Activation by mineral acids

Certain mineral acids can be successfully used in the role of chemical activator of raw lignocellulose materials during activated carbons fabrication. Among several acids used for this purpose, the phosphoric acid seems to be the most appropriate agent from environmental and economic point of view. Some authors pointed out other advantages of application of phosphoric acid as activation agent, such as possibility of application of activated carbons in pharmaceutical and food industry, and absence of equipment corrosion (Kumar and Jena, 2016). Besides that, it seems that the presence of phosphoric acid required lower carbonization temperature and activation time compared with activation by physical agents.

In the study of Kumar and Jena from 2016 (Kumar and Jena, 2016), synthesis of activated carbons from Fox nutshell using phosphoric acid as chemical activators was described. The authors reported that activation was performed by process of impregnation of Fox nutshell by phosphoric acid in determinated impregnation ratios, and that the presence of activator led to the production of activated carbons with high values of specific surface area, having the positive impact on the yield of products, in the same time.

The study of Huang et al. (2014) emphasized the potential of water hyacinth as precursor for the production of the activated carbon. The authors applied the phosphoric acid as an activator and produced mesoporous carbons, suitable for role of adsorbents in aqueous solutions. The phosphoric acid has several roles in the activation process, such as impact on the better development of mesoporous structure and producing surface oxygen containing functional groups responsible for the potential adsorption process of different pollutants.

Cheung et al., (2017) used waste bamboo scaffolding as a starting material for activated carbon production, obtaining products with a high value added. The activated carbons were produced by process of thermal activation in the presence of the phosphoric acid. The authors discussed that phosphoric acid has role in process of pyrolytic decomposition of the starting lignocellulose materials, promoting the processes of depolymerization, dehydration and redistribution of lignocellulose components matrix. The activated carbon produced in this study has specific surface area of 2500 m^2 g^{-1} and was further used as efficient adsorbent of textile dyes.

The presented studies revealed significant impact of phosphoric acid in activation process, which is reflected in efficient decomposition of organic matter present in the starting materials via process of depolymerization, dehydration, char prevention and development of surface-active groups.

Besides phosphoric acid, some authors emphasized the role of other mineral acids, such as sulfuric acid, in the process of activation. Karagöz et al., (2008) produced activated carbons form sunflower oil cake. The process of activation was performed in the presence of sulfuric acid applied by impregnation in different mass ratios with starting material. The authors found that the experimental optimization of the amount of activation agent and temperature strongly affectthe adsorption properties of obtained activated carbons.

Gomez et al, (2010) submitted commercial activated carbon to process of chemical modification in order to produce carbon-based catalysts with high acidic characteristics and desirable surface chemistry. The materials were used in the reaction of oxidative degradation of acid dye in the presence of hydrogen peroxide. The role of sulfuric acid during activation is different than previously described roles of different chemical agents. The results of this study have shown that the presence of sulfuric acid

does not affect significantly the textural properties development. However, the presence of sulfuric acid mainly affected the nature of groups introduced on the surface of the activated carbons. The presence of thiol and sulphonic acid functional groups dominates over different oxygen-containing groups, such as carboxylic, carbonyl, esters and others.

2.3.2.3. Activation by hydroxides and carbonates of alkali and alkaline earth metals

Among many activation agents, alkali hydroxides, particularly potassium hydroxide, have been reported as chemicals that provide the production of activated carbons with high values of surface areas and pore volumes.

Cardoso et al, (2008) used waste of cork powder and prepared activated carbons in the presence of potassium- hydroxide as activator. The activator was introduced by process of impregnation of raw materials in changed impregnation ratios. The optimal experimental conditions led to production of activated carbons of 1300 m^2g^{-1} and pronounced microporosity. The authors observed that great advantaged of application of KOH in activation process was the production of activated carbons with narrow distribution of micropores.

González et al. (1997) used olive stones to obtained chars in the presence of KOH as activating agent. The goal of the study was to produce microporous carbons. However, authors discussed that porosity of activated carbons, depends both on optimal impregnation ratio between KOH and starting material, as well as carbonization temperature. At higher carbonization temperatures the KOH reacts with the carbon and improves the porosity of the samples.

Hafizuddin et al, (2021) used sodium hydroxide for surface modification of palm kernel shells and coconut shells with goal to obtained microporous activated carbons. The study revealed efficiency of sodium hydroxide as activator since effective improving of the textural properties of activated carbons. The authors found that increase of the amount of sodium hydroxide in the activation process resulted in the removal of volatile components from the char. In the same time, sodium hydroxide breaks chemical bonds between alkyl and aromatic components of starting lignocellulose materials, when was used in a higher amount. Besides that, sodium hydroxide participates in the reaction of elimination and dehydration of organic matrix (Hafizuddin et al., 2021).

The literature review shows that among alkaline hydroxides, such as Na_2CO_3 and K_2CO_3, have been also used as chemical activators in the process of activated carbons production from raw lignocellulose materials. Xia et al, (2016) prepared bamboo-based activated carbons in the presence of different activated agents: KOH, NaOH, K2CO3 and Na_2CO_3. The results showed that presence of KOH led to production of the activated carbon in yield of 39.82% achieving extraordinary values of specific surface area of 3441 $m^2 g^{-1}$, and with significant part of micropore structure. On the other hand, the presence of Na_2CO_3 as chemical agent resulted in low value of specific surface area, below 500 $m^2 g^{-1}$, but the yield of activated carbons was very high – 54.23%. The characteristic of K_2CO_3 and NaOH as activators were to produce activated carbons with high portion of ultra-micropore (Xia et al., 2016).

2.3.3. Hydrothermal carbonization

Hydrothermal carbonization represents the alternative way to the conventional pyrolytic method to produce activated carbons from biowaste lignocellulose materials. The carbonization in a hydrothermal reactor assumes the presence of water solution, and the application of relatively low temperature, usually not higher than 250 ⁰C. The carbonization occurs under the presence of saturation pressure, while the reaction time is commonly in the range of an hour to 24 hours. After the carbonization, process product is known as hydrochar with a significantly higher content of carbon in comparison with starting lignocellulosic material. Hydrochar can be applied in produced form for many applications but also can be submitted to additional treatment in activated carbons production (Diaz et al, 2022). The additional treatment implies pyrolytic carbonization followed by a physical or chemical activation process. In that manner, the carbon content increase, and the textural properties of the activated carbons has been improved.

Hydrothermal carbonization of raw lignocellulose precursors stabilizes the macrocellular structure of the starting biomass. The results of some study shown that carbonized materials obtained with pre-treatment in hydrothermal process have combined morphology of preserved lignin structure and cellulose microspheres (Braghiroli et al., 2012). Several publications confirmed the study of Braghiroli et al, (2012), reporting that hydrothermal pre-treatment of lignocellulosic raw materials led to preserving the spherical morphology of particles, and, at the same time, the process contributes to improving porosity (Borrero-López et al, 2017).

Liu et al., (2010) produced two types of pinewood chars, by hydrothermal method and by conventional pyrolytic method in order to obtained effective adsorbent for the removal of the cooper. The results showed that char obtained by regular pyrolytic method possess less surface-active groups with oxygen than char produced in the hydrothermal process. The hydrothermal treatment led to production of surface-active groups such as carboxylic, lactone, carbonyl and phenolic. The authors reported that the specific surface areas of 21 and 29 m^2 g^{-1} were obtained for chars in hydrothermal and pyrolytic process, respectively. Based on this finding, authors concluded that both hydrothermal treatment and pyrolysis could develop porous materials structure through different carbonization process (Liu et al., 2010).

Fang et al., (2015) carbonized biomass of sugarcane bagasse, hickory and peanut hull in hydrothermal process using different carbonization temperatures from 200 ⁰C to 300 ⁰C. The results suggested that yield, specific surface area, and pore volume decreased with temperature increase, and hydrochar with the best developed textural properties were ones produced at 200 ⁰C. On the other hand, the hydrochars produced on higher temperatures showed better thermal stability (Fang et al, 2015).

Zhai et al., (2017) submitted sewage sludge and waste biomass to the process of hydrothermal carbonization to produce hydrochar. The authors investigated the effect of the reaction temperature on the textural properties and composition of char, with respect to energy consumption (Zhai et al., 2017). They found that activated carbon contained different surface active groups such as: phenolic, carbonyl, and carboxylic, and summarized that temperature effect is crucial for crystallinity and size of produced samples.

2.4. Applications of activated carbons from lignocellulose waste materials in environment protection

The pollutant emissions from different sources continually deteriorate air, water and soil quality and have strong impact on a human health. In fact, air and water pollution have emerged as one of the major problems caused by rapid development of the industrial activities and substantial population growth. Therefore, in order to achieve a sustainable development for future, pollution control is a crucial step. Since activated carbon provides a suitable pore size and large surface area for adsorption of wide range of volatile and soluble pollutants, their utilization offers a great potential in environment protection (Shendell, 2011).

2.4.1. Activated carbons as adsorbents in air pollution control

Most gaseous pollutants have a molecular size of less than 2 nm, therefore, activated carbons with developed microporosity can be suitable adsorbents for their removal. The source of air pollutants is various, including flue gas, power plants, fossil fuel combustion and transportation. A literature summary of the removal of gaseous pollutants using activated carbons synthetized using different chemical and physical methods, from different lignocellulose precursors, is presented in Table 1.

Table 1. The literature summary of preparation method and adsorption capacity toward gasses of activated carbons obtained from different lignocellulose biomass.

Lignocellulose precursor	Preparation method	Adsorption capacity	Reference
Coconut shell	10% KOH impregnation	40 mg g^{-1} SO$_2$; 22 mg g^{-1} NOx	Lee et al., 2003.
Coconut shell	Steam activation, Cu impregnation	116 mg g^{-1} SO$_2$	Tseng et al., 2003.
Coconut shell	Base impregnation	215.4 mg g^{-1} H$_2$S	Elsayed et al., 2009.
Palm shell	CO$_2$ activation, metal impregnation	121.7 mg g^{-1} SO$_2$, 3.7 mg g^{-1} NO	Sumathi et al., 2010.
Bamboo chip	80% H$_3$PO$_4$	0.25 mg g^{-1} l CO$_2$	Wang et al., 2008
African palm stone	H$_3$PO$_4$ activation	160 mg g^{-1} CO$_2$	Vargas et al., 2011.

Successful application of activated carbon from lignocellulose materials in air pollution control depends on the adsorption capacity of an activated carbon. For that, activated carbon needs to undergo modification through either controlling the conditions of activation or by post-activation surface treatments.

2.4.2. Activated carbons as adsorbents in water pollution control

The activated carbons have been employed as adsorbents of a wide range of contaminants and carcinogenic compounds such as pharmaceuticals, metallic and non-metallic pollutants, and dyes from aqueous solutions (Din et al., 2017). In comparison with other adsorbents (zeolite, clays, and polymers)

activated carbons show better performance and stability in terms of adsorption (Regti et al., 2017). Activated carbons have been one of the most effective adsorbents for organic and inorganic pollutants. The versatility of adsorption capacity, surface area, and porous structure of activated carbons are the main characteristics that made themt suitable for application as adsorbents (Briones et al., 2011).

In Table 2, the literature data show that activated carbons have been employed as effective adsorbents of different soluble pollutants: metallic and non-metallic ions, organic compounds (dyes, phenolic compounds, pesticides, pharmaceutics, etc.).

Table 1. Literature data for applications of activated carbons for the removal of different inorganic and organic compounds from aqueous solutions

Lignocellulose precursor	Activator	Adsorption capacity	Reference
Acacia	N_2	37.2 mg g^{-1} Cr	Danish et al., 2012
Tropical almond shells	Steam, CO_2	114.8 mg g^{-1} Pb	Largitte et al., 2016
Water hyacinth	H_3PO_4	118.8 mg g^{-1} Pb	Huang et al., 2014
Water hyacinth	NaCl	56.50 mg g^{-1} Acid Blue 50	Tarapitakcheevin et al., 2013
Walnut shell	KOH	52.67 mg g^{-1} S	Li et al., 2018
Cashew nut shell	H_2SO_4	80.33 % F	Alagumuthu and Rajan, 2010
Walnut cake	H_3PO_4	70.39–243.04 mg g^{-1} Methylene blue	Maguana et al., 2018
Bamboo cane powder	H_3PO_4	2600 mg g^{-1} Lanaysn orange	Wong et al., 2018
Avocado kernels	CO_2	90 mg g^{-1} Phenol	Gonzalez-Garcıa, 2018
Argan nut shell	H_3PO_4	1250 mg g^{-1} Bisphenol A	Zbair et al., 2018
Date stones	Steam	228.047 mg g^{-1} Endrin	El Bakouri et al., 2009
Olive stones	CO_2	282.6 mg g^{-1} Ibuprofen	Ahmed, 2017

The precursors of the activated carbon are low cost and available biomass which can be the used as replacement for available commercially, non-renewable sources. To produce activated carbons from the waste lignocellulose biomass there are many different types of activation processes that are being used. It was observed that appropriate selection of precursors, carbonization process and optimum activation *conditions* are the most significant parameters which improve the adsorption capacities of activated carbons towards removal of inorganic, organic and pharmaceutics pollutants from water (Gonzalez-Garcıa, 2018, Li et al., 2018).

2.5. Pesticides as water pollutants

Nowadays, it is not necessary to point out the significance of the fresh water and its protection. People around the world are becoming aware that with the increase in human population on Earth and various industrial processes, nature and surface water bodies are under enormous threat. The water pollution happens every day over the world.

With the growth of the modern civilization, the water pollution with organic and inorganic compounds starts to be emerged environmental problem. A high number of synthetic organics like industrial chemicals, pesticides, dyes, and pharmaceuticals have been released daily into many wastewaters, entering surface and ground waters and accumulating in the nature (Brillas, 2014).

Pesticides are the chemical substances used for increase of the agricultural production. As artificial organic compounds, pesticides can remain in the environment for many years and may be transported over a long distance (Scholtz et al., 2002). Pesticide residues in soil and water are significant environment threats and have been classified as carcinogen pollutants (Dich et al., 1997). Among many pesticides, glyphosate-based herbicides as systemic, broad-spectrum herbicide are widely used, therefore contributed to concerns about their environmental impact.

Chemically, glyphosate is N-(phosphonomethyl) glycine (Figure 6), with chemical formula $C_3H_6NO_5P$ and molar mass of 169.08 g/mol. The glyphosate is odourless crystalline solid, non-volatile, and stable in the air (Kanissery et al., 2019).
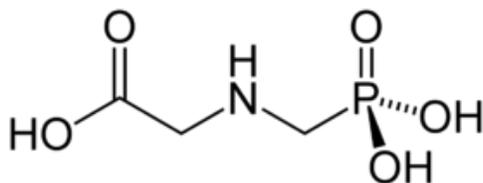
Figure 6. Chemical formula of glyphosate

Due to improper practices and excessive application, the presence of glyphosate has been observed in aquatic and terrestrial environments (Hanke et al., 2010). The glyphosate has been detected in soil, crop products, animals fed by the crop products, humans, and freshwater (Perez et al., 2011). In literature, there are numerous studies that suggested that glyphosate induces disruption of intelligence and has impact on reproductive and nervous systems (Muneer and Boxall, 2008; Echavia et al, 2009). According to the International Agency for Research on Cancer and World Health Organization, glyphosate has been classified as substance with carcinogenic effect to humans and belonging to group 2A (Morley and Seneff, 2014).

Glyphosate in soils can be almost completely degraded due to several microbiological degradation routes, but mainly due to glyphosate oxidoreductase enzyme. Process of glyphosate degradation is depending on many factors in soils, such as soils constituents, acidity, presence of aerobic conditions, etc. (Duke, 2020). However, some authors found that glyphosate degradation is not pronounced in soils with good adsorption properties, probably due to low bioavailability (Kanissery et al., 2019).

2.6. Pharmaceutics as water pollutants

Due to the enormous growth of the world's population and everyday consumption of wide range of pharmaceutics, mostly drugs, the presence of these chemical-based products is detected worldwide in surface and ground water bodies. The pharmaceuticals have been released into environment and have significant impact on aquatic systems. The pharmaceutics can reach the environment in different ways, primarily through untreated wastewater of pharmaceutic industry. The pharmaceutics can be regarded as "emerging pollutants" nowadays, including different class of the drugs: antibiotics, non-steroidal anti-inflammatory drugs, drugs for diabetes, etc. The metabolism of many drugs in a human body is incomplete; the high number of drugs or their metabolites can be excreted through urine, and released into the communal water. Inadequate treatment of communal wastewaters is common in many countries and directly leads to the presence of pharmaceutics in surface waters (rivers and lakes), as well as ground waters (Pouretedal et al., 2014).

Among different kinds of pharmaceuticals, antibiotics have been frequently used for prevention and healing of infections caused by microorganisms and pathogens. The presence of antibiotics in the environment has a strong negative impact on ecosystems since they can act on the development of antibiotic-resistant bacteria (Pouretedal et al., 2014). On the other hand, non-steroidal anti-inflammatory drugs are used on a daily basis in pain control of many diseases of muscular and skeletal system. This pharmaceutics are highly water-soluble compounds, and many of them are not easily degradable showing harmful impact on waters ecosystems. The removal of non-steroidal anti-inflammatory drugs from wastewaters is quietly difficult due to highly solubility and polarity of these compounds (Wazzan, 2021).

Over the last decades, the application of antidepressants strongly increases, which was particularly noticed during the Covid-19 pandemic. The way they get into the environment is similar to the one described above for other types of pharmaceutics. One of the most frequently used antidepressants belongs to the class of benzodiazepines, known as diazepam. This antidepressant shows sedative and muscle relaxant effects. The diazepam undergoes to the process of biotransformation and can be released from human body as variety of metabolites, with complex and unpredictable impact on the ecosystems (Sulaiman et al, 2016).

In recent years, one of the most used drugs for diabetes type 2 control is metformin with wide variety of different brand names: *Axpinet*, *Diagemet*, *Glucient*, *Glucophage, Metabet*. The metformin has also been used for treated gestational diabetes and polycystic ovary syndrome. It is also used to help prevent type 2 diabetes with patients at high risk of developing it. According to chemical name, metformin is 3-(diaminomethylidene)-1,1-dimethylguanidine, with structure presented in Figure 7.
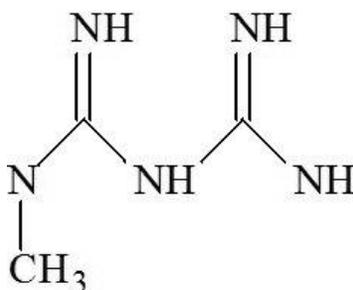
Figure 7. Chemical formula of metformin

Based on the physical-chemical properties of metformin, this chemical is not volatile, but due to presence of the polar amine groups it shows high water solubility and highly basic nature (Briones et al., 2016).

Today, metformin is an emerging concern in pharmaceutical and communal wastewaters. After metformin consummation, the non-metabolized drug is excreted from the human body, easily penetrating into environment. Due to several negative side effects, metformin has been the focus of many scientific studies in several aspects: medicine research and research related to the environmental impact, where many studies have been focused on wastewater treatment.

Some researchers indicate that high attention should be directed toward metformin's presence in the environment since this pharmaceutical is a potential endocrine disruptor and shows toxicity properties. However, according to the USEPA, there are no set standards for metformin presence in the environment, while the German Federal Agency demands a concentration of metformin less than 3 ppb in drinking water (Briones et al., 2016).

There are many investigated methods for metformin removal from real wastewaters: coagulation using low-cost clay with biodegradable polymeric flocculant (Amin et al., 2016), ozonisation (Scheurer et al., 2012), photocatalysis at TiO_2 nanoparticles (Prashanth et al. 2021), UV/Fe/peroximonosulfate process (Karimian et al. 2020) etc. Among all these methods, it seems that adsorption process on different adsorbents were the most successful, with the degree of removal usually higher than 95% (Briones et al., 2016).

Cusioli et al., (2020) developed adsorbent based on residues of Moringa plant in process of functionalization with Fe-nanoparticles. The adsorbent described in this study shown high efficiency of nearly 94% in metformin removal from wastewater. The authors described in details the adsorption process with aspect of kinetics and thermodynamics of the adsorption. The obtained adsorption capacity was relatively high and confirmed the potential using of suggested material in real systems (Cusioli et al., 2020).

Recently, Niaei and Rostamizadeh, (2020) performed metformin adsorption from aqueous solution using adsorbent obtained by hydrothermal method and additionally impregnated by iron. The adsorption system has shown good correlation with Langmuir adsorption model with moderate value adsorption capacity of 14.99 mg g^{-1}, but with high reusability (Niaei and Rostamizadeh, 2020). At the same time, group of researchers lead by Kalumpha (Kalumpha et al, 2020) published study where used *Zea mays tassel* for production of low-cost activated carbon in pyrolytic process and phosphoric acid as activator. For relatively short equilibrium time, the authors obtained the values for adsorption capacity derived from Langmuir isotherm of 44.84 mg g^{-1} for metformin removal.

Based on the presented literature survey, it seems that adsorption techniques can be successfully applied, although additionally research should be done toward developing of new, highly efficient and low-cost adsorbents. The potentially applicable adsorbent besides high values of adsorption capacity should exhibit a higher degree of recovery and reusability.

3. ADSORPTION

The adsorption is one of the most popular and the most efficient method used for the removal of contaminants from wastewaters. The advantages of adsorption process can be summarized through several issues: adsorption is of cost-effective and easy to operate, the process of adsorption is environment-friendly since does not require additional chemicals, and the adsorption is a non-destructive process with possible recovery and reusability of both adsorbents and adsorbates (Balasundram et al., 2017).

Adsorption process occurred on the surface of adsorbents and means transfer of adsorbate molecule from a fluid bulk to the solid surface of adsorbents, caused by physical forces or by chemical bonds. The adsorption process was guided by 4 major steps that controlled the adsorption rate. These steps include: (i) mass transfer from bulk to the boundary film, (ii) external transfer of adsorbate to the adsorbent surface; (iii) internal adsorbate transfer into porous area and finally (iv) – interaction of adsorbate with active sites (Lopičić et al., 2019). In the most cases, the adsorption is reversible. The opposite process is *desorption,* which is responsible for the release of adsorbate molecules from the surface.

The adsorption process can be completely described using appropriate adsorption isotherm models, adsorption kinetics models, particle diffusion models as well as thermodynamics models.

3.1. Adsorption isotherms

The adsorption isotherms describe the adsorbent-adsorbate interaction and have crucial role in optimizing the adsorbents application. On the other hand, several mathematical models have been proposed to describe kinetic process of adsorption as well as the adsorption mechanism (Tien, 2019).

Based on experimental adsorption data, the mechanism of adsorption process at specified temperature – T in equilibrium, can be explained by adsorption isotherms. The nature of interaction between adsorbent and adsorbate can be described as physical, chemical or combined interaction mechanisms. There are numerous isotherm models used in literature for different adsorption systems, but for heterogeneous adsorption system consisting from solid adsorbent and dissolved adsorbate molecules, two mostly used two-parameter models are Freundlich and Langmuir model (Tien, 2019). Beside them, three parameter models can also be used (Sips, Redlich-Peterson, Dubinin–Radushkevich etc)

3.1.1. Langmuir isotherm model

Langmuir isotherm model (Langmuir, 1918) primarily described gas adsorption on solids, but successfully can be applied on various adsorption systems. The main assumption in Langmuir model is based on finite number of energetically homogeneously distributed surface-active sites. The adsorbate cover surface in in form of monolayer and there is no interaction between adsorbate. The Langmuir isotherm model in non-linear form is expressed by Eq. (1).

$$q_e = \frac{q_{\max} K_L C_e}{1 + K_L C_e} \qquad (1)$$

Where q_e represents the amount of adsorbate adsorbed at equilibrium (mg g^{-1}), C_e – adsorbate concentration in solution in equilibrium (mg L^{-1}), K_L – Langmuir constant (L mg^{-1}) and q_{max} is maximum monolayer adsorption capacity (mg g^{-1}).

The *Eq.* 1 of Langmuir model can be expressed in linear form of equation – *Eq.* 2.

$$\frac{C_e}{q_e} = \frac{1}{q_{max} \cdot K_L} + \frac{C_e}{q_{max}}$$

(2)

One of the most important characteristics of the Langmuir isotherm model is dimensionless constant, known also as Langmuir separation factor, R_L. The R_L can be calculated from Eq. 3:

$$R_L = \frac{1}{1 + K_L \cdot C_0}$$

(3)

Based on the experimental data for C_0 and derived K_L, the values R_L has multiple meaning. For values $R_L > 1$, the adsorption is unfavourable, if the R_L is equal to 1, the adsorption process is linear; if the R_L lies between 0 and 1 the adsorption is favourable, and finally, when R_L is equal to 0, the adsorption process can be described as irreversible.

Numerous studies dealing with adsorption from aqueous solutions refer Langmuir model as a most appropriate for describing the investigated adsorption system.

Song et al., (2013) investigated adsorption of phenol and methylene blue on activated carbon obtained from rice husk in the presence of alkali hydroxide as activator. The authors find that adsorption data for both investigated adsorbates can be described by Langmuir model, suggesting monolayer adsorption. The authors calculated the theoretical adsorption capacities based on the size of phenol and methylene blue molecule and obtained results close to those derived from experimental data.

Mojoudi et al, (2019) prepare, characterized and applied as adsorbents activated carbons form sludge in the process of chemical act

ivation by KOH. The adsorption process studied adsorption phenol on series of activated carbons prepared in this study. The fitting of adsorption results has shown best agreement with Langmuir adsorption model for investigated microporous activated carbons, with maximum adsorption capacity of 434 mg g^{-1}.

Investigating the metformin adsorption on Fe-impregnated zeolite adsorbents, Niaei and Rostamizadeh, (2020) also shown that adsorption data shown best fit with Langmuir isotherm model, indicating monolayer adsorption and homogenous distribution of surface-active sites.

Rodriguesa and co-authors (Rodriguesa et al., 2023) used palygorskite from Guadalupe (Brazil) in the process of organo-modification by cetyltrimethylammonium ammonium bromide in order to synthesize the efficient adsorbent for glyphosate removal. The glyphosate removal reached nearly 90% and adsorption process was described by Langmuir model, with maximum glyphosate adsorption capacity of 11.69 mg g^{-1}.

3.1.2. Freundlich isotherm model

Freundlich isotherm model (Freundlich, 1906) described multilayer adsorption where adsorbed molecules can interact to each other. The Freundlich non-linear isotherm model is given by Eq. (4).

$$q_e = K_d \cdot C_e^{\frac{1}{n}} \tag{4}$$

However, many researchers preferred linear form of the Freundlich reaction, and the linear expression is given in Eq. 5.

$$\ln q_e = \ln K_F + \frac{1}{n} \ln C_e \tag{5}$$

Where K_F (mg g^{-1})(mg L^{-1})$^{1/n}$ is the Freundlich constants related with adsorption capacity, while n is associated with adsorption intensity and depending on surface heterogeneity; C_e is adsorbate concentration in solution in equilibrium (mg L^{-1}).

Freundlich isotherm model describes significant information regarding to the adsorption surface and heterogeneity of the adsorption active sites, but there are some limitations of the model. The model is empirical one, and valid only in specific range of concentrations. Further, the Freundlich model does not predict the maximal value of adsorption capacity, which is frequently used as parameter for describing of adsorbent efficiency toward investigated adsorbates. Although certain drawbacks exist, the Freundlich model has been frequently used in many published studies dealing with adsorption from aqueous solutions in environmental chemistry.

Zaini and co-workers (Zaini et al., 2023) published study where palm kernel shell was used in different process of chemical activations in order to synthetized activated carbons. The study has shown different impact of activating agents on the textural development of the activated carbons samples. Adsorbents were tested in the adsorption of methane in the gas storage process.. Each adsorption system was fitted with appropriate isotherm model, and Freundlich equation shown best fit with experimental data, indicated multilayer adsorption of methane.

Ojediran et al., (2021) investigated the mechanism and isotherm modelling of malachite green adsorption in acid functionalized maize cob in batch adsorption experiments. The amino-functionalized maize cob has shown excellent textural properties with specific surface area of 1329 m^{2}g^{-1}. Based on the mathematical interpretation of experimental results, the best fitting was obtained with Freundlich adsorption isotherm model, with coefficient of determination higher than 0.97.

Study of Bernal et al., (2018) refereed adsorption of different organic pollutants (phenol, salicylic acid, acetaminophen, and methylparaben) performed on activated carbon derived from the coconut shell in the process of chemical modification of HNO$_3$ along physical activation by heating. The results shown that adsorption behaviour of phenol and methylparaben on investigated adsorbent was best described by Freundlich isotherm model, while salicylic acid and acetaminophen followed different adsorption models (Bernal et al., 2018).

3.1.3. Redlich-Peterson isotherm model

The Redlich-Peterson isotherm model (Redlich and Peterson, 1959) is hybrid empirical model based on assumption of both Langmuir and Freundlich isotherm models. According to the Redlich-Peterson, adsorption is not occurred in form of ideal monolayer while adsorption sites can be both, energetically homogeneous and heterogeneous. The characteristics of the model are linear dependence on adsorbate concentration, achieving of equilibria over wide concentration range. The equation of the Redlich-Peterson isotherm model is based on three parameters, and it is presented by *Eq*. 6.

$$q_e = \frac{K_R \cdot C_e}{1 + a_R C_e^g}$$

(6)

The linear expression of the Redlich-Peterson model is more frequently used in the literature, and it is presented by Eq. 7.

$$\ln\left(K_R \frac{C_e}{q_e} - 1\right) = b_R \ln C_e + \ln a_R$$

(7)

Where K_R is Redlich-Peterson constant related to adsorption capacity, a_R is constant, while b_R is exponential parameter between 0 and 1. Based on b_R parameter the Redlich-Peterson model can be closer to Langmuir model for b_R values equal to 1 or can be closer to Freundlich isotherm parameter for $b_R = 0$ (Redlich and Peterson, 1959; Fo and Hameed, 2010).

Benhammou et al., (2005) investigated adsorption of cadmium, cooper, manganese, lead and zinc on natural Moroccan stevensite, adsorbent with moderate textural properties, with specific surface area of 134 m^2 g_{-1}, and the value of the cation exchange capacity was 76.5 mmol per 100 g. The adsorption models: Langmuir, Dubinin–Radushkevich, and Redlich–Peterson were employed to describe adsorption of studied cations, but the best fit was shown Redlich–Peterson model.

Belhachemi and Addoun (2011) performed study of comparative adsorption isotherms and modeling of methylene blue onto activated carbons produced from date pits. The adsorption results for methylene blue onto activated carbon were tested by Freundlich, Langmuir, Sips and Redlich-Peterson isotherm models. The authors refereed that three parameters' models such as Sips and Redlich – Peterson model showed the better fitting with the experimental adsorption results than the two parameters models such as Langmuir and Freundlich. .

Based on the literature data, it can be noticed that many of authors published their findings that Redlich-Peterson isotherm model based on three parameters shows higher accuracy with experimental data than isotherm models based on two parameters, like Langmuir and Freundlich. Group of authors leaded by Wu (Wu et al, 2010) give explanation for this finding and suggest new exponential linear model with variable exponent *a*. They performed adsorption study on activated carbons obtained from pistachio shell in process of chemical modification by NaOH.

3.2. Kinetic of the adsorption process

Kinetic adsorption models reveal rate of kinetic process and can give information about mass transfer, diffusion, and reaction on the adsorbent surface. The adsorption process on surface of solid adsorbent involves transport of adsorbate molecules from solution to the boundary layer (diffusion in mass), external mass transfer between the outer surface of the adsorbent and the surrounding liquid phase (diffusion through the boundary layer), diffusion within a particle and finally chemical or physical binding of adsorbate molecule to the active surface centres (Tien, 2019).

The experimental data obtained in adsorption kinetic can be fitted with appropriate kinetics model of zero-order kinetic model, pseudo-first order kinetic model, and pseudo-second order kinetic model, which are extensively used in investigation of the adsorption systems.

3.2.1. Pseudo-first order kinetic model

The *pseudo*-first-order model according to (Lagergren, 1989) can be expressed by *Eq. 8*.

$$q_t = q_e(1 - e^{k_1 \cdot t}) \tag{8}$$

The linearized form of *Eq. 8* is presented by *Eq. 9*:

$$\ln(q_e - q_t) = \ln q_e - k_1 t \tag{9}$$

Where q_t and q_e are the amounts of adsorbate adsorbed (mg g^{-1}) at predetermined time t and at equilibrium, respectively; the k_1 is the first-order rate constant (min^{-1}).

The presented form of pseudo-first order kinetic model has been used in numerous literature studies. Usually, the pseudo -first order kinetic model can be applicable under following experimental conditions: high concentration of the adsorbate, for initial stage of the adsorption process, and when limited number of the active adsorption cites existed on the adsorbent surface or when adsorption process occurred via limited number of the adsorbate interactions with adsorbent active sites (Wang and Guo, 2020).

Darwish et al, (2019) performed batch equilibrium adsorption study in order to investigate adsorption of methyl orange on nickel-oxide and copper-oxide nanoparticles. The adsorption was performed with respect to several different adsorption parameters, like initial concentration of the methylene blue, adsorption time, pH of the methyl blue solution and temperature. The experimental adsorption results were described in terms of the kinetic and authors concluded that pseudo-first order kinetic model was the most applicable for higher concentration of the adsorbate in initial states of the reaction process (Darwish et al., 2019).

Siyal et al. (2019) suggested the remediation and environmentally friendly process of water contaminant removal using fly ash based geopolymer as effective adsorbent of the sodium dodecyl benzene sulfonate. The authors found that when initial concentration of sodium dodecyl benzene

sulfonate increase from 100 to almost 900 ppm, the correlation coefficient (R^2) obtained in fitting pseudo first order model with experimental adsorption results increased in finally reached value of 0.937.

3.2.2. Pseudo-second order kinetic model

Ho end co-workers (1996) were the first scientists who applied pseudo-second order kinetic model to the adsorption results obtained for lead removal by peat (Ho et al., 1996). From then, the pseudo-second order model has been widely applied to describe kinetics of many different adsorption systems, dominantly for adsorption process of pollutants from aqueous solutions onto solids. According to Ho and McKay (Ho and McKay, 2000), the pseudo-second order kinetic model is given by *Eq.* 10.

$$q_t = \frac{q_e^2 \cdot k_2 \cdot t}{1 + q_e \cdot k_2 \cdot t}$$

(10)

Many authors perfered the linear form of the *Eq. 10*, given bellow by Eq. *11*:

$$\frac{t}{q_t} = \frac{1}{k_2 q_e^2} + \frac{t}{q_e}$$

(11)

Where q_t and q_e are the amounts of adsorbate adsorbed (mg g^{-1}) at predetermined time *t* and at equilibrium, respectively; k_2 is the *second*-order rate constant (g mg^{-1} min^{-1}).

Although, according to some authors, the application of the liner pseudo-second order kinetic model includes propagated errors, the linear form of this model is still widely applied (Wang and Guo, 2020).

The physical meaning of the pseudo second order kinetic model is related to the low initial concentration of adsorbate at final stages of the adsorption process, in a case when a huge amount vacant active cites on the surface of adsorbent exist (Wang and Guo, 2020). Many published studies connected with investigation of the kinetics of adsorption process confirmed above presented assumptions of Wang and Guo (2020) related to the application of pseudo-second order kinetic method.

Sabarinathan et al. (2019) investigated kinetics, thermodynamics and mechanism of the methylene blue adsorption on polyoxometalates. The authors found that the higher initial concentration of methylene blue corresponded to the lower values of coefficient of determination obtained in process of fitting experimental results with pseudo-second order kinetic model (Sabarinathan et al., 2019). Further, Simonin (2016) performed comparison of adsorption rates of pseudo-first and pseudo-second order kinetics models, and confirmed that pseudo-second order kinetic method very well described kinetics of adsorption at the final stage of the adsorption process. Finally, the pseudo-second order kinetic model could be characteristic for adsorbents reached by active adsorption sites distributed on the surface (Simonin, 2016). Xia et al, (2019) modified hydrochar by hydrogen-peroxide in the presence of ultrasonic treatment in order to obtained adsorbents suitable for lead ions removal. The results suggest that hydrogen-peroxide strongly affected on elemental composition and textural surface, as well as contributed in the developing of the surface present oxygen functional groups. The oxygen-containing functional groups were responsible for lead ions removal via different adsorption mechanisms, but mainly by complexation. The adsorption of lead was proven to follow the pseudo-second order kinetic model in sample modified by H_2O_2 (Xia et al., 2019).

3.2.3. Weber -Morris intraparticle diffusion model

Generally, the diffusion models are based on the assumption that the slowest step in the reaction could be the diffusion of the adsorbate molecule through the porous adsorbent.

Weber and Morris (1963) model describe diffusion of adsorbates between the particles of the adsorbents (intraparticle diffusions), and it is presented by *Eq. 12*.

$$q_t = C_{id} + k \cdot t^{1/2} \tag{13}$$

Where, q_t is the amount of the adsorbed adsorbate in time t, C_{id} -intercept of the linear plot, and k is Weber-Morris's diffusion constant, which value can be determined by the slope of the linear plot obtained as q_t vs. $t^{1/2}$.

Weber-Morris is widely used in order to describe rate-controlling steps in different adsorption processes. Generally, there are three interpretations of the Weber-Morris diffusion process (Wu et al., 2009):

(i)   In the case that a linear plot passed through the origin, the model can interpret that the adsorption process is controlled by diffusion.

   Wu et al., (1999) investigated pH depended copper (II) ions adsorption from solutions with four different chelating agents (EDTA, citric acid, tartaric acid, and Na-gluconate) on chitosan. The applied Weber-Morris intraparticle diffusion model showed that there was onlyy adsorption in the first stage, and that intraparticle diffusion was rate-limiting for the adsorption process.

   Gupta and co-workers (1990) tested the removal of Omega Chrome Red ME dye onto mixture of different proportions of the fly ash and coal. Several different parameters of the adsorption system were evaluated in the process of the dye removal: adsorbate concentration, particle size, temperature and pH of the solution. The effects of the investigated parameters on the kinetic of the adsorption were estimated. They found that adsorption mechanism involved rapid rate of dye adsorption in the initial stage, controlled by intraparticle diffusion (Gupta et al., 1990).

(ii) Secondly, if the plot does not pass through the origin, several other processes can control adsorption.

   Choi et al., (2007) proposed new kinetic model for benzene adsorption onto granular and powdered activated carbons. The authors found that benzene adsorption can be summarized in three different stages. The first stage was described as initial adsorption on the external surface; the second: adsorption occurred through phased stages with intraparticle diffusion as a rate-limiting process; and third: the adsorption is constant without interactions of aqueous solution with adsorbent surface.

   Dizge et al. (2008) performed adsorption of Remazol Brilliant Blue, Remazol Red 133 and Rifacion Yellow HED on fly ash. The adsorptions were investigated in respect to various initial concentrations of dyes, pH, different adsorbent particle sizes and temperature. The authors shown that external mass transfer and intraparticle diffusion model can be applied on the experimental adsorption results of investigated adsorption systems. Besides that, external mass transfer along with intraparticle diffusion were rate-limiting process (Dizge et al., 2008).

(iii) Finally, for some adsorptions process the multilinearity of plots q_t vs. $t^{1/2}$ was observed and several steps are involved in the whole process.

Ozer et al, (2007) used chemically modified agricultural waste (peanut hull) as an adsorbent for the removal of textile dye methylene blue from an aqueous solution. It was found that the adsorption of methylene blue on investigated adsorbent occurred by three processes (three linear stages) defined as external diffusion, intraparticle diffusion, and finally, adsorption, but only intraparticle diffusion was the process that controlled the kinetics of the adsorption (Ozer et al., 2007).

Akmil-Basar et al., (2007) investigated adsorption of the malachite green on two different activated carbons with different porosity, prepared from pine sawdust in the presence of polyethylenetetraphtalate, activated by $ZnCl_2$. The Weber-Morris diffusion model was applied to the obtained adsorption results and two linear stages were observed for the malachite green adsorption. The first linear plot indicated that there is no external surface adsorption for short adsorption times. In the second stage, the intraparticle diffusion model can be considered as a rate-limiting step that controlled the adsorption process (Akmil-Basar et al., 2007).

3.3. Thermodynamics of the adsorption process

The interactions between adsorbate molecules and solid surface are strongly temperature dependent, and thermodynamic aspects of the removal process represent one of the most significant considerations in the terms of adsorption. The studies related to thermodynamics give the information about spontaneity and feasibility of the adsorption process. Based on the experimental adsorption data, different thermodynamic parameters such as Gibbs free energy (ΔG^0), reaction heat or enthalpy (ΔH^0), reaction entropy (ΔS^0), and activation energy (E_a) can be calculated.

The thermodynamic parameter Gibbs free energy (ΔG^0) for the adsorption process can be calculated from the *Eq*.13:

$$\Delta G = -R \cdot T \cdot \ln K_d \tag{13}$$

where R is the gas constant of 8.314 J K^{-1}·mol^{-1}, K_d is the equilibrium constant, and T (K) is the temperature. The K_d value is calculated from the *Eq*. 14:

$$K_d = q_e/C_e \tag{14}$$

where q_e is the amount of adsorbate adsorbed at equilibrium (mg g^{-1} or mmmol g^{-1}), and C_e is the equilibrium concentration of adsorbate in solution (mg L^{-1} or mmmol g^{-1}).

The ΔG^0 is a thermodynamic parameter referring to the spontaneity of the adsorption process. If the ΔG^0 value is negative, the spontaneity and feasibility of the adsorption processes are confirmed, while the positive value indicates opposite trends. Many adsorption studies refer spontaneous process for

different pollutant removals on the solid adsorbents. Allahkarami et al, (2023) described a mechanistic understanding of adsorption of phenol onto activated carbon composite. The phenol adsorption increased by increasing the adsorption temperature, and thermodynamic study of the adsorption indicated spontaneous process over investigated temperature range (Allahkarami et al., 2023). However, there are a limited number of adsorption studies dealing with non-spontaneous adsorptions. For example, Amin et al, (2017) investigated the adsorption of textile dye malachite green on *Acacia nilotica* waste in the process of batch adsorption. The thermodynamic of the adsorption process was non-spontaneous based on a positive ΔG^0 value and controlled by the entropy of the system (Amin et al., 2017). Nwosu et al., (2012) prepared activated carbon from biowaste material in a pyrolytic process activated by CO_2. The authors performed temperature driven adsorption of Pb(II) and Cd(II) and found that adsorption was non-spontaneous for the Pb(II) ions and spontaneous for the Cd(II) in investigated adsorption system. The ΔG^0 values at 35⁰C were 6.71 kJ mol^{-1} and -2.55 kJ mol^{-1} for Pb(II) and Cd(II) ions, respectively (Nwosu et al., 2012).

The other thermodynamic parameters, standard enthalpy (ΔH^0) and entropy (ΔS^0) of adsorption can be estimated from the Van 't Hoff equation (15):

$$\ln K_D = -\Delta H/RT + \Delta S/R \tag{15}$$

where K_D is the equilibrium constant calculated from the ratio of the C_e and C_t, i.e., concentrations of adsorbate in equilibrium and adsorption time t, respectively; T is the temperature (K), and R is the universal gas constant (kJ/mol K) (Ghosal and Gupta, 2017).

4. EXPERIMENTAL

4.1. Materials

4.1.1. Preparation of water hyacinth lignocellulose materials

The water hyacinth (WH) plant (Karbala, Iraq) was used as the raw material for obtaining of activated carbons. The raw WH was washed with distilled water. The roots and stalks without leaves were chopped and dried in oven for 24 h. The dried WH was boiled in 0.25 M hydrochloric acid to remove metallic oxides, rinsed with distilled water and finally dried in vacuum freeze dryer for 24 h. The dry WH was crushed and ground in rotary mill, and finally sieved in order to obtained particle sized from 1.4 – 2.0 mm.

4.1.2. Agents used for acid carbons synthesis

The $ZnCl_2$ ($\geq$98%), supplied from Sigma-Aldrich, was used as activating agent in process of chemical activation during activated carbons synthesis.
The phosphoric acid (purity of 85% (w/v)) used for the impregnation of dry WH material was supplied from Sigma Aldrich.

4.1.3. Chemical compounds used as water pollutant models

The herbicide glyphosate – GP ($\geq$99%), used in adsorption study as a compound-model of pesticide pollutant, was purchased from Merck.
The anti-hyperglycaemic drug metformin hydrochloride (MT), supplied by Sigma Aldrich, CAS-No. 1115-70-4, with purity $\leq$100%, was used as a model of pharmaceutic pollutant.

The chemical formulas of glyphosate and metformin are given in Figs. 3 and 7, respectively.

4.2. Synthesis of activated carbons

The synthesis of activated carbons is procedure consisting of three steps: (i) preparation of the water hyacinth weed biomass into starting material; (ii) chemical activation process by $ZnCl_2$ or H_3PO_4, and (iii) conversion of activated starting material into active carbon by carbonization.

4.2.1. Synthesis of activated carbons activated by $ZnCl_2$

The activated carbons prepared by chemical activation of dry WH (Section 4.1.1) with $ZnCl_2$ were synthetized according to procedure described in literature (Liou, 2010). The impregnation ratio was calculated as the ratio of the weight of $ZnCl_2$ in the solution to the weight of the dry WH. The impregnation ratio was 0.0, 0.5, 1.0, 1.5, 2.0, 2.5 and 3.0.
The 40 g of dry WH sample was added to 150 ml of solution with appropriate mass of $ZnCl_2$ and stirred at 60 ºC during 4 hours. The solid and liquid phases were separated by filtration through Buchner funnel and dried at 105 ºC during 24 h. The drying process was applied prior to carbonization in order to avoid the loss of the sample caused by rashly steam development. The carbonization of activated WC was carried out in electrical furnace with nitrogen flowing (150 cm^3 min^{-1}) and heating rate of 15 ºC min^{-1}. The carbonization during 80 min was conducted at following temperature: 400 ºC, 500 ºC, 600 ºC and 700ºC.

The obtained active carbons were rinsed with 0.5 M HCl in order to remove activating agent, washed with hot distilled water until neutral pH and finally dried at 110 ⁰C for 12 h. The dry samples were weight in order to calculate the yield.

The yield of activated carbons was calculated from mass ratio between starting WH after drying process and activated carbon (Eq. 16)

$$Y = \frac{m_{dry\,WH}}{m_{AC}} \cdot 100\% \qquad\qquad (16)$$

where Y – is yield of the synthesis, m_{dry} – mass of dry WH and m_{AC} – mass of activated carbon.

The synthetized activated carbons were denoted according to the type of chemical activator, impregnation ratio and carbonization temperature, *i.e.* $0.5ZC_{500}$ means that chemical activator was $ZnCl_2$, while impregnation ratio and carbonization temperature were 0.5 and 500⁰C, respectively.

4.2.2. Synthesis of activated carbons activated by H₃PO₄

The procedure of chemical activation by H_3PO_4 was the same as previously described with $ZnCl_2$. The dried and grounded WH was impregnated with a H_3PO_4 solution in 0.5 to 3.0 ratios, with an increment of 0.5.

20 g of dry WH sample was added to 80 mL of solution, with an appropriate mass of H_3PO_4, and stirred at 60 ⁰C for 4 h. The solid and liquid phases were separated by filtration through a Buchner funnel and dried at 105 ⁰C for 24 h.

The carbonization of impregnated WH was performed in an furnace equipped with nitrogen flowing (150 cm^3 min^{-1}) and a heating rate of 15 ∘C min^{-1}. The carbonization was conducting over 80 min at the temperatures: 400 ⁰C, 500 ⁰C, 600 ⁰C, 700 ⁰C, and 800 ⁰C. The synthetized materials were rinsed with distilled water heated at 80 ⁰C until neutral pH was achieved, and finally dried at 110 ⁰C for 12 h.

The AC were marked and denoted according to the type of chemical activator, impregnation ratio and carbonization temperature, i.e. $0.5PC_{500}$ means that chemical activator was H_3PO_4, while impregnation ratio and carbonization temperature were 0.5 and 500 ⁰C, respectively.

A schematic illustration of the raw WH pre-treatment and procedure for synthesis of activated carbons is given in Figure 8.

Preparation of raw Water Hyacinth material

Raw WH → (Leaves separation; Water washing) → Clean WH roofs and stalks → (a) Chopping, Drying. (b) Boiling in HCl; Washing; (c) Vacuum freeze drying. → Dry and pre–treated WH material →

→ (Grounding and sieving) → Dry and pre–treated WH material, particle size <2 mm.

Activated carbons obtained by activation with $ZnCl_2$

Dry and pre–treated WH, size < 2 mm. → (Impregnation Ratio $ZnCl_2$: Dry WH 0.5, 1.0, 1.5, 2.0, 2.5 and 3.0.) → Suspension dry WH + $ZnCl_2$ → (Separation; Drying.) →

→ Activated WH → (Carbonization 400 °C – 800 °C.) → Carbonized materials → (Rinsing; Drying.) → ACTIVATED CARBONS

Activated carbons obtained by activation with H_3PO_4

Dry and pre–treated WH, size < 2 mm. → (Impregnation Ratio H_3PO_4 : Dry WH 0.5, 1.0, 1.5, 2.0, 2.5 and 3.0.) → Suspension dry WH + H_3PO_4 → (Separation; Drying.) →

→ Activated WH → (Carbonization 400 °C – 800 °C.) → Carbonized materials → (Rinsing; Drying.) → ACTIVATED CARBONS

Figure 8. Schematic presentation of the activated carbons synthesis by activation process with $ZnCl_2$ and H_3PO_4 (Mohammad et al., 2022).

4.3. Characterization methods

The synthetized active carbons were characterized used different analytic methods: elemental analysis, nitrogen adsorption-desorption isotherms and scanning electron microscopy.

- In order to determinate the content of carbon, hydrogen, nitrogen and sulphur in raw materials and active carbons elemental analysis was used. The analysis was performed using elemental analyser instrument (Thermo Scientific - FlashEA1112 Automatic Elemental Analyzers). Prior to analysis, the samples were dried in oven at 110 ⁰C for 24h.
- The textural properties of active carbons were obtained from adsorption-desorption nitrogen isotherms at -196 ⁰C (Micromeritics' ASAP® 2020). Prior to analysis the samples were outgassed at 110 ⁰C during 12 hours. The specific surface area (S_{BET}) was calculated according to Brunner-Emmett-Teller method (Rouquerol et al., 2007), the total pore volume (V_T) was estimated from N_2 adsorption isotherm according to Gurvich rule, and represents the liquid molar volume adsorbed at pressure p/p_0 of 0.999 (Gregg & Sing, 1983; Rouquerol et al., 1998). The volume of micropores were determinated by Dubinin-Radushkevich method (Dubinin, 1966), while mesopores volume was calculated based on desorption N_2 isotherm, using Barrett, Joyner, Halenda (BJH) method (Barrett et al., 1951).
- FTIR spectroscopy was employed in order to detect and analyse the presence of the surface-active functional groups (Thermo Nicolet iS 5 FTIR). Prior to measurement the samples were mixed with KBR in order to prepare pastilles. The KBr pastilles were prepared by mixing 2 mg of activated carbon samples with 200 mg of KBr. The spectra were recorded in wave-numbers range from 400 and 4000 cm^{-1}. The band assignation was performed based on available data and literature publications.
- The morphology of the active carbons was characterized by scanning electron microscopy (SEM - JEOL, JSM 6360 LV). Prior to the analysis, the samples were dried until constant mass (24 h at 110 ⁰C) and gold coated.
- The point of zero charge (PZC) analysis was done in order to determine the effect of the pH of adsorbate solution on the surface charge of activated carbon selected in this study. The procedure was well-known, and previously described in the literature (Liu et al., 2019). The 10 mM solution of NaCl was adjusted between 2 and 12 using HCl or NaOH solution (0.1 M). The 100 mg of activated carbon was added to the 50 mL^3 of NaCl solution, and the suspension was mixed at room temperature for 48 h. After the separation of the solid phase by centrifugation, the final supernatant pH value was measured. The intersection point for curve pH_{final} vs. $pH_{initial}$ and the line that represents the bisector have been taken as pH_{PZC}.

4.4. Adsorption – desorption study

Batch adsorption experiments were carried out in a shaker with thermoregulation (KS 4000I Control Shaker 115V IKA 3510001, IKA®-Werke GmbH & Co., KG, Staufen, Germany). After adsorption was finished, the solid and liquid phase were separated by centrifugation (Hettich Universal 320, Hettich GmbH & Co., KG, Tuttlingen, Germany) at 17,000 rpm for 15 min. The adsorbate concentration in the solution before and after adsorption was analyzed by spectrophotometer (UV-VIS 1800, Shimadzu, Kyoto, Japan), monitoring the peaks at $\lambda_{max} = 234$ nm and $\lambda_{max} = 264$ nm, for metformin and glyphosate, respectively.

The percentage of the removal (R) of the adsorbates from the aqueous solutions was determined using the following equation:

$$R = \frac{(C_0 - C_e) \cdot 100\%}{C_0} \qquad\qquad (17)$$

The amount of the adsorbed pollutant (q_t, mg g^{-1}) in time t per mass of adsorbent was calculated according to the following equation:

$$q_t = \frac{(C_0 - C_t) \cdot V}{m_{ads}} \qquad\qquad (18)$$

where C_0 and C_e are initial MT/GP concentrations and MT/GP concentration after adsorption time t (mg L^{-1}), respectively; V is the volume (mL) of the MT/GP solution, and m_{ads} is the adsorbent mass (mg).

In preliminary experiments, linearity between the concentration of MT or GP standard solutions and absorbance was determined according to the Beer–Lambert law. According to Clark et al, 1993 the absorbance within range of 0.1 to 1.0 is ideal to maintain the linearity in Beer-Lambert law (Clark et al., 1993).

The calibration curves for MT and GP are presented in Fig. 9. Based on the curve, MT solutions in the concentration range 1–15 mg L^{-1}can be measured directly, while a concentration above 15 mg L^{-1} were diluted prior to measurement. The concentration range of the GP solution used for adsorption experiments was in the range of 1–25 mg L^{-1}, and all concentration higher than 25 mg L^{-1} were measured after dilution.
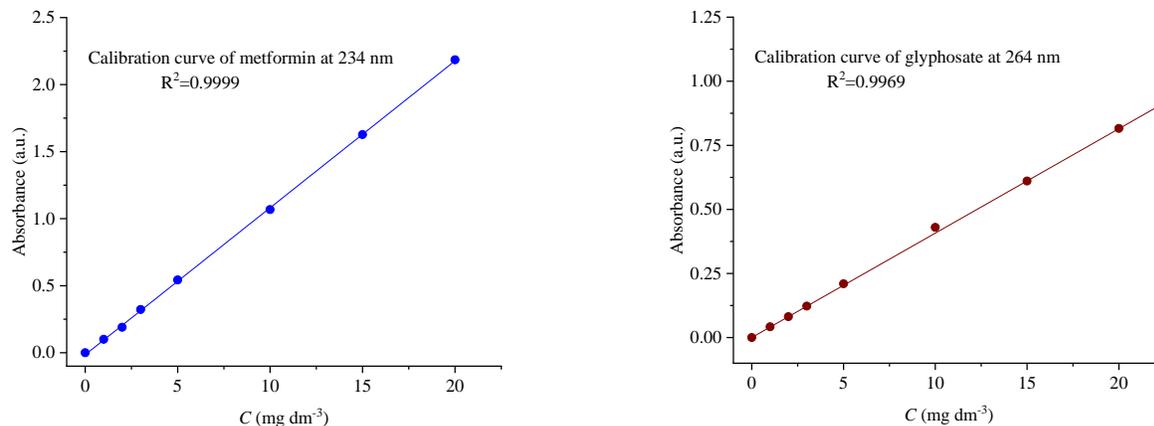
Figure 9. The calibration curve for: a) metformin, and b) glyphosate

The effect of the adsorbent mass, adsorbate initial concentration, contact time, pH, and temperature on the adsorption of MT and GP were investigated.

4.4.1. Experimental conditions for Metformin adsorption

The impact of the ***adsorbent concentration*** on the amount of removed MT was tested after 120 min with the following concentrations of the activated carbons: 100 mg L^{-1}, 150 mg L^{-1}, 200 mg L^{-1}, 250 mg L^{-1}, 300 mg L^{-1}, 400 mg L^{-1}, and 500 mg L^{-1}. The initial concentration of MT solution was 20 mg L^{-1}, and temperature during experiment was kept constant on 25⁰C. The pH of MT solution was unadjusted (6.8).

To study the ***effect of the initial MT concentration*** on the adsorption, experiments were carried out at the temperature of 25 ⁰C using a mass concentration of the adsorbent of 250 mg L^{-1} and an initial MT concentration of 10; 20; 40; 60; 80, and 100 mg L^{-1}. The pH of MT solution was unadjusted (6.8). The ***effect of contact time*** and equilibrium time of metformin adsorption was monitored at predetermined time intervals during 240 min.

The ***effect of pH*** was tested in the pH range from 2.0 to 12.0, while all the other parameters were kept constant (initial MT concentration of 20 mg L^{-1}, adsorbent concentration of 250 mg L^{-1}, and adsorption time of 120 minutes at 25 ⁰C). The pH was adjusted using 0.1 mol L^{-1} NaOH and 0.1 mol L^{-1} HCl solutions. The initial pH value of metformin solution without adjusting was 6.8, and the adsorption on this pH value has also been included into experimental investigations.

The dependence of the amount of adsorbed MT on ***temperature*** was investigated in the temperature range from 25 ⁰C to 50 ⁰C. The initial MT concentration in this experiment was set on 40 mg L^{-1}, while other adsorption parameters were kept constant: adsorbent concentration of 250 mg L^{-1}, and adsorption time of 120 minutes. The pH of MT solution was unadjusted (6.8).

4.4.2. Experimental conditions of Glyphosate adsorption

The **effect of the adsorbent concentration** (*adsorbent mass per volume*) on the amount of removed glyphosate was tested for 120 min in the range of 50 mg L^{-1} to 625 mg L^{-1}, using glyphosate solution with initial concentration of 100 mg L^{-1}. The pH value of GP solution was unadjusted – obtained by dissolving of pesticide in distillate water (3.9).

The **effect of contact time** and equilibrium time of glyphosate adsorption was monitored at predetermined time intervals during 240 min, at 25 °C, with starting GP concentration of 100 mg L^{-1} and concentration of the adsorbent of mass of adsorbent of 250 mg L^{-1}.

To study the **effect of the initial GP concentration** on the adsorption, experiments were carried out at the temperature of 25 °C, using a mass concentration of the adsorbent of 100 mg L^{-1} and an initial adsorbate concentration of 50, 75, 100, 125, 150 and 200 mg L^{-1}. The pH value of glyphosate solution was unadjusted.

The **effect of pH** was tested in the pH range from 2.0 to 12.0, while all the other parameters were kept constant (initial glyphosate concentration of 100 mg L^{-1}, adsorbent concentration of 250 mg L^{-1}, and adsorption time of 120 minutes). The pH was adjusted using 0.1 mol·L^{-1} NaOH and 0.1 mol·L^{-1} HCl solutions. The pH value of glyphosate solution without adjusting was 3.9 (unadjusted value), and adsorption on this pH value has been also included into experiment.

The dependence of the amount of adsorbed glyphosate on **temperature** was investigated in temperature range from 25 °C to 50 °C (298 K – 323 K). The initial glyphosate concentration of 75 mg L^{-1} was used in the experiment with temperature changes, while other adsorption parameters were kept constant: adsorbent concentration of 250 mg L^{-1}, and adsorption time of 120 minutes.

4.4.3. Desorption study and reusability test

Desorption experiments were conducted in order to select the best desorbing agent to be employed in the process of the adsorbent regeneration. Before desorption, the adsorbent saturation was done from adsorbate solution, according to the following experimental procedure: 100.0 mg of adsorbent was saturated by MT or GP molecules using 400.00 mL of 100 mg L^{-1} adsorbate solution (either MT or GP solution) during 120 min (previously estimated equilibrium time) at 25 °C. During adsorption test, the pH of MT or GP solution were at unadjusted pH values. After saturation, the MT/GP-saturated adsorbent was separated from the solution by centrifugation, rinsed with distilled water, and dried under the vacuum at room temperature. The desorption was firstly performed using 0.1 M NaOH, 0.1 M HCl, and 0.1 M NaCl, and then using mixtures of 0.1 M HCl and 96% ethanol in defined volume ratios. Trough desorption experiment, the MT/GP-saturated adsorbent was constantly shaken for 2 h at room temperature. The ratio of saturated adsorbent (mg) and desorption agent (mL^3) was 1:4. The concentration of desorbed MT or GP in the supernatant was determinate by UV-Vis spectrometry, while the desorption was estimated using *eq.* (19):

$$Percentage\ of\ desorption\ (\%) = \frac{C_{desorp.}}{C_{adsorp.}} \cdot 100\ \% \qquad (19)$$

In eq 19, C_{ads} and C_{des} denote the amounts of adsorbed / desorbed adsorbate, respectively. The recovered adsorbent was washed with distilled water, dried at 100 °C for 24 h, and reused in the follow adsorption cycle which was conducted under previously determined optimal adsorption parameters.

5. RESULTS AND DISCUSSION

The results of the characterization techniques and adsorption studies are presented in this section of doctoral dissertation, and followed by appropriate discussion and comparison with the literature data.

5.1. Characterization

The selection of the adsorbents obtained in the presence of two different chemical agents as activators were based on the results of the characterization.

5.1.1. Yield of activated carbon synthesis

The yields of activated carbons obtained after chemical activations with $ZnCl_2$ and H_3PO_4 and subsequent carbonization process are presented in Figure 10a and 10b, respectively.
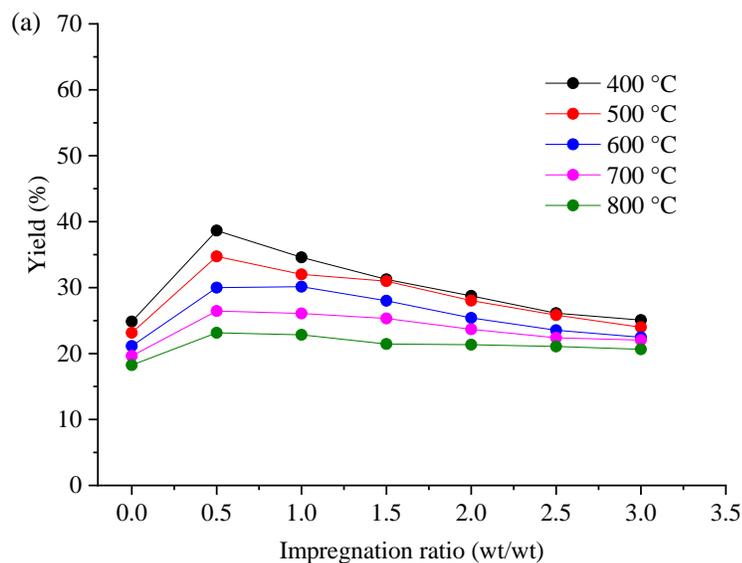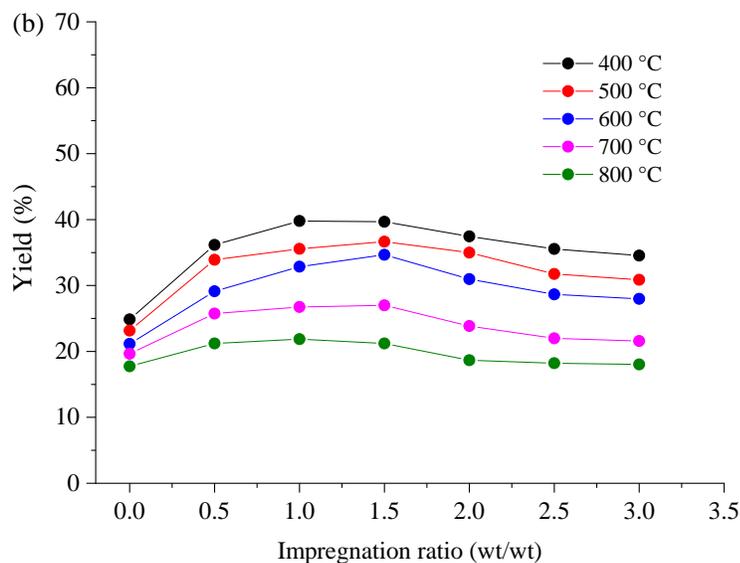
Figure 10. The effect of impregnation ratio and temperature of carbonization on the yield of activated carbons obtained from dry water hyacinth impregnated by:

a) $ZnCl_2$ (Mohammed and Kijevčanin, 2022) and b) H_3PO_4 (Mohammed et al, 2022).

It was observed that activated carbons obtained with impregnation ratio 0 (i.e. without applied $ZnCl_2$) and temperature range 400 ⁰C – 800 ⁰C had relatively low yield in the range of 17.8 – 24.9 %. This fact can be related to a high content of volatile matter and relatively low lignin content in raw WH material used for the preparation of activated carbons. According to the literature, activated carbons obtained by pyrolysis without prior activation showed significant weight loss attributed to gasses extraction (CO, CO_2 and CH_4) (Mohammad and Kijevčanin, 2022).

The activation agent and applied carbonization temperature have a significant impact on the yield of activated carbons (Fig. 10). The activated carbons obtained with impregnation ratio 0 (i.e. without applied $ZnCl_2$ or H_3PO_4) have lower yields than samples subjected to impregnation. Generally, the best yields were obtained for lowest carbonization temperature (400⁰C) no matter what chemical agent was used for the activation process. With temperature increase the yield of activated carbon decreased regardless the amount of applied $ZnCl_2$ or H_3PO_4 which was explained by the promotion of the tar volatilization at higher temperatures (Qian et al., 2007). For each carbonization temperature it was observed that the amount of the $ZnCl_2$ has a similar impact on yield, i.e. activated carbon yields continually decreased with the impregnation ratio higher than 0.5 (Fig. 10a). The similar trend was obtained for the samples impregnated by H_3PO_4, where the impregnation ratio higher than 1.5 lead to the decrease of activated carbons yield. This observation can be explained by larger evolution of volatiles compounds affected by dehydration agent either $ZnCl_2$ or H_3PO_4 (Liou, 2010).

35

5.1.2. Textural properties

It is very important to emphasize that surface development has been strongly connected to the adsorption properties. Therefore the detailed textural analysis has been performed and presented in this chapter with special focus on impact of synthesis parameters, i.e., amount of activation agent and carbonization temperature on the textural properties of activated carbons.

5.1.2.1. The effect of the impregnation ratio on the surface area of activated carbons

In order to determine the effect of the amount of applied chemical agents on the surface development and the specific surface area (S_{BET}),of the samples obtained at carbonization temperature of 400 ⁰C was correlated with impregnation ratio (from 0.0 to 3.0) and shown in Figure 11.
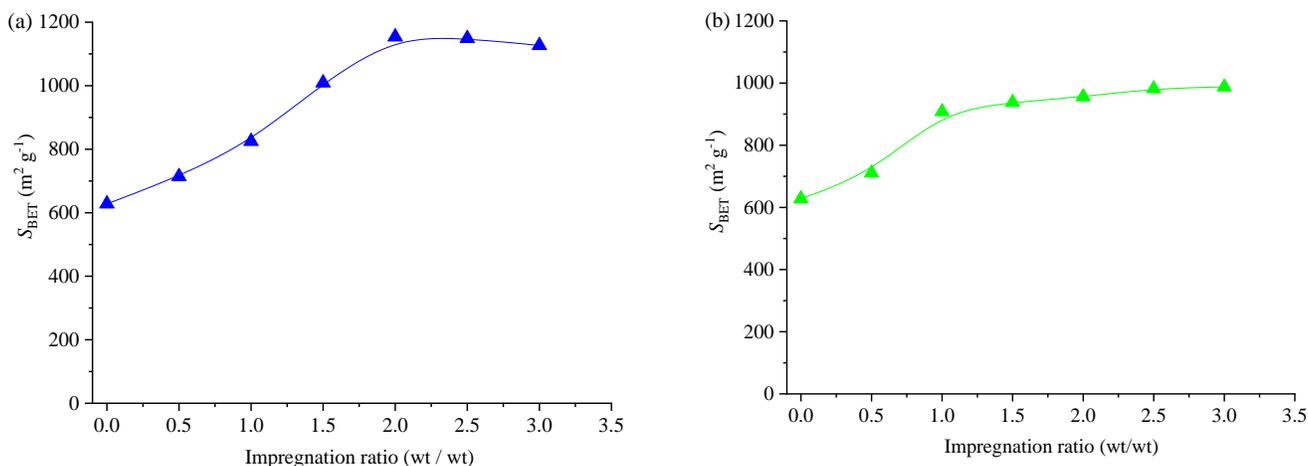
Figure 11. The influence of impregnation ratio of a) $ZnCl_2$ (Mohammed and Kijevčanin, 2022) and b) H_3PO_4 (Mohammed et al, 2022) on the specific surface area of activated carbons obtained by carbonization process at 400 ⁰C.

The sample of activated carbon obtained without impregnation showed the lowest value of S_{BET}, probably due to incomplete carbonization process. The introducing of $ZnCl_2$ lead to development of the specific surface and this trend continues up to impregnation ratio 2.0, and after that decreases for the higher impregnation ratios. These results are in accordance with literature data (Rodriguez-Reinoso and Molina-Sabio, 2004; Lua and Yang, 2005; Yorgun et al., 2009).

Yorgun and co-authors concluded that $ZnCl_2$ act as a dehydration agent during carbonization process, which resulted in carbon charring and formation of aromatic, porous structure (Yorgun et al., 2009). Therefore, the impregnation ratio of 2.0 was selected to be the optimal when activation process has been performed in the presence of $ZnCl_2$.

The application of the activation agent also had a significant act on the surface development for samples impregnated with H_3PO_4, as was expected. The application of phosphoric acid as chemical activator led to an increase in the specific surface area by increasing the impregnation ratio in range from 0 to 1.5. Further impregnation ratio increasing from 1.5 to 3.0, the surface area changes were negligible.. Therefore, the samples with an impregnation ratio of 1.5 were selected as an optimal for H_3PO_4 activation, and have been used for further synthesis.

5.1.2.2 The effect of the carbonization temperature on the surface area of activated carbons

In order to evaluate the optimal carbonization temperature, i.e., temperature which lead to the production of the activated carbons with the most developed specific surface area, the S_{BET} values of activated carbons obtained by impregnation with $ZnCl_2$ and H_3PO_4 in impregnation ratios 2.0 and 1.5, respectively, were correlated with carbonization temperature in the range from 400 ⁰C to 800 ⁰C (Fig. 12).
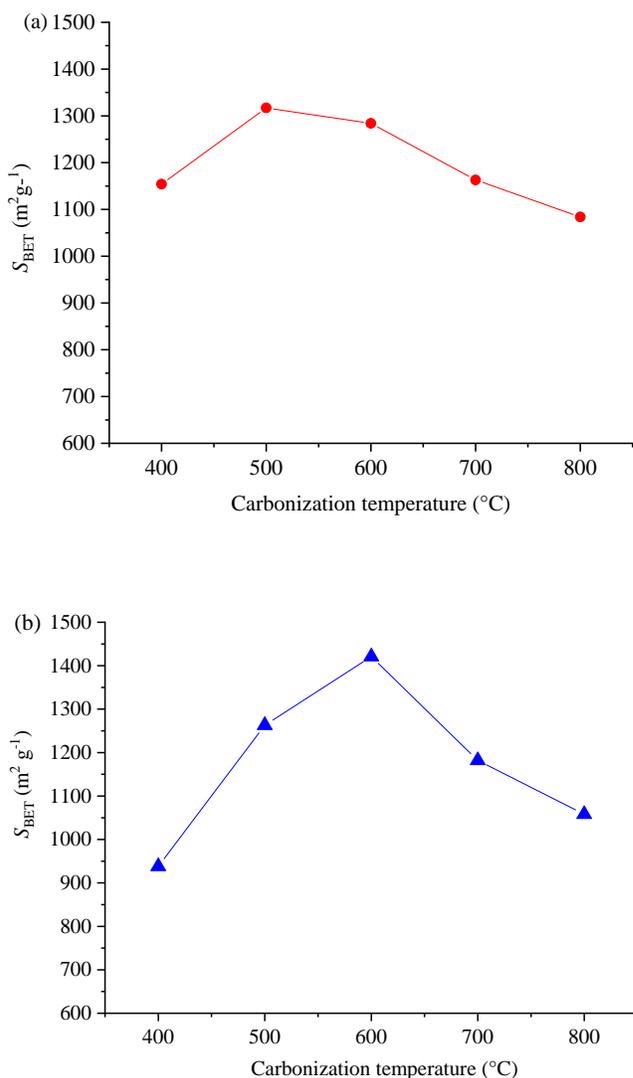
Figure 12. The influence of the carbonization temperature on the specific surface area of activated carbons obtained in the presence of a) $ZnCl_2$, with impregnation ratio of 2.0, and b) H_3PO_4, with impregnation ratio of 1.5 (Mohammed et al, 2022).

Carbonization temperature has a strong effect on the thermal degradation and the volatilization process of an impregnated sample, leading to an in-crease in the surface area (Castro et al., 2010). The activated carbon activated by $ZnCl_2$ shown significantly higher S_{BET} value for activated carbon obtained at 400 ⁰C than corresponding sample activated by H_3PO_4. The temperature increases up to 500 ⁰C led to

the production of the sample with the most developed S_{BET} of 1317 m^2 g^{-1}, while further increasing of temperature led to lower S_{BET} values (Fig. 12a). The results presented in Figure 12b showed that increasing activation temperatures from 400 ºC to 600 ºC caused a significant increase in S_{BET}, achieving the highest value of 1421 m^2 g^{-1} at 600 ºC. Further increases in carbonization temperature led to a decrease in the specific surface area, which can be explained by the shrinkage in the carbon structure, resulting in a reduction in textural properties (Kumar and Jena, 2016). Similar trends have also been found for the BET surface area of activated carbon obtained through the H$_3$PO$_4$ activation of other lignocellulosic precursors (Corcho-Corral et al., 2006; Deng et al., 2010; Kumar and Jena, 2016).

In order to check the effect of carbonization temperature on micro- and meso- porosity of the activated carbon, textural parameters such as micropore volume (V_{mic}), mesopore volume (V_{meso}) and total pore volume (V_{tot}) of the samples activated with ZnCl$_2$ in impregnation ratio of 2.0, and H$_3$PO$_4$ in impregnation reatio of 1.5 are presented in Table 3.

Table 2. Pore volumes of activated carbons activated by ZnCl$_2$ (impregnation ratio of 2.0) (Mohammad and Kijevčanin, 2022), and H$_3$PO$_4$ (impregnation ratio of 1.5) obtained by carbonization in the temperature range from 400ºC to 800ºC

Temperature	ZnCl$_2$ activation			H$_3$PO$_4$ activation		
(ºC)	V_{tot}	V_{mic}	V_{meso}	V_{tot}	V_{mic}	V_{meso}
	(cm^3 g^{-1})	(cm^3 g^{-1})	(cm^3 g^{-1})	(cm^3 g^{-1})	(cm^3 g^{-1})	(cm^3 g^{-1})
400	0.602	0.301	0.298	0.618	0.242	0.372
500	0.697	0.152	0.541	0.685	0.266	0.415
600	0.670	0.135	0.527	0.741	0.294	0.446
700	0.605	0.113	0.485	0.645	0.225	0.418
800	0.554	0.081	0.470	0.598	0.192	0.404

V_{tot}-total pore volume; V_{mic}-micropore volume; V_{meso}-mesopore volume

Based on results in Table 3, the total pore volume and mesopore volume of samples obtained by ZnCl$_2$ activation increased with increasing final carbonization temperature from 400ºC to 500ºC, while further increasing of temperature led to surface development decreasing. The similar trend was observed for samples obtained in the presence of H$_3$PO$_4$, but increasing of pore volume was observed for increasing temperature up to 600 ºC.It was also observed that higher carbonization temperatures reduced microporosity, and had positive impact on mesoporosity development, which was in agreement with literature data (Rodriguez-Reinoso and Molina-Sabio, 2004; Qian et al, 2007; Gómez-Tamayo et al., 2008). According to Rodriguez-Reinoso and Molina-Sabio, the ZnCl$_2$ has important role in producing micro and meso porosity in the carbonization process up to 500ºC, but at higher temperatures the reaction of ZnCl$_2$ with the char is negligible (Rodriguez-Reinoso and Molina-Sabio, 2004). The decrease in textural properties in temperatures higher than 500ºC can also be attributed to a sintering effect at high temperature, followed by shrinkage of the char, and realignment of the carbon structure (Mohanty et al., 2006). On the other hand, Kumar and Jena (2016) found that influence of the phosphoric acid and to developed of pore structure of activated carbons produced from lignocellulose material are crucial. The authors found that increasing of the temperature of carbonization above 700 ºC led to the reduction of pore volume (Kumar and Jena, 2016). Boonpoke (2015) produced the microporous activated carbons from water hyacinth lignocellulose materials with specific surface area in range 912-1066 m^{2}g^{-1}

(Boonpoke, 2015). Wu et al., (2016) also confirmed that raw water hyacinth can be successfully used for the production of activated carbons with highly developed surface by process of chemical activation and carbonization. The group has synthetized carbons with specific surface area of 1380 m^2 g^{-1} (Wu et al., 2016). Using different lignocellulose materials with similar activation procedure with $ZnCl_2$ in the presence of NaOH it was possible to synthetized activated carbons with high specific surface area around 2000 m^2 g^{-1} (Yang and Qiu, 2011).

5.1.2.3. Selection of the activated carbons

Based on the results of the performed analysis presented in subsections 5.2.1 and 5.2.2 samples of activated carbon obtained in the presence of $ZnCl_2$ (impregnation ratio 2.0, carbonized at 500 ⁰C – 2.0ZC$_{500}$) and in the presence of H_3PO_4 (impregnation ratio of 1.5, carbonized at 600 ⁰C -1.5PC$_{600}$) were selected as ones with the best surface characteristics.

In order to summarize the effect of both the optimal impregnation ratio and carbonization temperature, on the improvement of the textural and surface characteristics of the raw WH, this sample has also been characterized. The adsorption-desorption isotherms of nitrogen at -196 ⁰C of raw WH, 2.0ZC$_{500}$, and 1.5PC$_{600}$ are presented in Figures 13, 14, and 15, respectively.
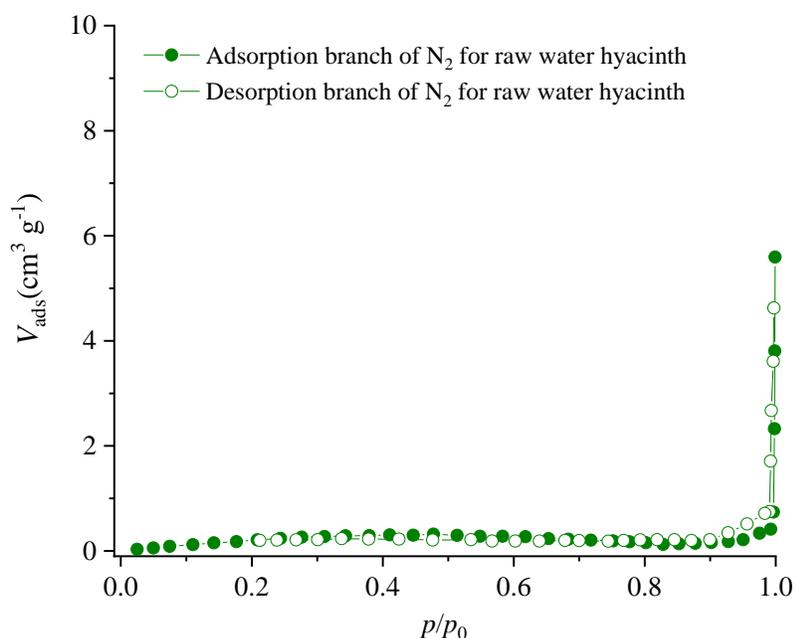
Figure 13. The adsorption–desorption isotherms of nitrogen for raw water hyacinth (Mohammed et al., 2022).
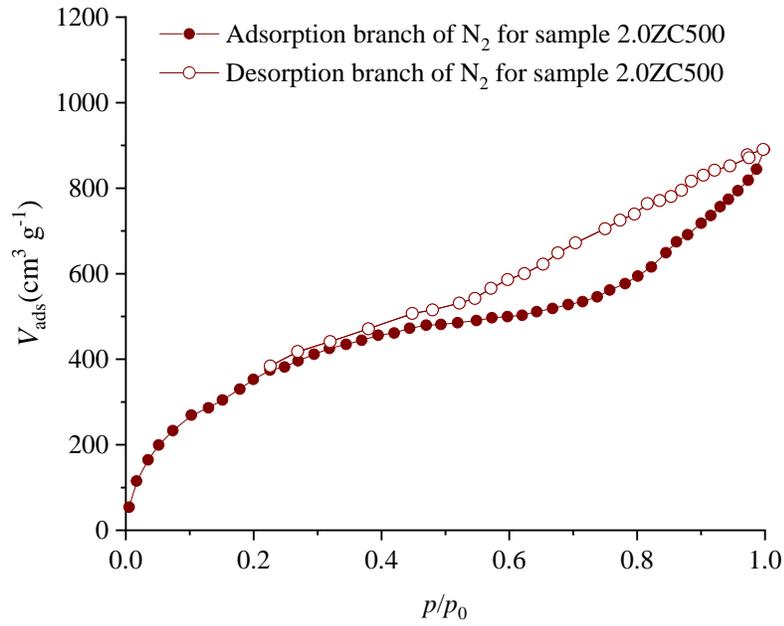
Figure 14. The adsorption–desorption isotherms of nitrogen of the sample 2.0ZC$_{500}$.
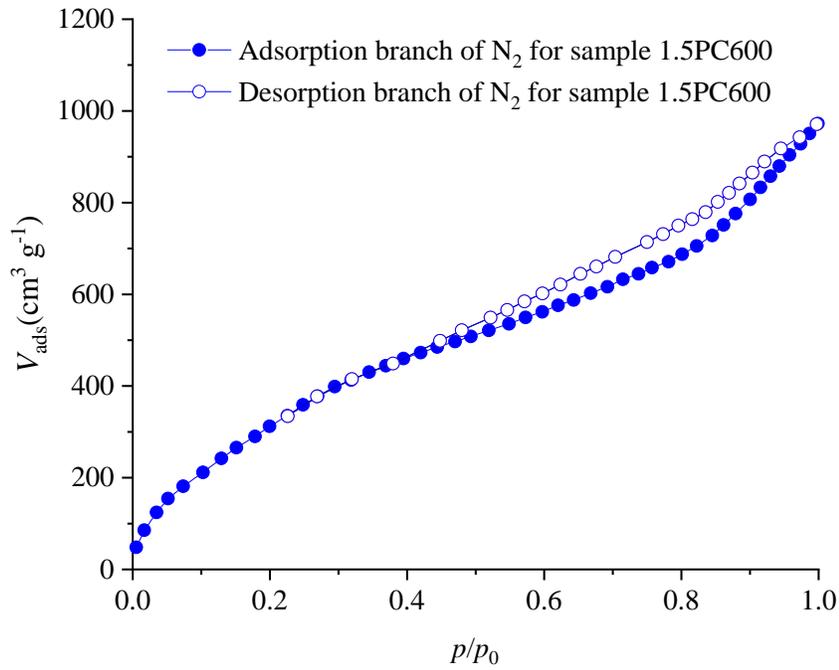
Figure 15. The adsorption–desorption isotherms of nitrogen of the sample 1.5PC$_{600}$ (Mohammed et al., 2022).

The summarized textural properties of raw water hyacinth, $2.0ZC_{500}$, and $1.5PC_{600}$ are given in Table 4.

Table 4. Textural properties of the raw water hyacinth material, and selected adsorbents (Mohammad et al., 2022, Mohammad and Kijevčanin, 2022)

Sample	S_{BET} (m^2 g^{-1})	V_{tot} (cm^3 g^{-1})	V_{mic} (cm^3 g^{-1})	V_{meso} (cm^3 g^{-1})	D_P (nm)
WH	2.4	0.00872	-	-	-
$2.0ZC_{500}$	1317	0.697	0.152	0.541	3.1
$1.5PC_{600}$	1421	0.741	0.294	0.446	2.8

Based on the adsorption–desorption isotherm of raw WH (Figure 13) and the results from Table 4, it can be noticed that the amount of adsorbed nitrogen and the S_{BET} and V_{tot} values are quite low. The raw WH has characteristics of a macroporous material, and the V_{mic}, V_{meso}, and D_p cannot be calculated based on the obtained adsorption branch. These results are expected for raw lignocellulose material. On the other hand, the impregnation process followed by carbonization under optimal conditions dramatically increased the textural properties of the treated samples. The prepared activated carbons show both micro- and mesoporosity regardless the type of chemical activator.

The sample $2.0ZC_{500}$ had slightly lower specific surface area in comparison to sample $1.5PC_{600}$ but almost 78% of its porosity belonging to the mesopores (Figures 14 and 15, Table 4). The sample $1.5PC_{600}$ has a higher value of micropore volume then $2.0ZC500$ and the percentage of the mesoporosity obtained for the ratio of V_{meso} to V_{tot} is equal to 60.2%. Based on these values, both samples can be described as a dominantly mesopores materials, which is a crucial characteristic for the access of the adsorbate molecules to the interior of the adsorbent particles. Several researchers also found that activated carbons derived from different lignocellulose precursors showed micro-and mesoporosity after treatment with phosphoric acid (Prahas et al., 2008; Hui et al., 2015).

According to the literature, the pores can be divided into three different classes: < 20 Å micropores, 20 Å < mesopores < 50 nm Å, and > 50 Å macropores (Groen et al., 2003). The micropores and mesopores, which have been developed mostly during the activation–carbonization process, are the most significant to the adsorbing capability.

The pore diameter distribution for both, $2.0ZC_{500}$ and$1.5PC_{600}$ lies between 10 Å and 40 Å, which clearly shows that the pore diameter is at the beginning of the mesopore range, with an average pore diameter (Dp) of 31 Å and 28 Å, respectively.

5.1.3. Elemental analysis

Elemental analysis was performed in order to evaluate the effect of temperature and the applied activation agent on the chemical composition of the activated carbons in comparison with the starting raw WH material. The result of the elemental analysis of dry WH and activated carbons prepared in the presence of $ZnCl_2$ (impregnation ratio of 2.0) along with the selected activated carbon obtained by H_3PO_4 activation of the raw material ($1.5PC_{600}$) are presented in Table 5. The major organic elements in all investigated samples are carbon and oxygen.

Table 5. The results of the elemental analysis (Mohammed and Kijevčanin, 2022, Mohammed et al., 2022).

Sample	Content of elements (wt%)				
	C	H	O^a	N	Ash
Dry WH	41.22	6.23	47.07	1.54	3.94
$2.0Z\ C_{500}$	81.57	3.15	14.20	0.27	0.81
$1.5PC_{600}$	81.56	3.47	13.78	0.28	0.91

[a] The oxygen content was calculated by difference

The major organic elements in all investigated samples are carbon and oxygen. Compared to the activated carbons, the raw WH has higher content of ash (3.94%), consisting mainly of silica-oxides and metal-oxides (Liou, 2010). The treatment with HCl prior to the activation process led to the leaching of metal cations and therefore the ash content was reduced. During the carbonization process, along with temperature increase, the content of carbon also increased, which was expected (Liou, 2010). The carbon content was 41.22% while the oxygen content in raw WH was calculated to be 47.07%. The results of the elemental analysis of 1.5PC600 reveal that the content of carbon, hydrogen, oxygen, nitrogen, and ash was 81.56%, 3.47%, 13.78%, 0.28%, and 0.91%, respectively. The elemental analysis shows that content of the major elements in samples $2.0ZC_{500}$ and $1.5PC_{600}$ are similar (Mohammad et al., 2022, Mohammad and Kijevčanin, 2022).

5.1.4. SEM analysis

The Scanning Electron Microscopy (SEM) was used to show the difference in the morphology between the raw WH material and selected activated carbons obtained by $ZnCl_2$ activation with the impregnation ratio 2:1, and carbonized in temperature range from 400 ⁰C to 700 ⁰C. The SEM images were recorded using magnification of 3000 times and presented in Fig. 16. (Mohammad and Kijevčanin, 2022).
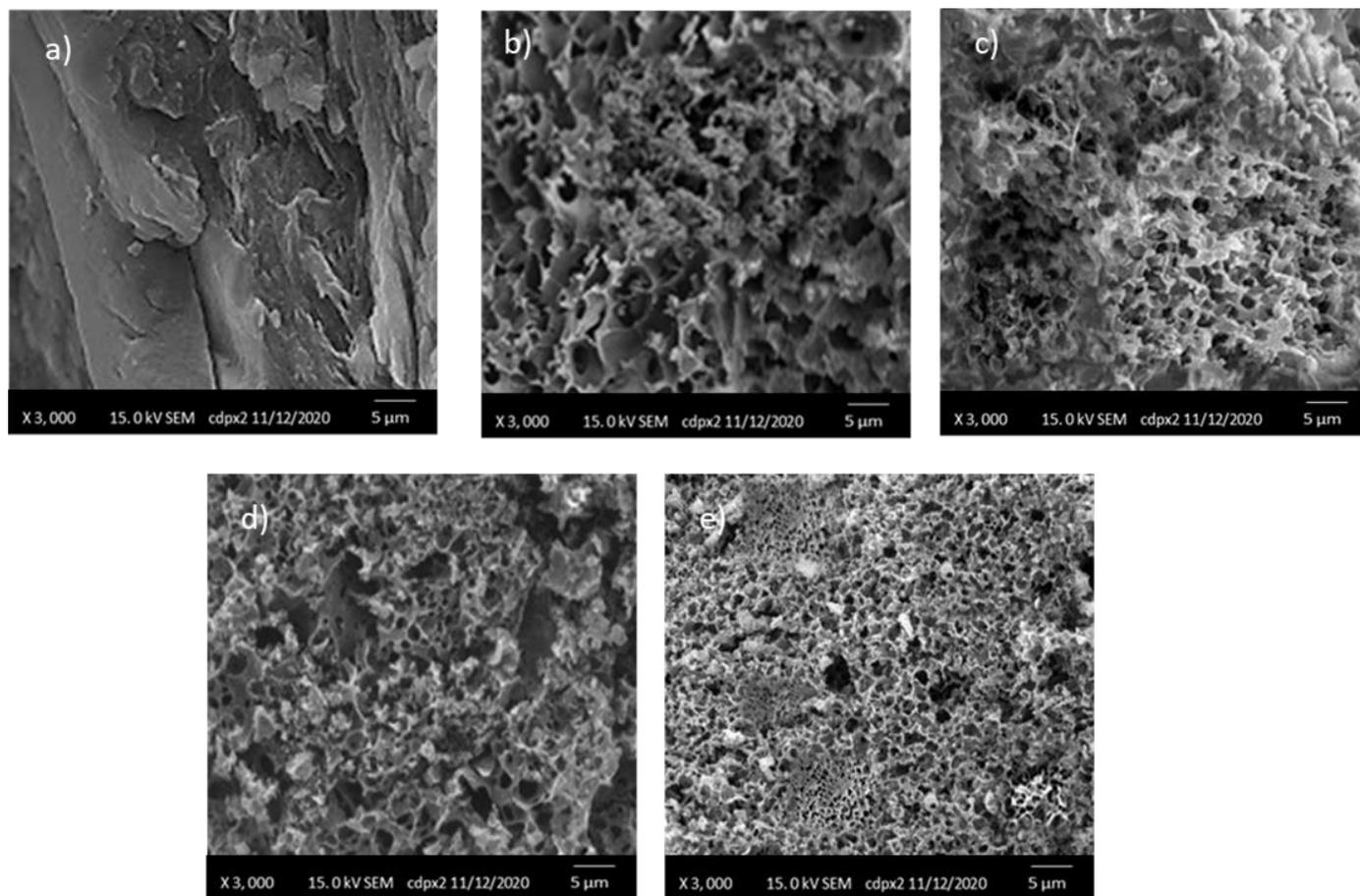
Figure 16. The SEM images of a) raw WH; b) 2.0ZC400; c) 2.0ZC500; d) 2.0ZC600; e) 2.0ZC700 (Mohammed and Kijevčanin, 2022).

From Fig. 16 significant difference in surface morphology can be observed between raw WH and activated carbons obtained by activation with $ZnCl_2$ at different temperatures. The surface of the raw WH is moderately developed with parts of a smooth area but after impregnation and carbonization, the raw WH biomass turns to be more porous with more open structures (Fig. 16). The increase of the carbonization temperature led to a reduction in small cracks in the activated carbon surfaces which could be responsible for the reduction of textural properties. According to the textural analysis the mesopore formation was dominantly responsible for the surface development (Table 1). Since the mesopores are those with diameter from 2 – 50 nm, they are not visible in Fig. 16, where macroporous structure can be noticed.

In order to compare the effect of the H_3PO_4 as activation agent with the effect of the $ZnCl_2$ on the morphology of the surface, the SEM image of 1.5PC600 is presented in Fig. 17.
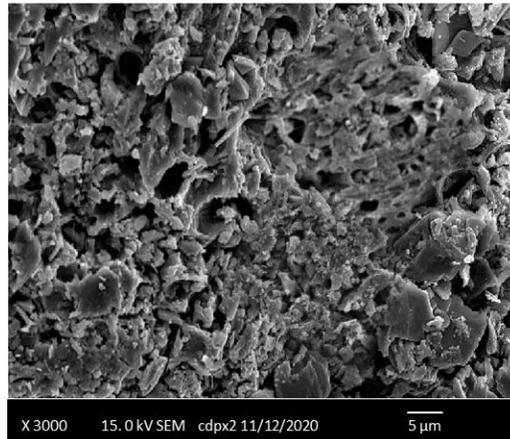
Figure 17. The SEM images of 1.5PC600 (Mohammad et al., 2022)

After the chemical activation process by H_3PO_4 and carbonization at 600 ⁰C, the morphology of the sample starts to be more developed, with open canals and cracks. Furthermore, the presence of different sizes and shapes of macrostructure pores can be noticed. Also, there is no significant difference in the morphology of the samples obtained in the presence of investigated chemical activators. Therefore, it can be assumed that the composition of the starting of raw lignocellulose material and carbonization temperature play more important roles than compound used as activator.

5.1.5. FTIR analysis

The presence of the specific surface functional groups along with the surface development, represent two major characteristics of the good adsorbents. Therefore, in order to determine the major functional groups present on the surface of the selected adsorbents, the FTIR spectra of the raw WH, $2.0ZC_{500}$ and $1.5PC_{600}$ are recorded and presented in Fig. 18a, 18b and 18c, respectively.
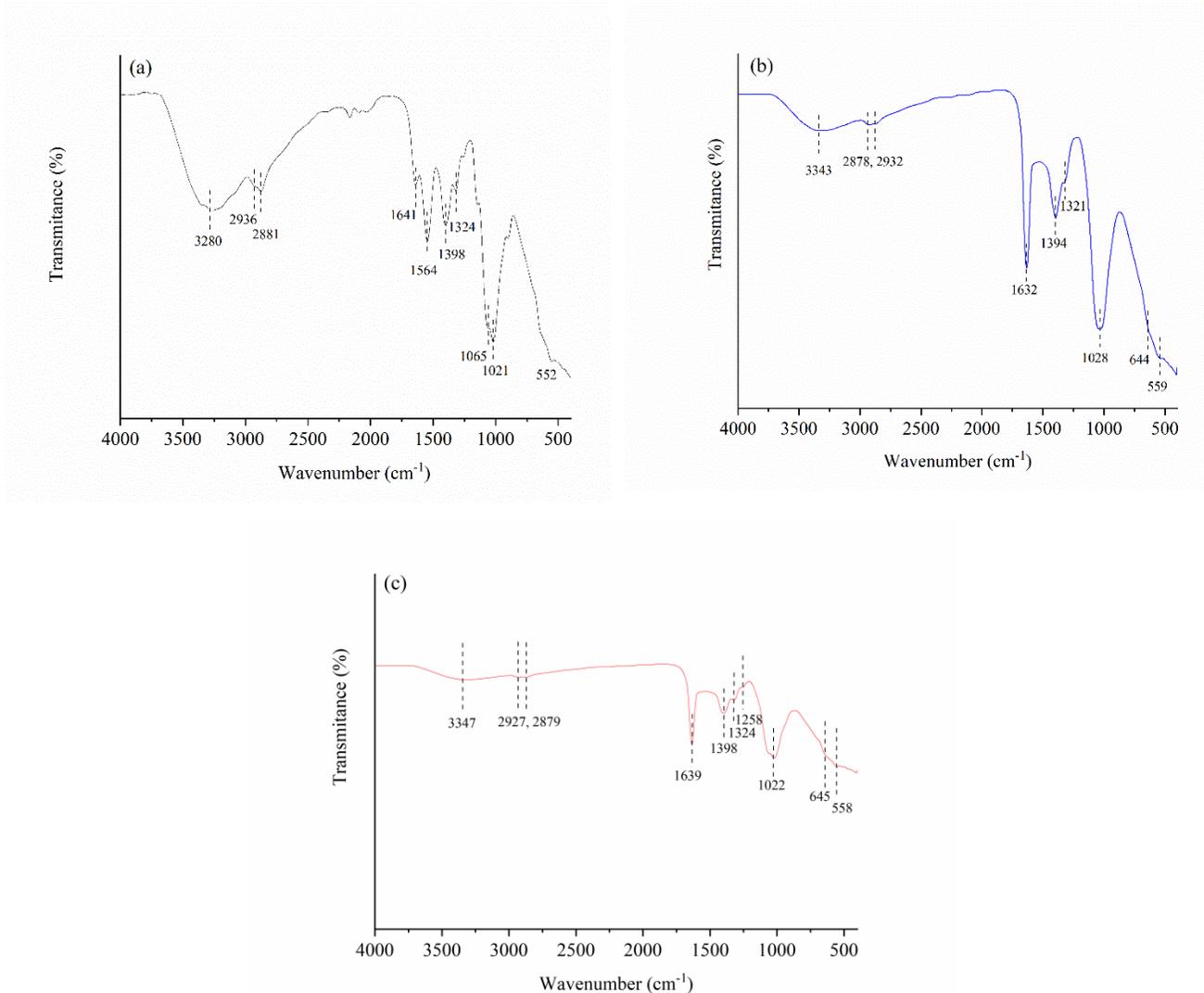
Figure 18. FTIR spectra of a) Raw WH material; b) $2.0ZC_{500}$; and c) $1.5PC_{600}$ (Mohammed et al., 2022).

The assignations of the IR bands from Figure 18a and 18b were based on the literature source on infrared spectroscopy absorption (Infrared Spectroscopy Absorption Table) and presented in the Table 6.

45

Table 6. The results of FTIR analysis, band assignation for samples 2.0AC500 and 1.5PC600.

	Samples		Bands assignation	Reference
Raw WH	2.0ZC500	1.5PC600		
	Wavenumber (cm^{-1})			
3280	3343	3349	the O–H stretching vibration	Infrared Spectroscopy Absorption Table
2936	2932	2927	the C–H stretching vibrations of the –CH$_2$–	
2881	2878	2879	the C–H stretching vibrations of the –CH$_3$	
1641	1632	1639	aromatic C=C bond and/or to the carbonyl group (C=O)	
1564	/	/	Characteristic band of uronic acid	Sun et al. (2000)
1398	1394	1398	O-H bending vibration of carboxylic group	Infrared Spectroscopy Absorption Table
1324	1321	1324	O-H bending vibration of phenol structure	
	/	1258	P=O symmetric vibration	Huang et al. (2014)
1065 (a)	/	1065(c)	(a) mannose-containing hemicelluloses	Liu et al., (2021)
			(c) C–O–P symmetrical vibration	Huang et al. (2014) Kilic et al., (2010)
1021	1028	1022	the C–O stretching vibrations	Huang et al. (2014)
/	644	645	aromatic structures	Huang et al. (2014) Kilic et al., (2010)
552	559	558	aromatic structures	

Based on the results of the FTIR analysis it can be concluded that activated carbons derived from water hyacinth biowaste by the process of chemical activation followed by carbonization, had different organic functional groups present on the surface. Also, the presence of aromatic structures confirmed the converting of lignocellulose structure into graphene-like carbon material (Asif and Saha, 2023).

The presence of different functional groups at the activated carbons surface and their interaction with organic pollutants usually presents a crucial factor during adsorption process. Aromatic structures on the adsorbents surface are involved in hydrophobic and π-π interaction, while carboxylic and hydroxylic groups can participate in the hydrogen-bonding and electrostatic interaction with organic adsorbate molecules (Teo et al., 2022).

5.1.6. Point of zero charge

The surface charge is adsorbent characteristic with strong impact on the adsorption process. The point of the zero charges for the selected adsorbents 2.0ZC500 and 1.5PC600 is given in Figs. 19a and 19b, respectively.
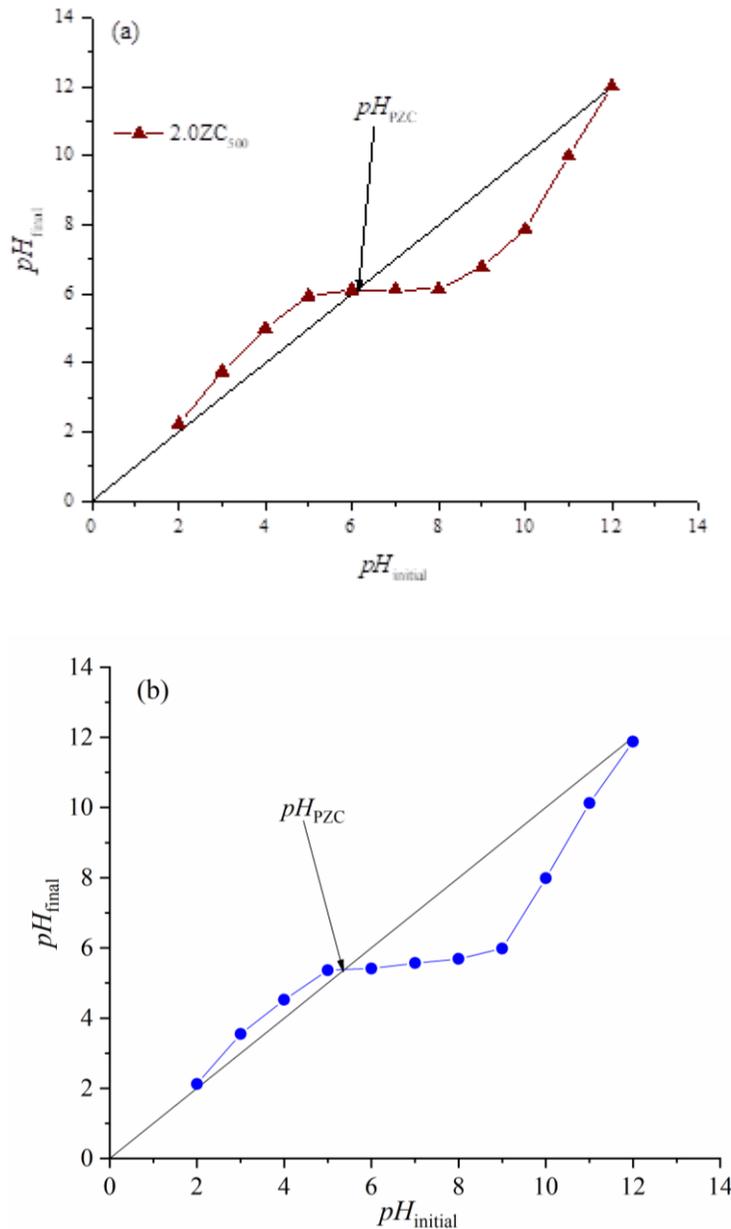
Figure 19. The point of the zero charges for activated carbons: a) 2.0ZC$_{500}$; and b) 1.5PC$_{600}$ (Mohammed et al., 2022).

The point of zero charge was determined to be at pH = 6.17 and pH = 5.35 for the samples 2.0ZC500 and 1.5PC600, respectively. The surface of these activated carbons below these values is positively charged and negatively charged above the pH$_{PZC}$ values. This fact has strong impact on the adsorption of pollutants at different pH values of the starting solution. Therefore, more appropriate

discussion will be given in the subchapter 5.2.3., where the pH of the adsorbate solution will be correlated with the pH$_{PZC}$ of adsorbents.

5.2. Adsorption study

In this chapter the adsorption properties of 2.0ZC$_{500}$ and 1.5PC$_{600}$ were tested toward two harmful pollutants, selected from pesticide and pharmaceutic class of compounds, namely glyphosate and metformin. In a complete and comprehensive adsorption study the following parameters of the adsorption system will be evaluated:

A. Effect of the adsorbent concentration.

B. Effect of the adsorbate concentration

C. Effect of the adsorption time

D. Effect of the pH on adsorption process

E. Effect of the temperature on adsorption process.

Based on the experimental results of the adsorption study performed from A to D section, the appropriate adsorption, kinetics, intra-particle diffusion and thermodynamic models will be applied to explain the phenomenon of interaction between tested adsorbates (metformin and glyphosate) and the surface of the obtained adsorbents. The adsorption behaviour of the selected adsorbents will be discussed and correlated by the textural characteristics and other relevant adsorbents characteristics (presence of the specific surface functional groups, surface charge, etc.).

5.2.1. Effect of the adsorbent mass on GP and MT removal

The effect of the adsorbent concentration (mg L^{-1}) on the amount of the adsorbed MT on 2.0ZC$_{500}$ and 1.5PC$_{600}$ activated carbons are presented in Fig. 20.
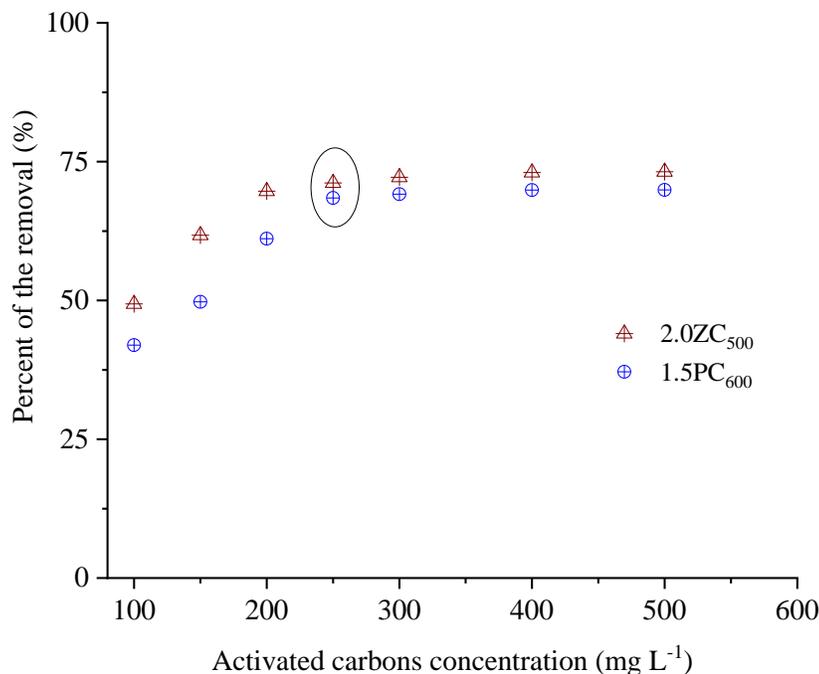
Fig. 20. The influence of the adsorbent mass on the percentage of metformin removal

($C_{MT} = 20$ mg L^{-1}; $T = 25$ ºC; $t = 120$ min; pH without adjusting - 6.8).

The results show that the percentage of MT removal increased from 41.9% to 61.0% when as adsorbent was used 1.5PC$_{600}$, and from 49.4% to 73.2% for adsorption in range of the adsorbents concentration from 100 mg L^{-1} to 250 mg L^{-1}. The concentrations of both activated carbons higher than 250 mg L^{-1} did not significantly affect the removal of metformin. Therefore, a concentration of adsorbent of 250 mg L^{-1} was chosen for further adsorption experiments for metformin adsorption.

The effect of the adsorbent concentration (mg L^{-1}) on the amount of the adsorbed glyphosate on 2.0ZC$_{500}$ and 1.5PC$_{600}$ are presented in Figure 21.
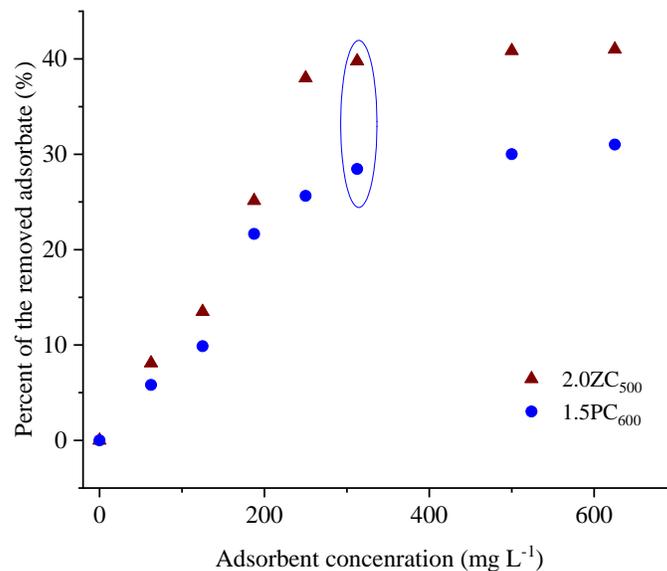
Figure 21. The influence of the adsorbent mass on the percentage of glyphosate removal
(C_{GP} = 100 mg L^{-1}; T = 25 ⁰C; t = 120 min, pH without adjusting – 3.9).

Under the defined experimental conditions of the adsorption tests, the percent of the removed glyphosate has been significantly lower comparing to the percent of the metformin removal on the same adsorbents. The glyphosate removal achieved 30 % and 41% for adsorption onto 2.0ZC$_{500}$ and 1.5PC$_{600}$, respectively for the activated carbons concentration of 250 mg L^{-1}.

Based on the literature interpretations in similar adsorption systems, the increasing concentration of the adsorbents is not beneficial to the percent of the removed pollutant. Namely, the higher concentrations of adsorbent can lead to the aggregation of the adsorbent particles, decreasing the available surface area and, consequently, decreasing the removal of the adsorbate (Semerjian, 2010). Therefore, for the following adsorptions 250 mg L^{-1} was selected as the optimal concentration for both activated carbons.

5.2.2. Effect of the initial adsorbate concentration and contact time on the amount of the removed pollutant

The influence of the initial adsorbate concentration on the amount of the adsorbed metformin (q_t) from the beginning of the adsorption up to 360 min is presented in Figs. 22a and 22b for adsorbents 2.0ZC$_{500}$ and 1.5PC$_{600}$, respectively.
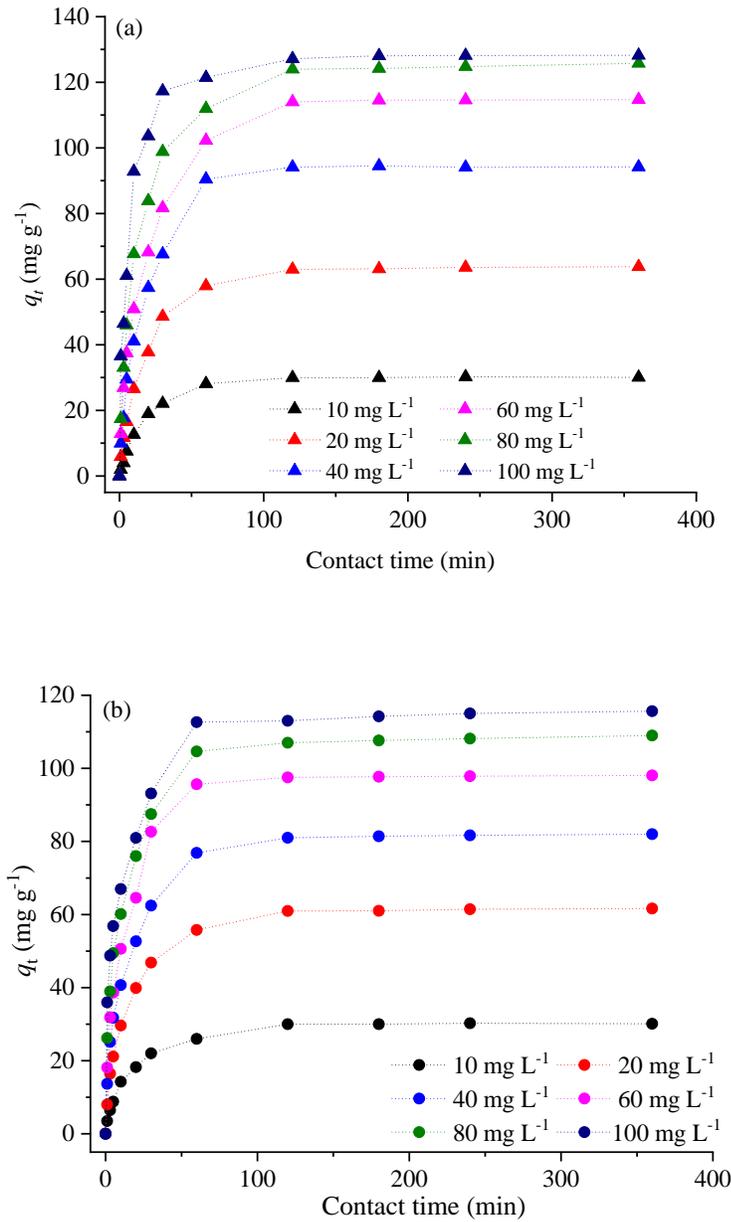
Figure 22. The influence of the initial metformin concentration on the amount of the adsorbed pollutant over time t on a) 2.0ZC$_{500}$, and b) 1.5PC$_{600}$ (Mohammed et al., 2022). (C_{ads}= 250 mg L^{-1}; T = 25 ºC, pH without adjusting 6.8).

The results presented in Figs. 22a and 22b show that for all investigated initial metformin concentrations the q_t approached a plateau after 120 min. Due to this result, 120 min was taken as the equilibrium adsorption time.

Generally, the adsorbent 2.0ZC$_{500}$ show slightly better adsorption properties toward metformin than 1.5PC$_{600}$. For the higher metformin concentration (80 mg L^{-1} and 100 mg L^{-1}) the q_t is higher for approx. 10% when adsorption was performed on 2.0ZC$_{500}$. On the other hand, the lower initial concentration of metformin of 10 mg L^{-1} and 20 mg L^{-1} led to the remarkably similar q_t values of roughly 30 mg g^{-1} and 60 mg g^{-1} regardless of the used adsorbent. Although the activated carbon 1.5PC$_{600}$ has higher value of S_{BET}, it seems that other textural parameters, such as mesopore volume can be more crucial factor for the adsorption process.

For the initial concentrations of metformin higher than 40 mg L^{-1}, more than 50% of metformin was adsorbed within the first 15 min, while for the lower concentrations of adsorbate (10 mg L^{-1} and 20 mg L^{-1}), half of the totally adsorbed metformin was removed in 20 min. The drastic increase in adsorption for such short times may be due to the availability of vacant adsorption sites on the adsorbate surface. With increasing contact time, adsorption sites become occupied, and adsorption equilibrium is reached. After an equilibrium time of 120 min, there is no significant increase in the amount of adsorbed metformin no matter which activated carbon was used.

The influence of the initial adsorbate concentration on the amount of the adsorbed glyphosate for different contact times is presented in Figs. 23a and 23b for adsorbents 2.0ZC$_{500}$ and 1.5PC$_{600}$, respectively.
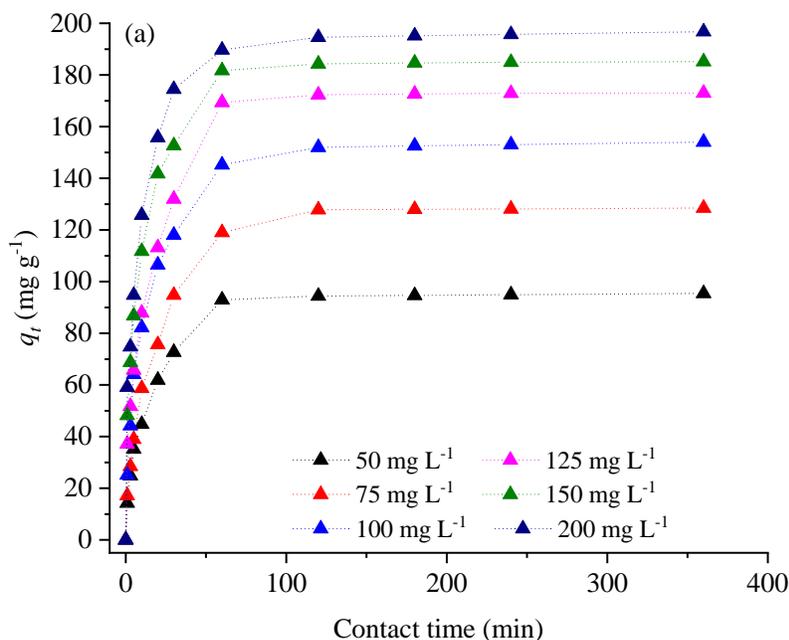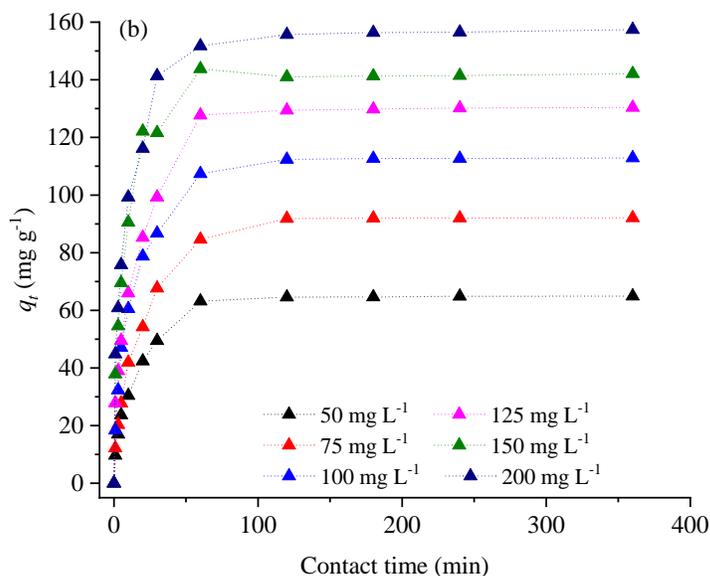
Figure 23. The influence of the initial glyphosate concentration on the amount of the adsorbed pollutant over time t on a) $2.0ZC_{500}$ (Mohammed and Kijevčanin, 2022), and b) $1.5PC_{600}$. ($C_{ads}= 250$ mg L^{-1}; $T = 25$ ℃, pH without adjusting 3.9).

The activated carbon $2.0ZC_{500}$ shown better adsorption affinity toward glyphosate then $1.5PC_{600}$. The value q_t was higher for 32%, 28%, 26%, 25% 23% and 20% for initial concentration of 50 mg L^{-1}, 75 mg L^{-1}, 100 mg L^{-1}, 125 mg L^{-1}, 150 mg L^{-1}, and 200 mg L^{-1}, respectively when the $2.0ZC_{500}$ was used as an adsorbent. Based on this result, it can be assumed that surface characteristics of activated carbon obtained in the presence of $ZnCl_2$ are more suitable for interaction with glyphosate than surface of activated carbon obtained in the presence of H_3PO_4 as activator.

The adsorption of glyphosate occurred relatively fast on both tested adsorbents since the half amount of pollutant has been removed within the first 10-20 minutes. After 120 minutes the amount of the adsorbed glyphosate seems to be constant, with minor increase up to 360 minutes. Therefore, the equilibrium time for glyphosate adsorption was estimated on 120 minutes, and it is the same as in the process of the metformin adsorption.

5.2.3. Effect of the pH of adsorbate solution

The pH of the adsorbate solution is known to be an essential parameter that affects adsorption behaviour. The pH of the adsorbate solution affects the adsorbent surface charge and surface ionization of the adsorbate material (Yu et al., 2016).

The effect of the initial pH of the metformin solution on the percentage removal of metformin was studied by varying the initial pH under constant process parameters on both adsorbents. The results of the metformin adsorption under a range of the pH of initial solutions from 2–12 are shown in Figs. 24a and 24b, for 2.0ZC500 and 1.5PC600, respectively.
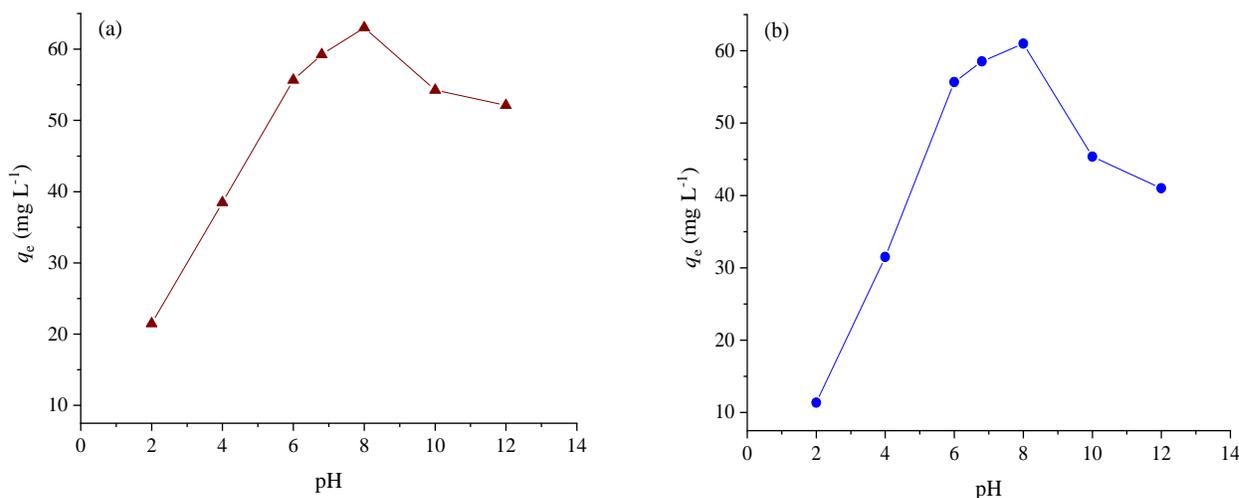
Figure 24. The effect of the initial pH of metformin solution for a) $2.0ZC_{500}$, and b) $1.5PC_{600}$ (Mohammed et al., 2022). ($C_{MT} = 20$ mg L^{-1}; $C_{ads.} = 250$ mg L^{-1}; $T = 25$ ℃; $t = 120$ min).

From Fig. 24 it was observed that the uptake of metformin increased when the pH value changed from 2.0 to 8.0 and then decreased when the pH increased from 8.0 to 12.0. These phenomena can be attributed to the surface charge of $2.0ZC_{500}$ and $1.5PC_{600}$ and the speciation of metformin at the different pH values. The point of zero charge (Figure 19) was determined to be at pH 6.17 and pH 5.35 for $2.0ZC_{500}$ and $1.5PC_{600}$, respectively. The surface of activated carbons below these values is positively charged and negatively charged above the pH$_{PZC}$ value.

At a pH below a pK$_{a1}$ of 2.8, metformin is mainly present in solution as a bi-protonated species, and, at the same time, the surface of the activated carbons is positively charged. Therefore, repulsive interactions between adsorbent and adsorbate occurred, and the lowest amounts of adsorbed metformin of 21.47 mg g^{-1} and 11.36 mg g^{-1} for $2.0ZC_{500}$ and $1.5PC_{600}$, respectively were observed at pH = 2.0. Further, at $4.0 < pH < 10.0$, metformin is mainly present in a monoprotonated form, while the surface of the adsorbent starts to be negatively charged above 5.35 and 6.17 for $2.0ZC_{500}$ and $1.5PC_{600}$, respectively. Hence, the significant increase in adsorbed metformin can be noticed above the pH$_{PZC}$ with a maximum of adsorbed metformin at pH = 8.0. This adsorption behaviour has been caused by the attractive forces between the adsorbents surface and metformin. Finally, at pH values above the pKa$_2$ of 11.6, metformin is present in a molecular form, and adsorption only through the pore diffusion mechanism can be present

54

(Spessato et al., 2021). This adsorption behaviour is more pronounced for adsorption on $2.0ZC_{500}$, probably due to its higher mesopore volume.

It is important to point out that the native pH of the metformin hydrochloride solution was 6.8. At this pH value, the percentage of removed metformin were 59.24 mg g^{-1} and 58.51 mg g^{-1}, for $2.0ZC_{500}$ and $1.5PC_{600,}$ respectively, which is more than 94% of the amount of adsorbed metformin at the optimum pH.

The effect of the initial pH value of the glyphosate solution has been also studied on the adsorption process, in the range of pH solutions from 2–12, and results are shown in Figs. 25a and 25b, for $2.0ZC_{500}$ and $1.5PC_{600}$, respectively.
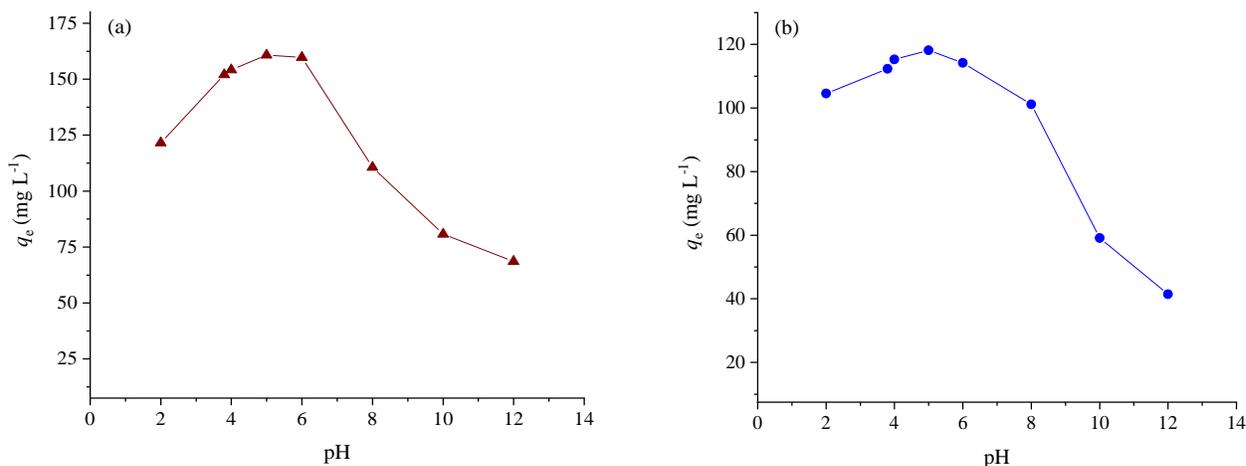
Figure 25. The effect of the initial pH of glyphosate solution for a) $2.0ZC_{500}$, and b) $1.5PC_{600}$
($C_{GP} = 100$ mg L^{-1}; $C_{ads.} = 250$ mg L^{-1}; $T = 25\ ^0C$; $t = 120$ min).

Like in the case of the most adsorption systems, the maximal uptake of adsorbate strongly depended on the surface charge of adsorbent and charge distribution of the adsorbate molecules. Glyphosate is molecule with three functional groups, where carboxylic and phosphoric represents two acidic groups, and secondary aliphatic amine as a base group. Therefore, glyphosate has four pK_A values, at pH of solution at 0.8, 2.23, 5.46 and 10.14 (Benetoli et al., 2010). At pH below the 0.8 the glyphosate is monoprotonated form with protonation on the secondary amine group. Above pH of 0.8 the dissociation of phosphoric group is occurred and until the pH of 2.23 glyphosate is present as neutral zwitter ion in the solution, where phosphoric group is deprotonated, and secondary amine group is protonated. When the pH of solution is above 2.23 the dissociation of the carboxylic acid happens, and the glyphosate form anionic specie. At pH of 5.46 the second deprotonation of phosphoric group starts, and finally, the deprotonation of amine group is above pH of 10.14 (Benetoli et al., 2010).

The results presented in Figs. 25a and 25b revealed that glyphosate adsorption strongly depended on pH of the solution. Under an acidic environment, at pH value 2, where glyphosate is in the form of zwitter ion, there is significant adsorption, probably due to the interaction of the deprotonated phosphoric group with the positively charged surface of the adsorbents. The maximum of the adsorption is achieved in the pH range from 3.8 to 5 where glyphosate exists in form of anion and surface of the adsorbents is

still positively charged; therefore, electrostatic interaction reached the maximum. With increase of pH value both, glyphosate and adsorbents are both in negatively charged form and adsorption portion guided by the electrostatic interaction decreases. In the alkaline condition, the adsorption still occurs, probably due to the pore diffusion process, which is more pronounced for $2.0ZC_{500}$ with more developed mesopore area. The glyphosate removal from unbuffered pH of glyphosate solution (which is nearly 4), for both tested adsorbents, is remarkably close to the optimal value. This finding favours the application of tested adsorbents in real systems since the adsorption process does not require the addition of extra acid or base to achieve an amount of adsorbed glyphosate almost equal to that obtained for optimal adsorption conditions.

5.2.4. Adsorption isotherm models

To elucidate adsorption data obtained for metformin and glyphosate removal on activated carbons $2.0ZC_{500}$ and $1.5PC_{600}$, the adsorption results were fitted with the most used isotherm models: Langmuir, Freundlich and Redlich-Peterson.

5.2.4.1. Adsorption isotherms for metformin removal

The non-linear fits of experimental data for metformin removal by $2.0ZC_{500}$ and $1.5PC_{600}$ with three different adsorption isotherm models, Langmuir, Freundlich, and Redlich–Peterson at 25 ⁰C are presented in Figs. 26a and 26b, while the calculated isotherms parameters are given in Table 7.
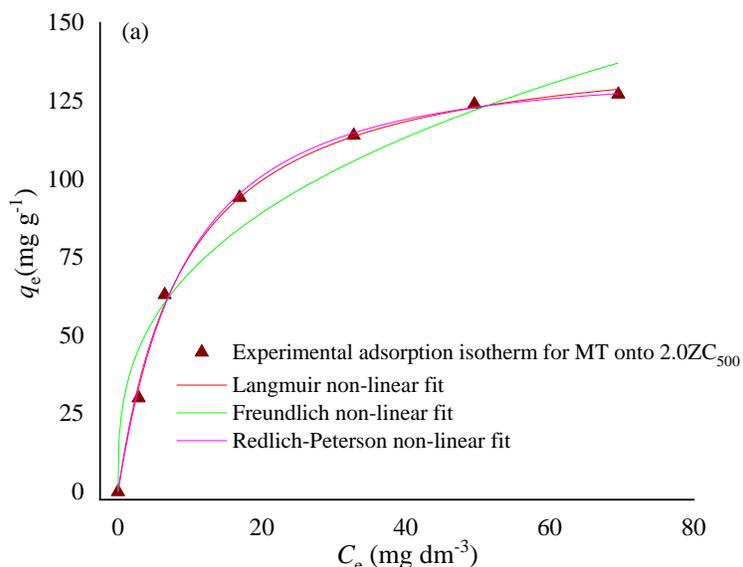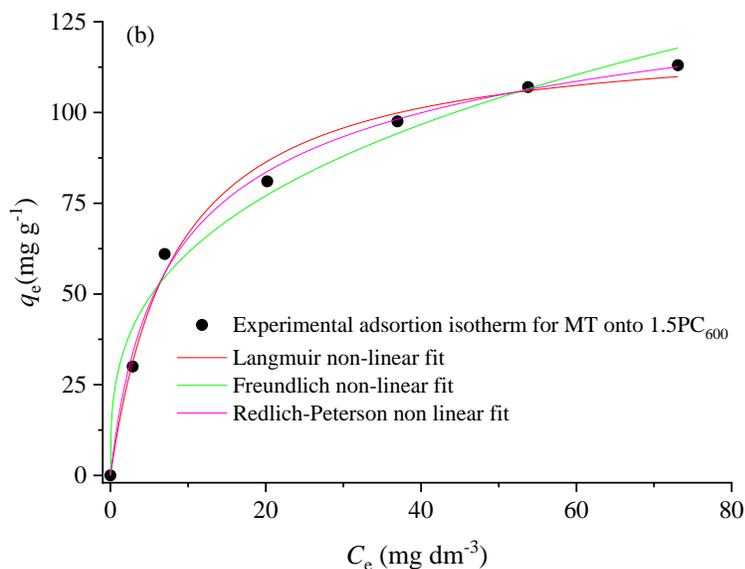
Figure 26. Adsorption isotherm of metformin onto a) $2.0ZC_{500}$, and b)$1.5PC_{600}$ (Mohammed et al., 2022). (C_{MT} = 10 mg L^{-1} – 100 mg L^{-1}; $C_{ads.}$ = 250 mg L^{-1}, T = 25 ℃, t_{eq} = 120 min, pH without adjusting 6.8).

Table 7. Calculated isotherm parameters for applied isotherm models for MT adsorption onto $2.0ZC_{500}$ and $1.5PC_{600}$.(Mohammad et al., 2022, Mahammad and Kijevčanin, 2022).

Isotherm model	Adsorption models parameters for MT adsorption			
Langmuir	K_L (L mg^{-1})	R_L	q_{max} (mg g^{-1})	R^2
$2.0ZC_{500}$	0.1073	0.483	146.05	0.998
$1.5PC_{600}$	0.1194	0.457	122.47	0.997
Freundlich	K_F (mg g^{-1}) (L mg^{-1})$^{1/n}$		n_F	R^2
$2.0ZC_{500}$	31.717		2.90	0.964
$1.5PC_{600}$	28.871		3.05	0.977
Redlich–Peterson	K_R (L g^{-1})	A (L mg^{-1})^n	n_R (g mg^{-1})	R^2
$2.0ZC_{500}$	14.31	0.078	1.053	0.997
$1.5PC_{600}$	19.163	0.246	0.894	0.995

K_L—Langmuir constant; R_L—Langmuir factor related with favorable adsorption; q_{max}—adsorption capacity, R^2—coefficient of determination; K_F—Freundlich constant; n_F—Freundlich factor related to heterogeneity of adsorption; K_R—Redlich–Peterson isotherm constants, A—Redlich–Peterson parameter; n_R—the exponent, which lies between 1 and 0.

Based on the values of the coefficient of determination (R^2) given in Table 7, the metformin adsorption could be best described by the Langmuir isotherm, followed by the Redlich–Peterson model, while the Freundlich model seems to be less suitable.

Langmuir's adsorption model can describe the metformin adsorption process as mainly homogeneous at energetically equal adsorption sites, where adsorbate molecules form the monolayer at the adsorbent surface. For a Langmuir-type adsorption process, the isotherm shape can be classified by a dimensionless constant separation factor R_L. The value of R_L indicates the shape of the isotherms to be either unfavourable ($R_L > 1$), linear ($R_L = 1$), favourable ($0 < R_L < 1$), or irreversible ($R_L = 0$).

For the investigated adsorption process of metformin on $2.0ZC_{500}$ and $1.5PC_{600}$, the calculated R_L have the value of 0.483 and 0.457, respectively (Table 7); therefore, these values are in the range between 0 and 1, and the adsorption of metformin on investigated activated carbons follow the same path, and can be regarded as a favourable process. Further, the Langmuir model predicts an adsorption maximum for each adsorption process. The values of the adsorption maximum (q_{max}) were 146.05 mg g^{-1} and 122.47 mg g^{-1}, for $2.0ZC_{500}$ and $1.5PC_{600}$, respectively. The obtained q_{max} values classify the investigated activated carbons as very efficient.

The literature review of q_{max} values for metformin adsorptions on different activated carbons derived from various types of biomasses, along with other adsorbents, is presented in Table 8.

Table 8. Comparison of metformin adsorption capacity of different adsorbents (Mohammed et al., 2022).

Adsorbent	Adsorption Parameters	q_{max} (mg g^{-1})	References
$2.0ZC_{500}$	$T = 25$ ºC, $C_{MT} = 10$–100 mg L^{-1}	146.05	Current Thesis
$1.5PC_{600}$	$S_{BET} = 1421$ m^2 g^{-1}; $T = 25$ ºC, $C_{MT} = 10$–100 mg L^{-1}	122.47	Mohammad et al., (2022)
Multi-walled carbon nanotubes, commercial	$S_{BET} = 250$–280 m^2 g^{-1}; $T = 295$ K, $C_{MT} = 10$–88 mg L^{-1}	79.94	Lofti et al. (2015)
Granular activated carbon	$S_{BET} = 1500$ m^2 g^{-1}; $T = 295$ K; $C_{MT} = 10$–88 mg L^{-1}	72.56	Lofti et al. (2015)
Graphene oxide	pH = 6; $C_{MT} = 8 - 40$ mg L^{-1}, contact time 160 min; $T = 288, 303$ and 318 K.	96.748 89.099 88.517	Zhu et al. (2017)
Activated carbon from agricultural waste	$T = 20$ ºC, $C_{MT} = 10$–200 mg L^{-1} pH = 7, contact time 125 min.	44.84	Kalumpha et al. (2020)
Sibipiruna activated carbon	$C_{MT} = 500$ mg L^{-1}, $T = 30$ ºC, pH = 13, contact time 360 min.	248.48	Spessato et al. (2021)
Water-treated clay Acid-treated clay	$S_{BET} = 9.5$ –11.5 m^2 g^{-1}; pH = 6, $C_{MT} = 1$–20 mg L^{-1} $T = 298$ K; contact time 30 min.	25.268 33.788	Elamin et al. (2021)
Fe-ZSM-5 nano-adsorbent	$T = 25$ ºC, $C_{MT} = 5$–20 mg L^{-1}, contact time 20 min.	14.992	Niaei and Rostamizadeh (2020)
Activated carbon from orange peel	$T = 323$ K, pH = 7; contact time 240 min.	50.99	Oluwatimileyin et al. (2020)
Hydrogen peroxide modified biochar	$T = 308.15$ K, $C_{MT} = 0.05$–3.6 mmol L^{-1}, contact time 24 h.	107.33	Huang et al. (2016)

Although some adsorbents presented in the literature (Spessato et al, 2021), like Sibipiruna activated carbon shown extraordinary adsorption capacity toward metformin of 248.48 mg g^{-1}, activated carbons investigated in this study have also exceptional values of q_{max}, which is higher than the majority of the q_{max} values obtained in the survey. Therefore, the activated carbons obtained in the present study can be considered for testing in real systems.

The Redlich–Peterson model has also shown particularly good agreement with the adsorption data, with a coefficient of correlation of 0.995. The Redlich–Peterson isotherm describes the adsorption equilibrium over a wide concentration range and can be applied in either homogeneous or heterogeneous systems due to its versatility. The good agreement of experimental results with the Redlich–Peterson adsorption isotherm was also found for dyes' adsorption on mesoporous activated carbon prepared from pistachio shells with NaOH activation (Wu et al., 2010).

The Freundlich isotherm fit, although with R^2 values higher than 0.96, seems to be the least suitable adsorption isotherm model to describe the metformin adsorption in investigated adsorption systems.

5.2.4.2. Adsorption isotherms for glyphosate removal

The isotherms for adsorption of glyphosate on 2.0AC$_{500}$ and 1.5PC$_{600}$ were studied, and results are corelated with Langmuir, Freundlich and Redlich-Peterson non-linear fit, and presented in Fig. 27 (a, and b).
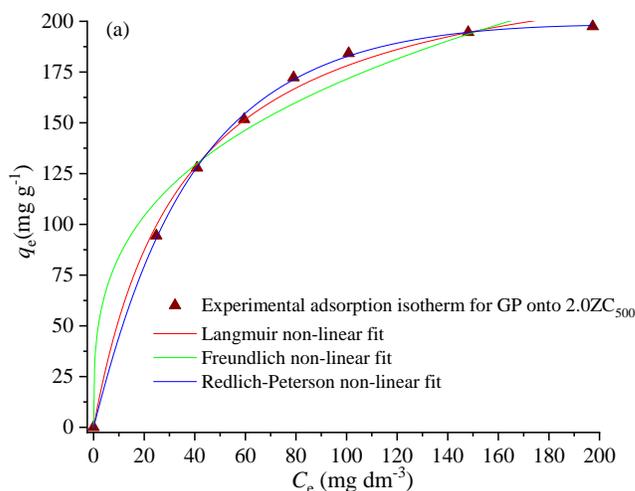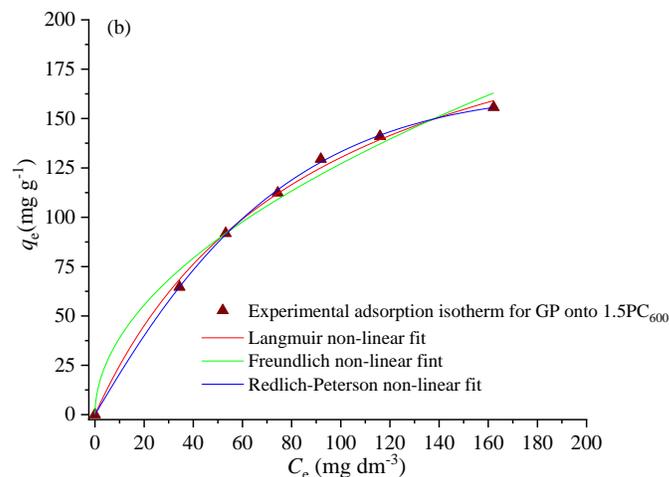
Figure 27. Adsorption isotherm of glyphosate onto a) 2.0ZC$_{500}$ (Mohammed and Kijevčanin, 2022) and b)1.5PC$_{600}$ (C_{GP} = 50 mg L^{-1} – 200 mg L^{-1}; $C_{ads.}$ = 250 mg L^{-1}, T = 25 ºC, t_{eq} = 120 min, pH without adjusting 3.9).

The calculated parameters for glyphosate adsorption on investigated activated carbons obtained based on non-linear fits of isotherms are presented in Table 9.

Table 9. Calculated isotherm parameters for applied isotherm models for GP adsorption onto 2.0ZC$_{500}$ and 1.5PC$_{600}$ (Mohammed and Kijevčanin, 2022; Mohammed et al, 2022).

Isotherm model	Adsorption models parameters for GP adsorption			
Langmuir	K_L (L mg^{-1})	R_L	q_{max} (mg g^{-1})	R^2
2.0ZC$_{500}$	0.0284	0.413	240.80	0.997
1.5PC$_{600}$	0.0111	0.947	246.91	1
Freundlich	K_F (mg g^{-1}) (L mg^{-1})$^{1/n}$		n_F	R^2
2.0ZC$_{500}$	41.15		3.23	0.965
1.5PC$_{600}$	11.87		1.94	0.990
Redlich–Peterson	K_R (L g^{-1})	A (L mg^{-1})^n	n_R (g mg^{-1})	R^2
2.0ZC$_{500}$	4.88	5.75·10^{-3}	1.23	0.999
1.5PC$_{600}$	2.10	6.10·10^{-4}	1.49	0.999

K_L—Langmuir constant; R_L—Langmuir factor related with favorable adsorption; q_{max}—adsorption capacity, R^2—coefficient of determination; K_F—Freundlich constant; n_F—Freundlich factor related to heterogeneity of adsorption; K_R—Redlich–Peterson isotherm constants, A—Redlich–Peterson parameter; n_R—the exponent, which lies between 1 and 0.

Generally, all investigated models could be applied to describe the investigation adsorption process ($R^2 > 0.960$). Based on the R^2 values, the Langmuir model seems to be the most suitable to describe glyphosate adsorption on $1.5PC_{600}$, while with slightly higher R^2 value of 0.999, Redlich-Peterson model can be applied on the adsorption glyphosate on $2.0ZC_{500}$.

The agreement of glyphosate adsorption on $1.5PC_{600}$ with Langmuir model indicated that surface of investigated adsorbent is energetically homogenous, and the binding sites are uniformly distributed with the same affinity. The adsorption process occurs until monolayer surface coverage and after saturation there is no additional interaction between adsorbate molecules. The monolayer adsorption capacity (q_{max}) according to the Langmuir model was 246.91 mg g^{-1}, and this predicted value is significantly higher than those presented in subchapter 4.2.2. where the highest q value of 155.67 mg g^{-1} has been obtained for glyphosate initial solution of 200 mg L^{-1}. Since the R^2 value for non-linear fit for glyphosate adsorption on $2.0ZC_{500}$ has value of 0.997, the Langmuir model should be discussed. Based on this model, the q_{max} value of 240.80 mg g^{-1} was obtained for glyphosate removal by $2.0ZC_{500}$. The values of R_L for glyphosate adsorption on both activated carbons lie in the range of $0 < R_L < 1$, where adsorption process is favourable, although the R_L value for $1.5PC_{600}$ is approaching to the linear adsorption.

The literature review of q_{max} values for glyphosate adsorption on different adsorbents including activated carbons derived from various types of biomasses, is presented in Table 10.

Table 10. Comparison of glyphosate adsorption capacity of different adsorbents (Mohammad and Kijevčanin, 2022).

Adsorbent	q_{max} (mg g^{-1})	References
$2.0ZC_{500}$	240.8	Mohammad and Kijevčanin (2022)
$1.5PC_{600}$	246.91	Current Thesis
Rice husk char	123.03	Herath et al. (2015)
Forest soil	161.29	Sen et al. (2017)
MnFe$_2$O$_4$–graphene composite	204.2	Yamaguchi et al. (2016)
Zr-MOF	256.54	Yang et al. (2018)
Resin D301	833.33	Chen et al. (2016)

According to the author best knowledge and acquisition of the literature data, it seems that present study of glyphosate adsorption brings the most efficient adsorbent in the class of the activated carbons derived from biomass. However, there are more powerful adsorbents toward glyphosate removal, such as Zr-MOF (Yang et al. 2018), and some extraordinary adsorbent such as Resin D301 (Chen et al. 2016).

5.2.5. Adsorption kinetics

The kinetic models were applied to the experimental adsorption results for metformin and glyphosate adsorption on selected adsorbents ($2.0ZC_{500}$ and $1.5PC_{600}$), to investigate the mechanism of the adsorption and potential rate-controlling steps, including the mass transport and chemical reaction processes.

5.2.5.1. Adsorption kinetics of metformin removal

The linear plots of the pseudo-first-order kinetic model, pseudo-second-order kinetic model, as well as Weber–Morris intraparticle diffusion model are given in Figs. 28 and 29 for metformin adsorption onto $2.0ZC_{500}$ and $1.5PC_{600}$, respectively, while the corresponding calculated kinetic parameters are presented in Tables 11 and 12.
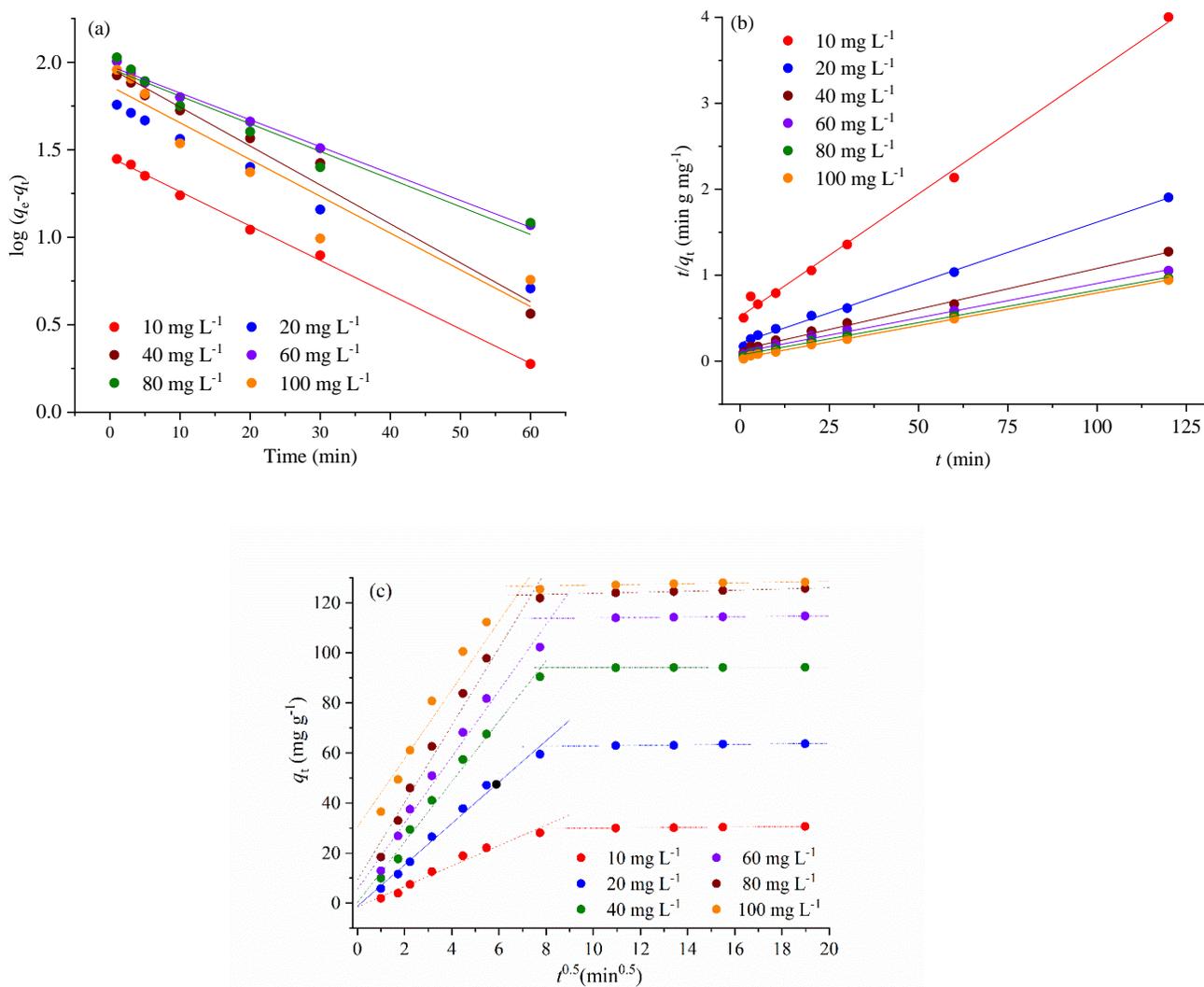
Figure 28. (a) Pseudo-first order kinetics model, (b) pseudo-second order kinetics model, and (c) Weber–Morris intra-particle diffusion model for adsorption of metformin on $2.0ZC_{500}$.

Table 11. The parameters calculated for pseudo-first order kinetic model, pseudo–second order kinetic model, and Weber–Morris intra-particle diffusion model for adsorption of MT on $2.0ZC_{500}$.

Model Parameters	C_0 (mg g^{-1})					
	10	20	40	60	80	100
q_e^{exp} (mg g^{-1})	29.98	63.01	94.13	114.01	124.02	127.16
Pseudo-first order kinetics model						
q_e (mg g^{-1})	28.64	56.62	92.53	95.13	92.26	73.18
k_1 10^{-3} (min^{-1})	8.51	7.77	9.64	6.69	6.86	9.12
R^2	0.998	0.994	0.981	0.995	0.963	0.901
Pseudo-second order kinetics model						
q_e (mg g^{-1})	34.97	70.92	105.26	125	128.58	131.58
$k_2 \cdot 10^{-4}$ (g mg^{-1} min)	15.8	9.41	6.85	6.24	8.11	14.4
R^2	0.996	0.997	0.996	0.996	0.999	0.999
Weber–Morris intra-particle diffusion model						
C_{id1}	0.145	0.214	0.311	5.60	9.26	30.362
k_{WM1} (mg g^{-1} min$^{-1/2}$)	4.08	8.27	12.0	13.21	15.45	13.699
R^2	0.988	0.984	0.987	0.977	0.975	0.931
k_{WM2} (mg g^{-1} min$^{-1/2}$)	0.081	0.102	0.121	0.1841	0.220	0.143
R^2	0.968	0.880	0.978	0.993	0.994	0.936

q_e^{exp}—experimentally obtained value of the amount of the adsorbed MT at equilibrium; q_e^{cal}-calculated value of the amount of the adsorbed MT, based on appropriate kinetic model; k_1-pseudo first order constant; k_2—pseudo-second order constant; R^2—coefficient of determination; k_{WM1}, k_{WM2}—Weber–Morris diffusion rate constants; C_{id}—intercepts of the linear plots, corresponding to initial adsorption .
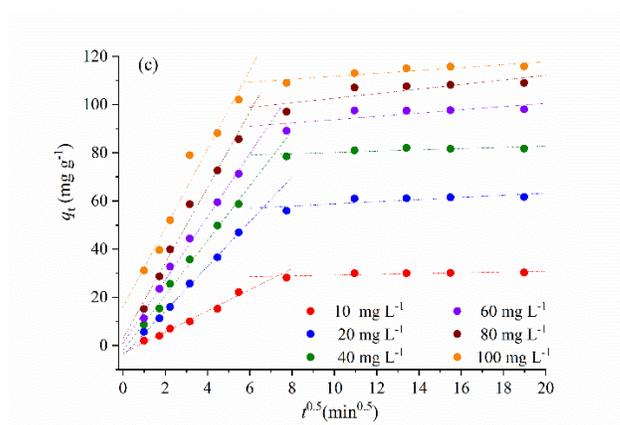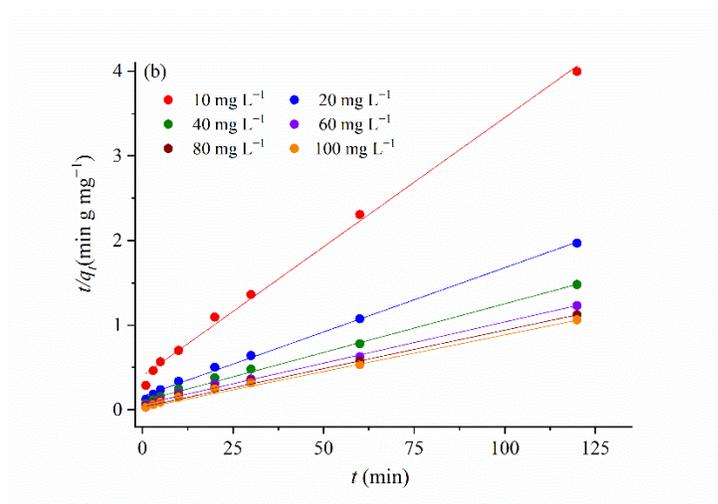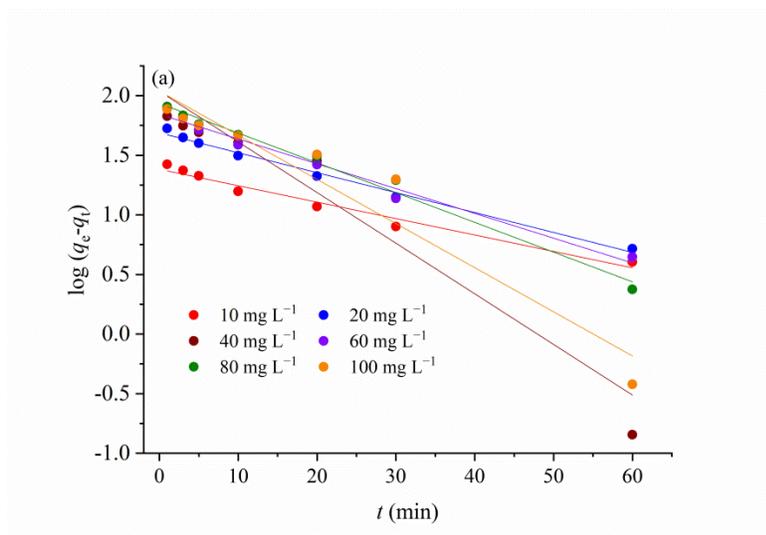
Figure 29. (a) Pseudo-first order kinetics model, (b) pseudo-second order kinetics model, and (c) Weber–Morris intra-particle diffusion model for adsorption of metformin on $1.5PC_{600}$ (Mohammed et al., 2022).

Table 12. The parameters calculated for pseudo-first order kinetic model, pseudo–second order kinetic model, and Weber–Morris intra-particle diffusion model for adsorption of MT on $1.5PC_{600}$.(Mohammed et al., 2022).

Model Parameters	C_0 (mg g^{-1})					
	10	20	40	60	80	100
q_e^{exp}(mg g^{-1})	30.01	60.99	81.02	97.52	107.00	113.01
Pseudo-first order kinetics model						
q_e (mg g^{-1})	24.11	48.76	59.34	69.77	86.22	109.19
k_1 10^{-3} (min^{-1})	5.99	7.25	8.42	9.03	10.9	16.4
R^2	0.972	0.991	0.899	0.983	0.987	0.929
Pseudo-second order kinetics model						
q_e (mg g^{-1})	32.79	65.79	86.96	104.17	111.11	119.05
$k_2 \cdot 10^{-3}$ (g mg^{-1} min)	2.34	1.44	1.24	1.18	1.35	1.45
R^2	0.996	0.998	0.996	0.996	0.997	0.996
Weber–Morris intra-particle diffusion model						
C_{id1}	1.40	3.37	9.26	11.172	11.57	11.68
k_{WM1} (mg g^{-1} min$^{-1/2}$)	3.46	7.69	9.23	11.64	20.56	29.536
R^2	0.962	0.987	0.980	0.974	0.976	0.988
k_{WM2} (mg g^{-1} min$^{-1/2}$)	0.031	0.086	0.119	0.069	0.247	0.327
R^2	0.985	0.969	0.980	0.994	0.999	0.946

q_e^{exp}—experimentally obtained value of the amount of the adsorbed MT at equilibrium; q_e^{cal}-calculated value of the amount of the adsorbed MT, based on appropriate kinetic model; k_1-pseudo first order constant; k_2—pseudo-second order constant; R^2—coefficient of determination; k_{WM1}, k_{WM2}—Weber–Morris intraparticle diffusion rate constants; C_{id}—intercept of the linear plot, corresponding to initial adsorption.

Based on the values of the kinetics parameters and correlation coefficient presented in Tables 11 and 12, the adsorption kinetics of metformin adsorption on $2.0ZC_{500}$ and $1.5PC_{600}$ are t best fitted by the pseudo-second order (PSO) kinetic model. The PSO kinetic model has usually been associated with the surface-reaction kinetic step, controlling the adsorption rate in solid/solution systems (Plazinski et al., 2009). There are accepted assumptions that the adsorption rate of the ion exchange reaction of the systems described by this model is responsible for the removal kinetics. According to the literature, the constant k_2 of the adsorption systems described by the PSO kinetic showed that it can be both dependent on and independent of the initial concentration of the adsorbate. The adsorption of metformin onto $2.0ZC_{500}$ and $1.5PC_{600}$ does not show the correlation between k_2 and the initial metformin concentration. This finding agrees with similar adsorption systems, where activated carbons were used as adsorbents (Kavitha et al., 2007; Rudzinski and Plazinski, 2008, Plazinski et al., 2009). Based on this, it can be assumed that regardless the differences in q_e values for metformin adsorption, both activated carbons tested in this study follow the same kinetics of the process.

Weber–Morris's equation has been used to describe intra-particle diffusion. Generally, if the regression of q_t versus $t^{1/2}$ is linear and passes through the origin, then intra-particle diffusion is the only rate-limiting step (Tan and Hameed, 2017). However, multi-linear curves are obtained for the adsorption of the metformin in the investigated concentration range onto $2.0ZC_{500}$ and $1.5PC_{600}$, (Figs. 28c and 29c). Each linear segment represents a controlling mechanism or several simultaneous controlling mechanisms during the adsorption process. The first sharper portion is attributed to the rapid adsorption on the external surface and the current interaction between metformin and the available sites on the adsorbent surface. The slopes of the first linear portion do not pass through the origin nether for adsorption on $2.0ZC_{500}$ nor $1.5PC_{600}$, indicating in both cases that intraparticle diffusion is not the rate-limiting step. Based on the values of C_{id} (Table 11 and Table 12), it can be concluded that the effective role of the boundary layer on the adsorption rate constant increased with an increase in the metformin concentration in the solution. This result agrees with the literature data, e.g., Raji and Pakizeh (2014) found that a higher bulk liquid concentration of the adsorbate led to an increase in both the rate constant and value of the boundary layer thickness (C_{id}) (Raji and Pakizeh, 2014).

The second portion describes the gradual layer adsorption stage, where intraparticle diffusion is rate limiting.

5.2.5.2. Adsorption kinetics of glyphosate removal

The kinetics of the glyphosate adsorption on the investigated adsorbents are also fitted with the pseudo-first and pseudo-second kinetic model, as well as with the Weber-Morris intraparticle diffusion model, and corresponding linear fits for glyphosate adsorption on $2.0ZC_{500}$ are presented in Fig. 30, while derived kinetics and intraparticle-diffusion parameters are presented in Table 13.
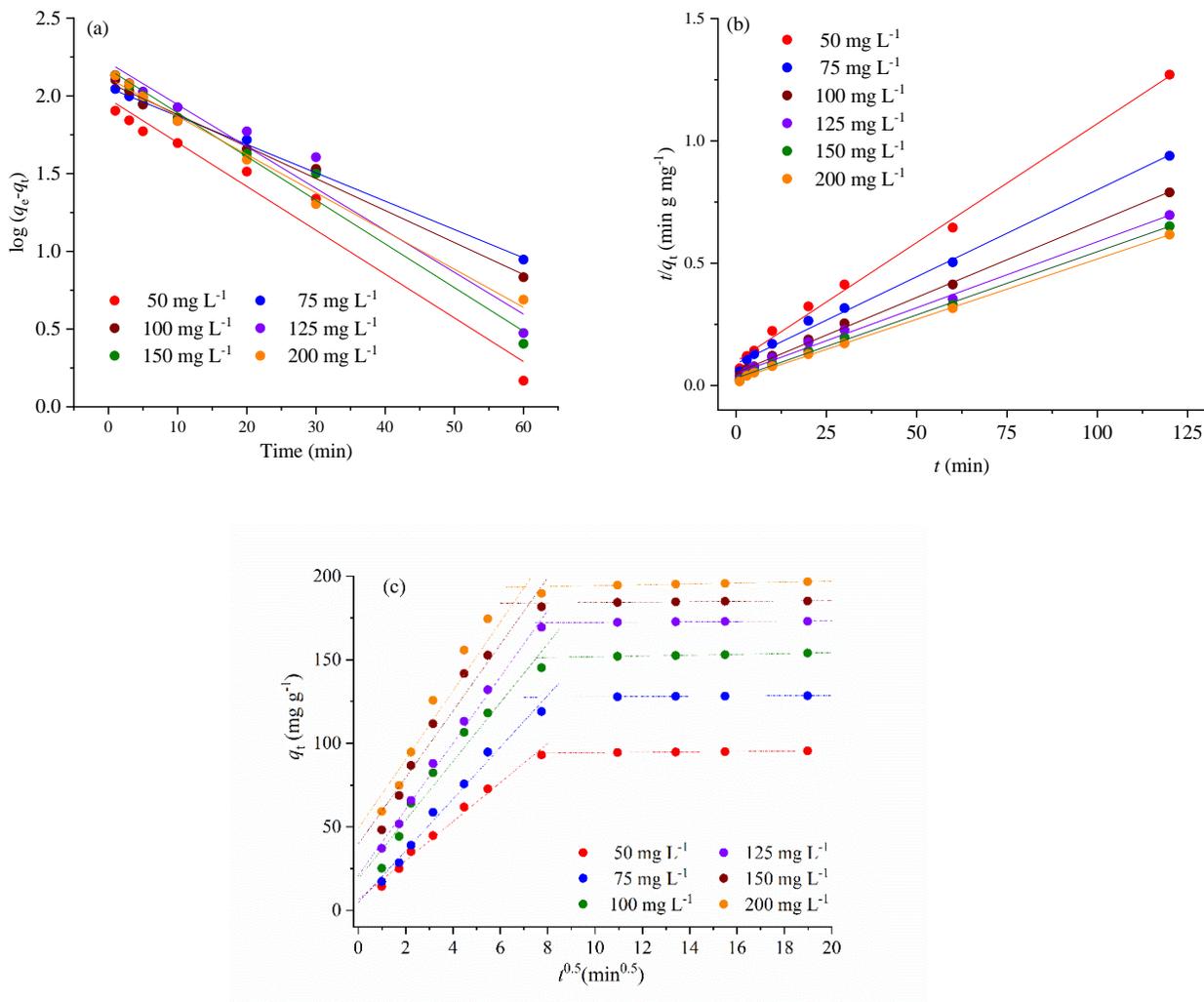
Figure 30. (a) Pseudo-first order kinetics model, (b) pseudo-second order kinetics model, and (c) Weber–Morris intra-particle diffusion model for adsorption of glyphosate on $2.0ZC_{500}$.

Table 13. The parameters calculated for pseudo-first order kinetic model, pseudo–second order kinetic model, and Weber–Morris intra-particle diffusion model for adsorption of glyphosate on 2.0ZC$_{600}$.

Model Parameters	C_0 (mg g^{-1})					
	50	75	100	125	150	200
q_e^{exp} (mg g^{-1})	94.43	127.84	151.99	172.31	184.24	194.59
Pseudo-first order kinetics model						
q_e (mg g^{-1})	95.74	112.82	121.81	163.53	148.49	130.13
k_1 10^{-3} (min^{-1})	12.2	1.9	8.9	11.7	12.2	10.7
R^2	0.966	0.997	0.992	0.963	0.982	0.990
Pseudo-second order kinetics model						
q_e (mg g^{-1})	98.03	133.33	156.3	178.57	188.68	196.08
$k_2 \cdot 10^{-3}$ (g mg^{-1} min)	1.22	7.40	11.0	7.67	10.68	11.8
R^2	0.999	0.999	0.994	0.999	0.998	0.999
Weber–Morris intra-particle diffusion model						
C_{id1}	6.43	4.69	18.79	20.73	39.54	48.95
k_{WM1} (mg g^{-1} min$^{-1/2}$)	11.67	15.48	17.58	19.82	19.93	20.58
R^2	0.9875	0.987	0.960	0.993	0.958	0.930
k_{WM2} (mg g^{-1} min$^{-1/2}$)	0.121	0.077	0.251	0.085	0.105	0.269
R^2	0.993	0.982	0.995	0.912	0.934	0.994

q_e^{exp}—experimentally obtained value of the amount of the adsorbed MT at equilibrium; q_e^{cal}-calculated value of the amount of the adsorbed MT, based on appropriate kinetic model; k_1-pseudo first order constant; k_2—pseudo-second order constant; R^2—coefficient of determination; k_{WM1}, k_{WM2}—Weber–Morris intraparticle diffusion rate constants; C_{id}—intercept of the linear plot, corresponding to initial adsorption.

The values of R^2 obtained for the applied kinetics models presented in Table 13 indicate that adsorption kinetics of glyphosate adsorption on 2.0ZC$_{500}$ follow the pseudo-second order kinetic model, with independent values of k_2 of the initial adsorbate concentration. Two linear stages have been obtained for Weber–Morris 'diffusion model, indicated two controlling mechanisms of the adsorption process. The slopes of the first linear fit do not pass through the origin, and therefore, the intraparticle diffusion cannot be the rate-limiting step. The C_{id} values suggest (Table 13) the that the role of the boundary layer is effective.

The kinetic modelling results for glyphosate removal on 1.5PC600 is presented in Fig. 31 (a-c), with derived parameters in Table 14.
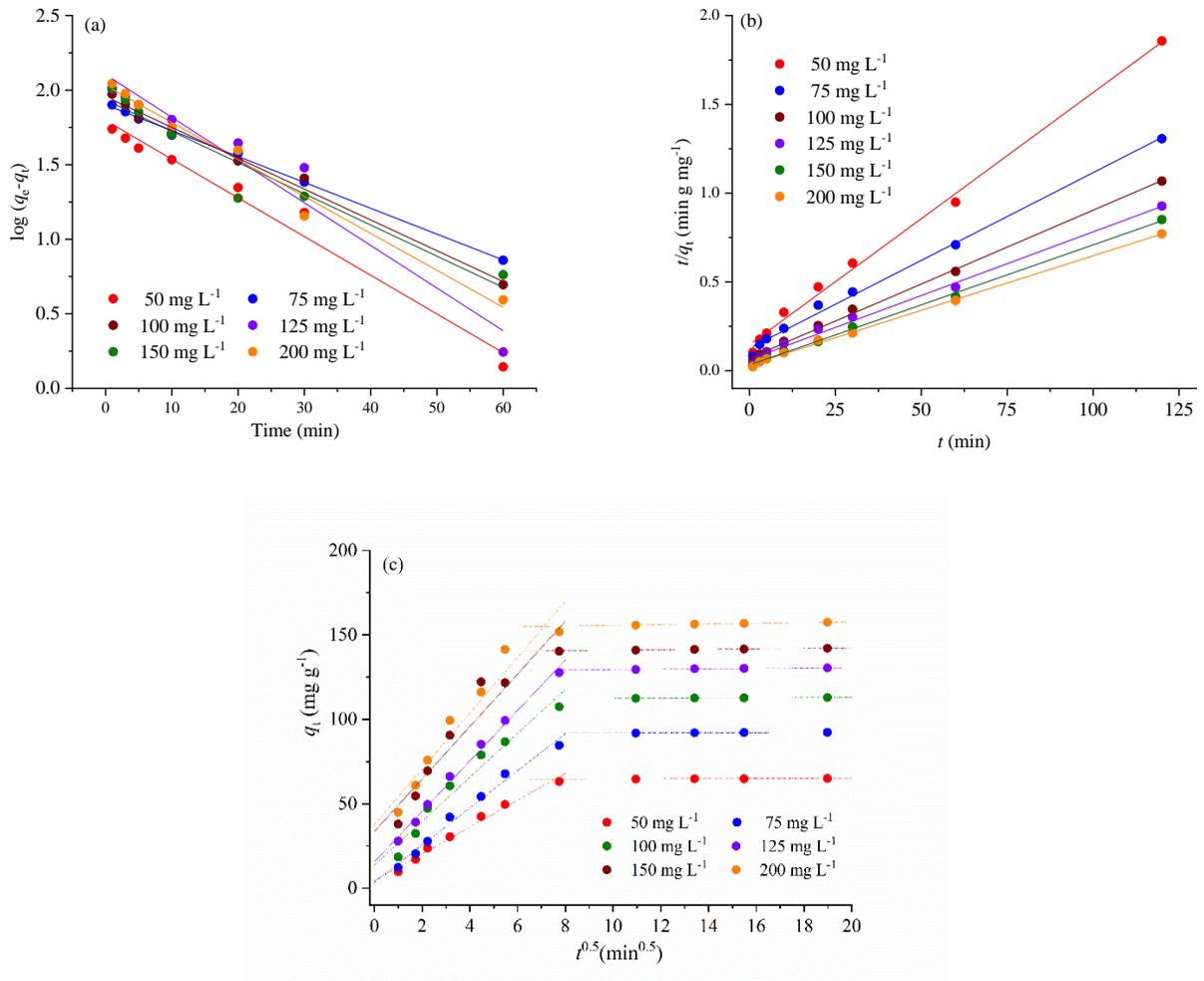
Figure 31. (a) Pseudo-first order kinetics model, (b) pseudo-second order kinetics model, and (c) Weber–Morris intra-particle diffusion model for adsorption of glyphosate on $1.5PC_{500}$.

Table 14. The parameters calculated for pseudo-first order kinetic model, pseudo–second order kinetic model, and Weber–Morris intra-particle diffusion model for adsorption of glyphosate on 1.5PC$_{600}$.

Model Parameters	C_0 (mg g^{-1})					
	50	75	100	125	150	200
q_e^{exp}(mg g^{-1})	64.6	91.87	112.36	129.45	141.01	155.67
Pseudo-first order kinetics model						
q_e (mg g^{-1})	62.72	79.87	90.68	127.09	110.74	107.48
k_1 10^{-3} (min^{-1})	11.3	7.56	8.99	12.4	14.3	10.8
R^2	0.975	0.998	0.991	0.956	0.976	0.984
Pseudo-second order kinetics model						
q_e (mg g^{-1})	67.11	96.15	116.28	133.33	144.93	158.73
$k_2 \cdot 10^{-3}$ (g mg^{-1} min)	1.79	1.0	1.19	1.21	1.74	1.38
R^2	0.999	0.999	1	0.999	1	1
Weber–Morris intraparticle diffusion model						
C_{id1}	3.46	4.36	13.58	15.52	33.52	37.63
k_{WM1} (mg g^{-1} min$^{-1/2}$)	7.95	11.02	13.03	14.95	15.55	16.52
R^2	0.987	0.986	0.960	0.994	0.912	0.930
k_{WM2} (mg g^{-1} min$^{-1/2}$)	0.038	0.042	0.066	0.113	0.137	0.209
R^2	0.963	0.987	0.985	0.962	0.990	0.986

q_e^{exp}—experimentally obtained value of the amount of the adsorbed MT at equilibrium; q_e^{cal}-calculated value of the amount of the adsorbed MT, based on appropriate kinetic model; k_1-pseudo first order constant; k_2—pseudo-second order constant; R^2—coefficient of determination; k_{WM1}, k_{WM2}—Weber–Morris intraparticle diffusion rate constants; C_{id}—intercept of the linear plot, corresponding to initial adsorption.

The glyphosate adsorption on 1.5PC$_{600}$, follow the same principles in the term of kinetics. The kinetic process obeys the pseudo-second order kinetic model, the k_2 are with independent values of the initial adsorbate concentration. Weber-Morris intraparticle diffusion model shows two linear stages, where the first linear portions do not pass through the origin. Therefore, the boundary layer has effective role, based on C_{id} values (Table 14).

The pseudo-second order kinetic model unambiguously described adsorption metformin and glyphosate on activated carbons 2.0ZC$_{500}$ and 1.5PC$_{600}$. Based on the results of comprehensive kinetic study, it can be concluded that differences in the adsorbents textural characteristic have an impact on the amount of the adsorbed pollutant, without impact on the kinetic rate. According to many authors, pseudo-second order model indicates that possible mechanism of investigated process included chemisorption of pollutants on adsorbent surface (Hameed, 2009).

5.2.6. The effect of temperature on metformin and glyphosate adsorption

The effect of temperature on metformin and glyphosate adsorption on selected adsorbents is given in Figure 32, and Figure 33, respectively.
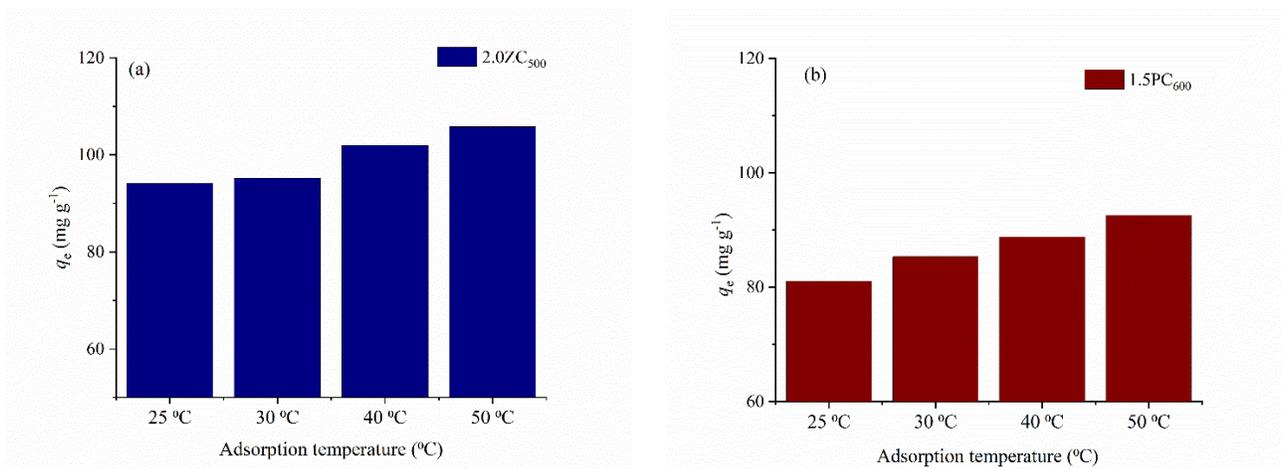
Figure 32. The effect of temperature on MT adsorption on: a) $2.0ZC_{500}$; and b) $1.5PC_{600}$.
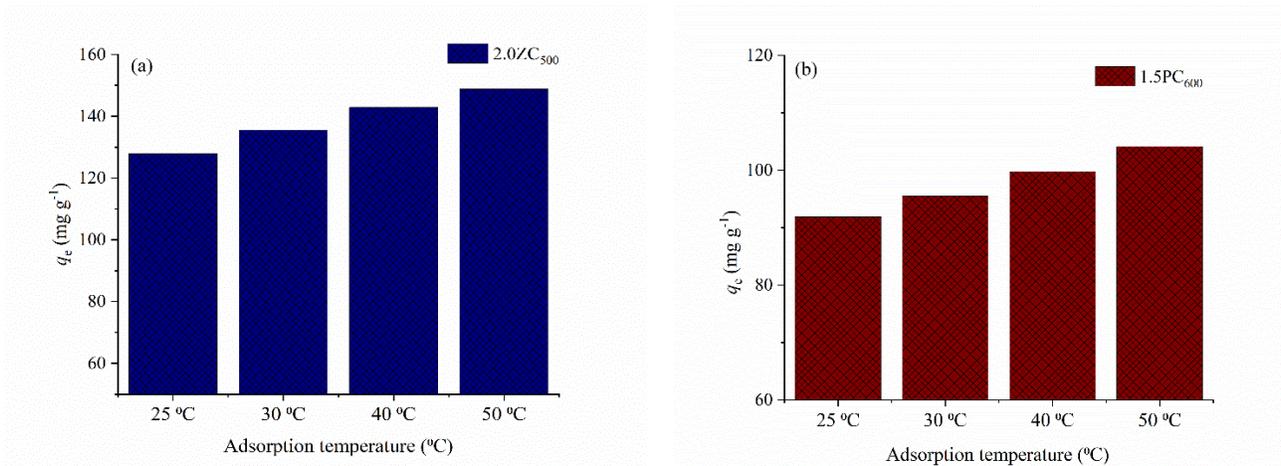
Figure 33. The effect of temperature on GP adsorption on: a) $2.0ZC_{500}$; and b) $1.5PC_{600}$.

For all investigated adsorption processes in this study, the removal of organic pollutant either metformin or glyphosate, increased with increasing temperature on both adsorbents $2.0ZC_{500}$ or $1.5PC_{600}$. However, metformin removal is less depended on temperature increasing in comparison to the glyphosate removal. The increasing of temperature from 25 ^{0}C to 50 ^{0}C slightly increased MT removal for 11.68 mg g^{-1}and 11.54 mg g^{-1} when as adsorbents were applied $2.0ZC_{500}$ and $1.5PC_{600}$, respectively (Figs. 32a and 32b). On the other hand, the glyphosate removal for the same temperature range was increased for 20.95 mg g^{-1}and 12.25 mg g^{-1}, in $2.0ZC_{500}$ and $1.5PC_{600}$, respectively (Figs. 33a and 33b). Therefore, the adsorption process of both pollutants can be characterized as *endothermic*. This finding is in agreement with literature data dealing with the influence of temperature on the

71

removal of these two organic pollutants from carbon-based materials (Sen et al., 2019, Pap et al., 2023).

5.2.6.1. Thermodynamic of the Adsorption

The thermodynamic study linear fits for MT adsorption on $2.0ZC_{500}$ and $1.5PC_{600}$ presented in Figure 34, while calculated thermodynamic parameters are presented in the Table 15.
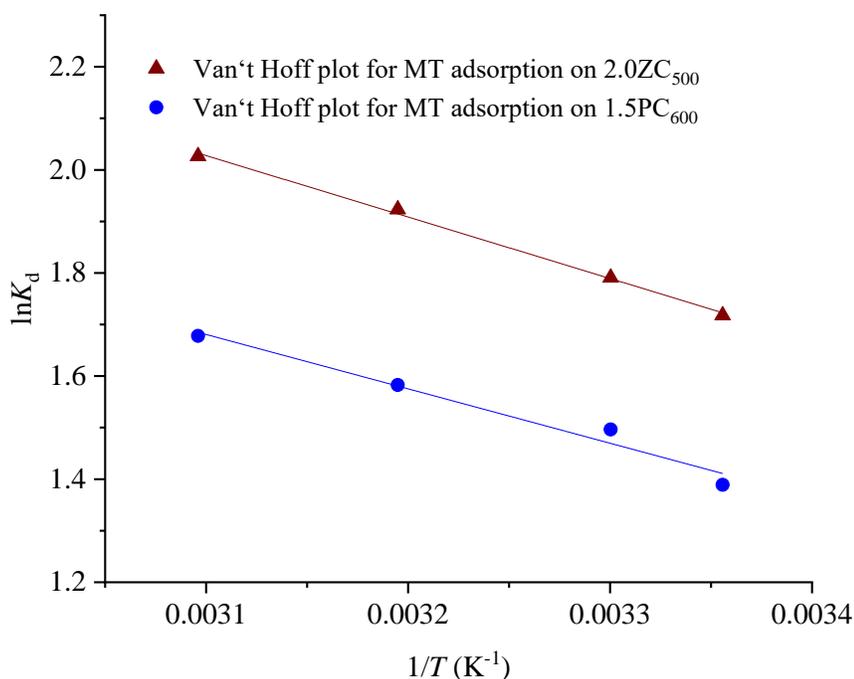
Figure 34. The Van 't Hoff plot for MT adsorption on $2.0ZC_{500}$ and $1.5PC_{600}$
($C_{MT} = 40$ mg L^{-1}; $C_{ads.} = 250$ mg L^{-1}; $T = 298$ K – 323 K; $t = 120$ min) (Mohammed et al., 2022).

Table 15. The thermodynamic parameters for metformin adsorption

Adsorbent	ΔH (kJ mol^{-1})	ΔS (J K^{-1}mol^{-1})	ΔG (kJ mol^{-1})
$2.0ZC_{500}$	9.91	47.55	-4.26
$1.5PC_{600}$	8.77	44.14	-3.44

Using the values of the slope and intercept from linear fits presented in the Fig. 34, the values of ΔH and ΔS were calculated. The obtained values indicate that metformin adsorption is slihgtly endothermic process, but for both adsorbents adsorption was spontanous since the ΔG values are below 0.

The thermodynamic of the glyphosate adsorption was also studied and Van't Hoff plot for the adsorption process on $2.0ZC_{500}$ and $1.5PC_{600}$ is presented in Figure 35, while calculated thermodynamic parameters are given in the Table 16.
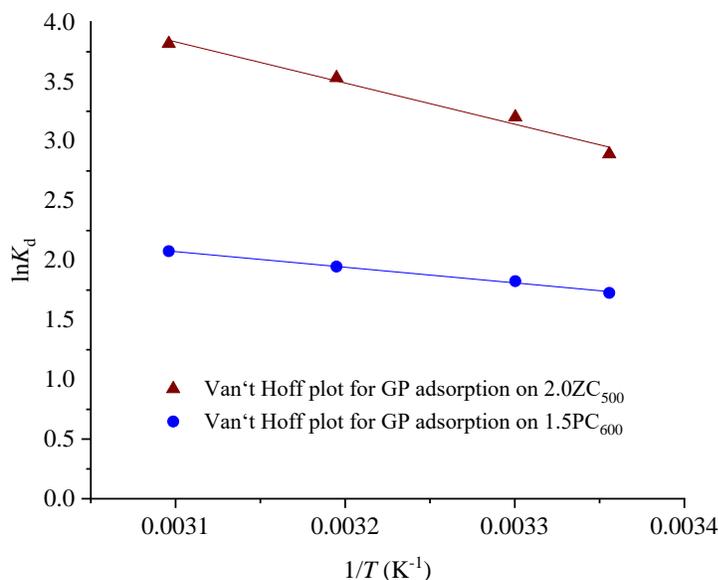
Figure 35. The Van 't Hoff plot for GP adsorption on $2.0ZC_{500}$ and $1.5PC_{600}$ ($C_{GP} = 40$ mg L^{-1}; $C_{ads.} = 250$ mg L^{-1}; $T = 298$ K – 323 K; $t = 120$ min).

Table 16. The thermodynamic parameters for glyphosate adsorption.

Adsorbent	ΔH (kJ mol^{-1})	ΔS (J K^{-1}mol^{-1})	ΔG (kJ mol^{-1})
$2.0ZC_{500}$	28.72	120.90	-7.31
$1.5PC_{600}$	10.90	51.03	-4.30

Similar trends in the thermodynamic behavior for adsorpton system glyphosate – activated carbons were oberved like for the metforimn adsorpton. The adsorption of glyphosate on 2.0ZC500 and 1.5PC600 is endotherminc process with higher temperature dependance than adsorpton of metformine under the same conditions. Besides that, the process is more spontaneous for the glyphosate adsrorption in comparing to the metformin adsorption. Based on the presented results, the temperature increase have benefitial effect for the amount of the both tested pollutants removal, which is already recorded in the literature as specific behavior for organic compounds adsorption. The temperature increase enhancing the rate of the molecular diffusion and in the same time, decreasing the solution viscosity. Hence, the adsorbate molecules easy travell through the external boundary layer and penetrate into the internal pores of the adsorbents (Wang et al., 2010).

This adsorption behavior has been reported in some literature studies for similar adsorptoin systems. Huang et al. (2016) used the biomass of *9999* to prepare biochar by process of the slow pyrolysis at 300⁰C, and then made activation of the biochar by hydrogen peroxide. The modified biochar was used for metformin adsorption and results of the thermodynamic study are in agreement with the results of the

adsorption study presented in this dissertation. The metformin adsorption on the biochar was spontaenous, but endothermic process (Huang et al., 2016). Marbawi et al. (2020) tested glyphosate adsorption on activated carbon loaded with manganese and iron, and found that process was spontaneous and endothermic, which was supported by the phenomenon that the glyphosate adsorption capacities increased with the increase of adsorption temperature (Marbawi et al., 2020).

5.3. Desorption and reusability study

The adsorbents reusability is one of the most important indicator for its empirical application in the real systems. Hence, finding the optimal and the most efficient desorption agent is often one of the essential task when some materials should be evaluated as adsorbents.

5.3.1. Desorption study of metformin

The desorption of metformin from previously saturated (experimental conditions are given in details in subsection 4.4.3) $2.0ZC_{500}$ and $1.5PC_{600}$ was performed using 0.1 mol L^{-1} NaOH, HCl, and NaCl, and results of the desorption study are presented in Fig. 36.
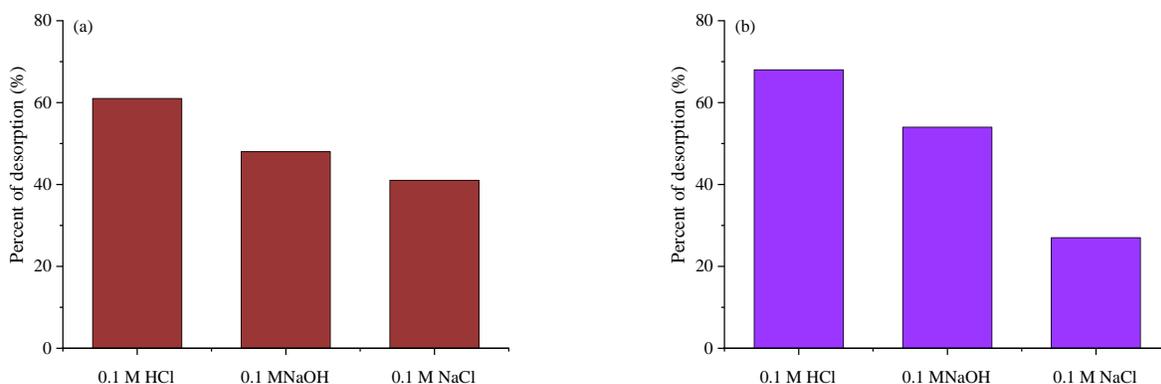
Figure 36. Desorption of metformin from metformin-saturated:

a) $2.0ZC_{500}$ and b)$1.5PC_{600}$ in 0.1 mol L^{-1} solutions of HCl, NaOH, and NaCl (Mohammed et al., 2022).

The experimental data indicate that in the presence of HCl, about 61% and 68% of adsorbed metformin is released from $2.0ZC_{500}$ and $1.5PC_{600}$, respectively. In the presence of NaOH and NaCl desorption, the percentages are found to be 48% and 41%, respectively for $2.0ZC_{500}$, and 54% and 27%, respectively for $1.5PC_{600}$. The obtained result for the desorption study agrees with the literature data. Several studies dealing with desorption found that the hydroxyl and carboxylic groups present on the surface of the adsorbent made it susceptible to easy desorption and regeneration (Herathet al., 2016; Bayuo et al., 2019).

Literature publications suggest that the desorption process for some adsorption systems is efficient in the presence of an acid–ethanol mixture (Valizadeh et al., 2016; Zhang et al., 2019). To achieve a higher amount of the desorbed MT than that obtained in the presence of 0.1 M HCl, as well as

to find the optimal desorption conditions for further test of adsorbent reusability, the desorption of metformin from $2.0ZC_{500}$ and$1.5PC_{600}$ was performed from mixtures of 0.1 HCl and 96% ethanol in different volume ratios (3:1, 2:1, 1:1, 1:2, 1:3), and results are shown in Fig. 37.
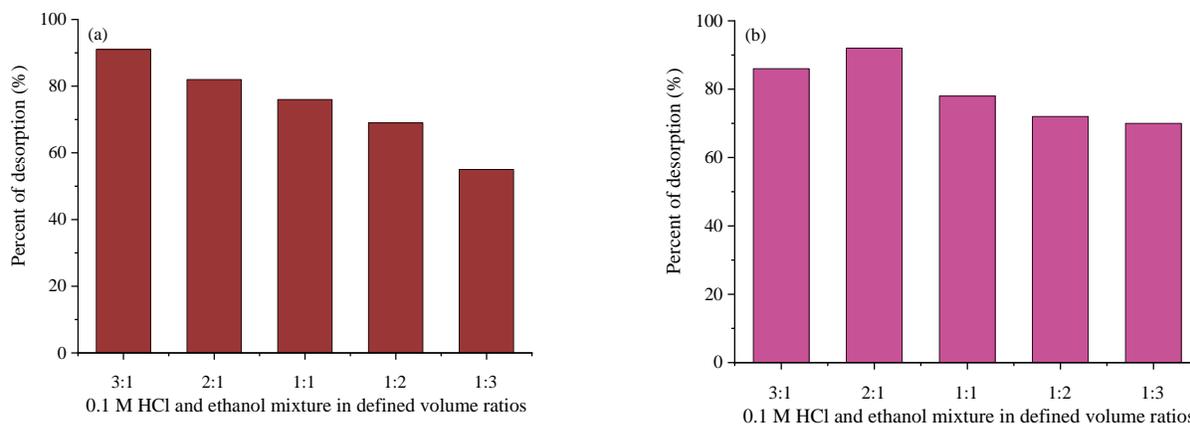
Figure 37. Desorption of metformin from:

a) $2.0ZC_{500}$ and b) $1.5PC_{600}$ using the 0.1 M HCl/ethanol mixture (Mohammad et al., 2022).

The results of desorption process of metformin from HCl/ethanol mixture revealed that the assistance of ethanol in desorption solution mixture significantly contributed to metformin desorption from both adsorbents. The portion of desorbed metformin from all tested HCl/ethanol desorption solutions were above the portion of desorbed pollutant from 0.1 M HCl.

The presence of small portion of the ethanol in desorption solution where 0.1M: ethanol ratio was 3:1 highly contributes to the metformin desorption from $2.0ZC_{500}$ (Fig. 35a). The further increase of ethanol portion in desorption solution has not beneficial effect of the metformin desorption, and the percent of the desorbed metformin decreased.

The metformin desorption efficiency for the adsorbent 1.5PC600 (Fig. 37b) achieved a maximum percent (92%) when as desorption solution was used $0.1 mol\ L^{-1}$ HCl and ethanol in 2:1 volume ratio. It was also observed that increase of the ethanol volume above previously defined value led to a decrease in the desorption efficiency.

The obtained results in this study indicated that adsorption of metformin onto $2.0ZC_{500}$ and $1.5PC_{600}$ occurred via different interactions (electrostatic interaction, hydrogen bonding, etc.). For further desorption experiments and testing of the reusability of $2.0ZC_{500}$ a mixture of HCl/ethanol with a volume ratio 3:1 will be used, while for the desorption of metformin from $1.5PC_{600}$ as optimal desorption solution will be used a mixture of HCl/ethanol with a volume ratio 2:1(Mohammad et al., 2022).

5.3.2. Desorption study of glyphosate

The desorption of glyphosate from previously saturated $2.0ZC_{500}$ and $1.5PC_{600}$ adsorbents was performed from 0.1 mol L^{-1} NaOH, HCl, and NaCl, and results of the desorption experiments are given in Fig. 38.
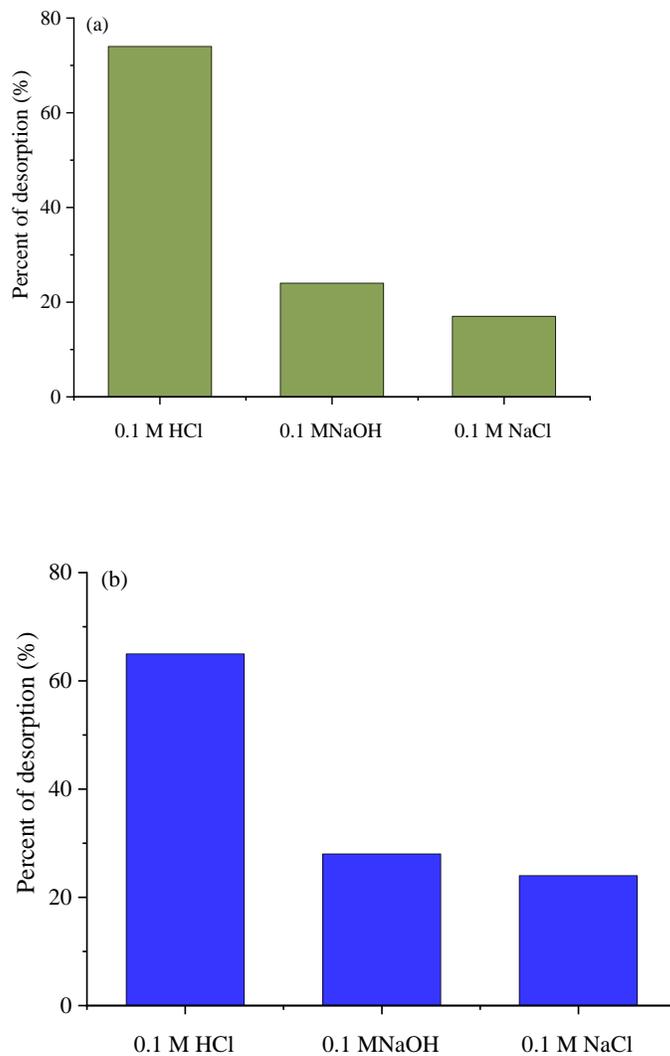
Figure 38. Desorption of glyphosate from glyphosate-saturated:

a) $2.0ZC_{500}$ and b) $1.5PC_{600}$ in 0.1 M solutions of HCl, NaOH, and NaCl.

The experimental results showed that in the presence of hydrochloric acid, about 74 % and 65 % of adsorbed metformin is released from $2.0ZC_{500}$ and $1.5PC_{600}$, respectively. The presence of NaOH and NaCl as desorption agents lead to percentages of desorbed pollutant of 28% and 24%, respectively for $2.0ZC_{500}$, and 24% and 15%, respectively for $1.5PC_{600}$. The observed values for the desorption study of glyphosate were similar like values of desorbed of metformin.

Further desorption investigates were directed toward optimization of the desorption mixture, and desorption was performed from the mixture of hydrochloric acid and ethanol. Therefore, desorption of glyphosate from $2.0ZC_{500}$ and $1.5PC_{600}$ was carry out from mixtures of 0.1 mol L^{-1} HCl and 96% ethanol in using predefined ratios of solution volumes: 3:1, 2:1, 1:1, 1:2, 1:3, and results are shown in Fig. 39.
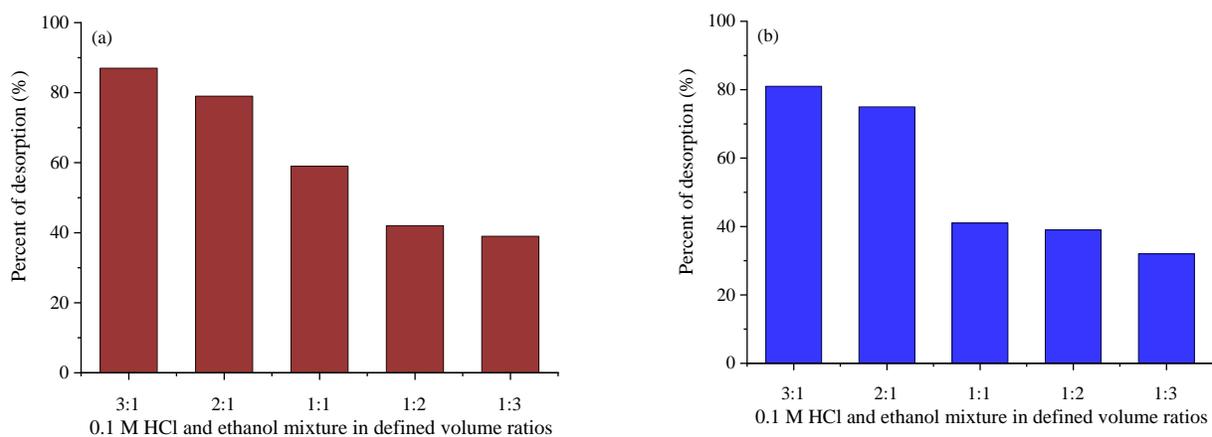
Figure 39. Desorption of glyphosate from:

a) $2.0ZC_{500}$ and b)$1.5PC_{600}$ using the 0.1 mol L^{-1} HCl/ethanol mixture (Mohammad et al, 2022)

Desorption processes from the mixture HCl/ethanol for glyphosate indicated that ethanol presence contributes to the glyphosate desorption in both cases, i.e. from $2.0ZC_{500}$ and $1.5PC_{600}$. T

The presence of small portion of the ethanol in desorption solution where 0.1M: ethanol ratio was 3:1 was considered to be the optimal desorption solution for glyphosate saturated $2.0ZC_{500}$. The desorption solution with a 2:1 HCl/ethanol ratio also contributes to the desorption of glyphosate, but not as much as the previous solution (Fig. 39a). The additionally increase of ethanol portion in desorption solution led to the decrease of the amount of the desorbed glyphosate.

The analogue behaviour of the glyphosate desorption from $1.5PC_{600}$ was observed at Fig. 37b. The desorption from the HCl/ethanol mixture with ratio of 3:1 achieved a maximum of 82%, while glyphosate desorption from the mixture with ratio of 2:1 was almost the same as desorption from HCl solution without ethanol. Further increase of the ethanol portion in desorption solution has negative effect on the glyphosate desorption and cannot be used for this purpose.

5.3.3. Reusability study

The adsorbents reusability after metformin adsorption were tested in five successive cycles using the desorption agents defined as an optimal in previous subchapter 4.2.1. The reusability study data are given in Fig. 40a and 40b for $2.0ZC_{500}$ and $1.5PC_{600}$, respectively.
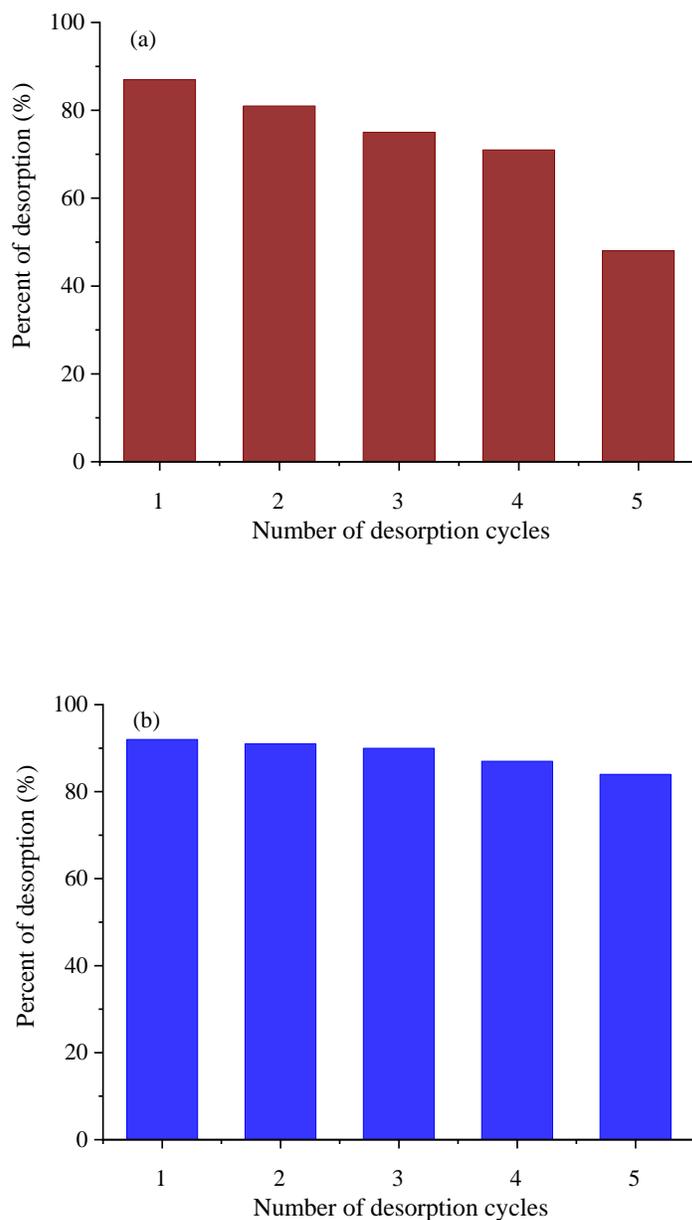
Figure 40. Desorption of metformin in five consecutive adsorption–desorption cycles from: a) $2.0ZC_{500}$, and b)$1.5PC_{600}$ (Mohammad et al., 2022). (Adsorption conditions: m_{ads}=100 mg, V=400 mL, C_{MT}=100 mg L^{-1}; T=25 °C, t_{ads}=120 min, pH 6.8. Desorption conditions: saturated adsorbent (mg) and optimal desorption agent (mL) ratio 1:4, t_{des}=120 min)

Desorption experiments for reusability study were performed from optimal desorption solution 0.1 M HCl/ethanol in a vol. ratio 3:1 and 2:1 for the $2.0ZC_{500}$ and $1.5PC_{600}$, respectively. The reusability of the $2.0ZC_{500}$ after metformin adsorption/desorption slowly decrease during five consecutive cycles, but after the 5th cycle keep almost 50 % of the desorption efficiency (Fig. 40a). On the other hand, the reusability determinate for the metformin adsorption/desorption process on $1.5PC_{600}$ shown that the this activated carbon could be regenerated without a significant loss in its initial efficiencies after five adsorption–desorption cycles, with percent of the desorbed MT of 84% after 5th cycle (Fig. 40b). On the other hand, the interaction of metformin with $2.0ZC_{500}$ seems to be stronger, and the percent of metformin desorption and adsorbent regeneration is not high as in the case of $1.5PC_{600}$. These results demonstrated that $1.5PC_{600}$ exhibits better reusability and stability to remove metformin from pharmaceutical wastewaters than $2.0ZC_{500}$, and potentially could be used as an effective adsorbent material in real systems.

The experimental values of percentage of desorption during reusability study for glyphosate are presented in Fig. 41. As an optimal desorption solution, the mixture of HCl/ethanol in ration 3:1 and 2:1 was used for 2.0ZC500 and 1.5PC600, respectively.
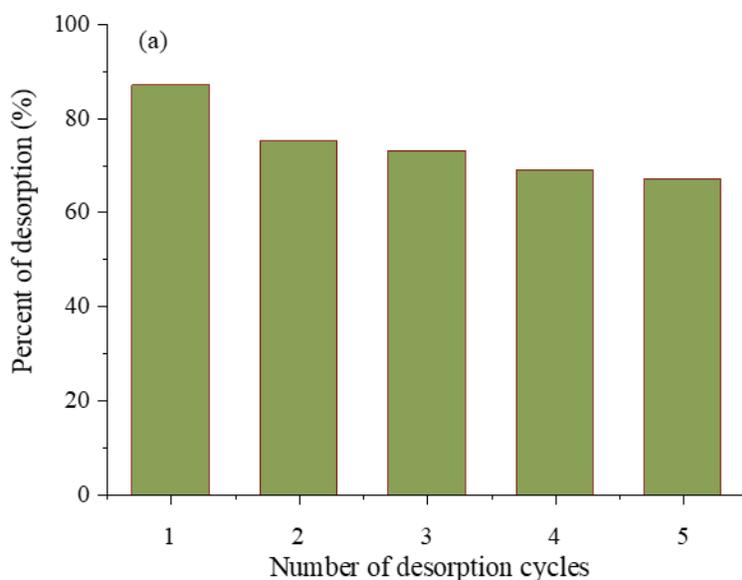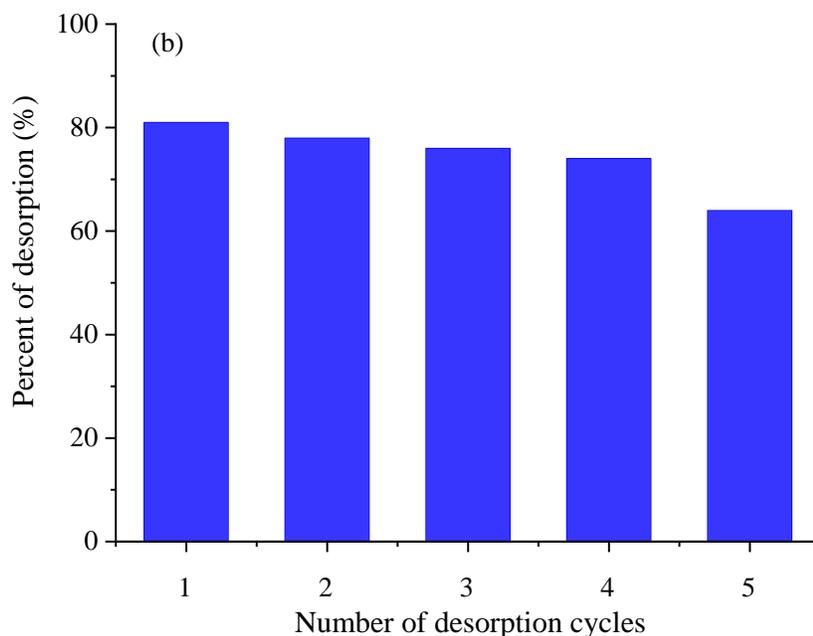
Figure 41. Desorption of glyphosate in five consecutive adsorption–desorption cycles from: a) 2.0ZC$_{500}$, and b)1.5PC$_{600}$. (Adsorption conditions: m_{ads}=100 mg, V=400 mL, C_{GP}=100 mg L^{-1}; T=25 °C, t_{ads}=120 min, pH 3.9. Desorption conditions: saturated adsorbent (mg) and optimal desorption agent (mL) ratio 1:4, t_{des}=120 min)

The results of the reusability study for the glyphosate adsorption/desorption shown similar trend as for reusability after metformin adsorption/desorption. The reusability of the 2.0ZC$_{500}$ after glyphosate adsorption/desorption slowly decrease after first cycle, but after five consecutive cycles the percent of the desorbed glyphosate was still high and has value of 67% (Fig.41a).

On the other hand, the reusability of 1.5PC600 after glyphosate removal almost the same during the cycles repeating and finally, has value of the desorbed pesticide of 64% (Fig.41b). The results demonstrate the reusability and stability of investigated activated carbons and can be recommended to further investigation to application in real systems.

6. CONCLUSION

The present doctoral dissertation investigated the utilization of water hyacinth biomass as a precursor for activated carbons and its application in the adsorption removal of organic pollutants.

The water hyacinth weed caused serious environmental problems in Karbala (Iraq). After the process of washing and drying it was used as starting raw matter for activated carbons synthesis. The AC were synthesized in the chemical activation process using $ZnCl_2$ and H_3PO_4, followed by controlled carbonization. The fabricated activated carbons were fully characterized by elemental analysis, low-temperature adsorption-desorption isotherms of N_2, FTIR analysis, SEM analysis, and analysis of the point of zero charges of the adsorbent.

The different impregnation ratios (IR) of $ZnCl_2$ in the scale of 0.5-3.5 were applied, while the temperatures of carbonization (T_{carb}) were 400 ⁰C, 500 ⁰C, 600 ⁰C, and 700 ⁰C. The IR and T_{carb} were two synthesis parameters that significantly impacted the yield of fabricated activated carbons and surface development. The IR = 0.5 and T_{carb} = 400 ⁰C led to the highest yield of activated carbons. Textural properties showed that the most developed surface of 1317 m^2 g^{-1} has the sample of activated carbon produced with an IR = 2.0 at T_{carb} = 500 ⁰C. Therefore, sample $2.0ZC_{500}$ was chosen to be tested in adsorption study and submitted for more detailed characterization. The SEM analysis revealed that the surface of the raw water hyacinth was moderately developed with parts of a smooth area but after impregnation and carbonization, the material was more porous. The FTIR analysis confirmed the presence of aromatic structures, along with carboxylic, carbonyl, and hydroxyl groups.

The range of IR of H_3PO_4 and raw water hyacinth were from 0.5 to 3.0, while carbonization was performed in a nitrogen atmosphere using T_{carb}= 400 ⁰C, 500 ⁰C, 600 ⁰C, 700 ⁰C, and 800 ⁰C. Although the best yield was got for the lowest temperature of 400 ⁰C, the sample at 600 ⁰C with an IR=1.5 showed the most expressed textural properties and a seriously high value of the specific surface area equal to 1421 m^2 g^{-1}. Both samples $2.0ZC_{500}$ and $1.5PC_{600}$ were dominantly mesoporous materials, with the mesopores volume of 0.541 L^3 g^{-1} and 0.446 L^3 g^{-1}, respectively. However, sample $1.5PC_{600}$ had a higher value of micropore volume than $2.0ZC_{500}$. The SEM analysis for sample $1.5PC_{600}$ confirmed the porous structure of the material. The FTIR spectrum $1.5PC_{600}$ confirmed the presence of aromatic carbon structures, carboxylic, carbonyl, and hydroxylic groups, as well as vibrations originating from activator, i.e., P=O and C–O–P structures. The pH_{PZC} (point of zero-surface charges) was found out to be at pH 6.17 and pH 5.35 for $2.0ZC_{500}$ and $1.5PC_{600}$, respectively.

The adsorption study of two proven organic pollutants: the pesticide glyphosate and pharmaceutic metformin was performed using different adsorption parameters: adsorbent concentration, adsorbate concentration, initial pH and temperature.

The impact of the adsorbent concentration on the percent of the removed glyphosate and metformin revealed that the optimal activated carbons concentration was 250 mg L^{-1}. The increasing concentration of the adsorbents above optimal was not beneficial to the percent of the removed pollutants.

For metformin adsorption $2.0ZC_{500}$ show slightly better adsorption properties than $1.5PC_{600}$; the adsorption was rapid and 120 min was defined as the equilibrium adsorption time. The impact of the starting metformin concentration revealed that lower initial concentrations of metformin (below 20 mg L^{-1}) had similar q_t values regardless of the used adsorbent. Despite the higher value of S_{BET} for $1.5PC_{600}$, other textural parameters, such as mesopore volume were crucial factors for the amount of the adsorbed pollutant. The activated carbon $2.0ZC_{500}$ showed better adsorption affinity toward glyphosate than $1.5PC_{600}$. The equilibrium time for the metformin removal was defined to be 120 minutes.

The adsorbed quantity of glyphosate and metformin strongly depends on the pH of a solution. The maximal amounts of the adsorbed metformin on $2.0ZC_{500}$ and $1.5PC_{600}$ were on pH 8. However, the percent of the removed metformin at the native pH (6.8) was more than 94% of the adsorbed quantity of metformin at the optimum pH of 8. The glyphosate removal was optimal at pH 5, and from the unbuffered pH of glyphosate solution for both tested adsorbents, the percent of glyphosate adsorption approached to the optimal value.

It was found that Langmuir isotherm could be used to best description of the metformin adsorption on both tested adsorbents, with values of maximum adsorption capacity - q_{max} of 146.05 mg g^{-1} and 122.47 mg g^{-1} for $2.0ZC_{500}$ and $1.5PC_{600}$, respectively. The obtained q_{max} values classify the investigated activated carbons as very efficient. Therefore, metformin adsorption could be described as homogeneous adsorption process that happened at adsorption sites with equal interaction energy, with assumption that during adsorption metformin forms the monolayer at surface of investigated adsorbents.

Glyphosate adsorption isotherms could be best described by the Langmuir isotherm model on the surface of $1.5PC_{600}$, while for glyphosate adsorption on $2.0ZC_{500}$ Redlich-Peterson isotherm equation can be successfully fitted. The q_{max} were 240.80 mg g^{-1} and 246.91 mg g^{-1} for glyphosate adsorption on $2.0ZC_{500}$ and $1.5PC_{600}$, respectively.

The pseudo-first kinetic model, pseudo-second kinetic model, and Weber-Morris intraparticle diffusion model were used to describe metformin and glyphosate adsorption on adsorbents $2.0ZC_{500}$ and $1.5PC_{600.}$ It was observed that the pseudo-second kinetic model best described all investigated adsorption systems. Weber-Morris intraparticle diffusion model shows two linear stages. The intraparticle diffusion wasn't the step that limited the adsorption rate, since the first Weber-Morris linear fit doesn't pass through the origin. This finding stands for both, metformin and glyphosate adsorption process. The significant role in the adsorption rate had the boundary layer.

The thermodynamic study showed that metformin adsorption is a slightly endothermic and spontaneous process for both adsorbents. Similar trends in the thermodynamic behavior for glyphosate adsorption on adsorbents $2.0ZC_{500}$ and $1.5PC_{600}$ was observed, but adsorption was in the most expressed dependence on temperature than metforimn adsorption under the same conditions.

The highest degree of desorbed metformin was observed using 0.1 mol L^{-1} HCl for $2.0ZC_{500}$, and in using the 2:1 mixture of 0.1M HCl and ethanol for $1.5PC_{600}$. The adsorbents $2.0ZC_{500}$ and $1.5PC_{600}$ can be successfully reused in 4 and 5 consecutive cycles.

The glyphosate desorption from both $2.0ZC_{500}$ and $1.5PC_{600}$ was the most expressed in the 0.1 M HCl. The $2.0ZC_{500}$ keep almost 67 % of efficiency after five consecutive cycles of glyphosate adsorption, while $1.5PC_{600}$ reached 64% of the starting efficiency.

The performed investigations indicated that water hyacinth biomass can be utilized as a starting lignocellulose material for fabrication of activated carbons in the suggested procedure via chemical activation. The estimated fundamental adsorption characteristics of activated carbons obtained in this study recommended these materials be tested in scale-up studies, and potentially can be successfully used in for application for treatment of real wastewaters.

References

Abdel-Fattah A. F., Abdel-Naby M. A., 2012. Pretreatment and enzymic saccharification of water hyacinth cellulose. *Carbohydrate Polymers* 87, 2109–2113.

Adegunloye D.V., Olosunde S.Y., Omokanju A.B., 2013. Evaluation of ratio variation of Water hyacinth on the production of pig dung biogas. *Intern. Res. J. Biol. Sci.* 2, 44-48.

Ahmed, M.J., 2017. Adsorption of non-steroidal anti-inflammatory drugs from aqueous solution using activated carbons: Review. *J. Environ. Manag.* 190, 274–282.

Akmil-Basar C., Onal Y., Kilicer T., Eren D. 2005. Adsorptions of high concentration malachite green by two activated carbons having different porous structures. *J. Hazard. Mater.* 127, 73–80.

Alagumuthu G., Rajan M., 2010. Equilibrium and kinetics of adsorption of fluoride onto zirconium impregnated cashew nut shell carbon. *Chem. Eng. J. Biochem. Eng. J.* 158, 451–457.

Allahkarami E., Monfared D.A., Silva L.F.O., 2023. Toward a mechanistic understanding of adsorption behavior of phenol onto a novel activated carbon composite. *Sci. Rep.* 13, 167.

Amin M.F., Heijman S.G.J., Rietveld L.C., 2016. Clay-starch combination for micropollutants removal from wastewater treatment plant effluent. *Water Sci. Technol.*, 73, 1719-1727.

Amin M. T., Alazba A. A., Shafiq M., 2017. Nonspontaneous and multilayer adsorption of malachite green dye by Acacia nilotica waste with dominance of physisorption. *Water. Sci. Technol.* 76, 1805–1815.

Asif, F.C., Saha G.C., 2023. Graphene-like carbon structure synthesis from biomass pyrolysis: A critical review on feedstock–process–properties relationship. C 9, 31.

Awashti M., Jeevanjot K., Shiwali R., 2013. Bio ethanol production through Water hyacinth via optimization of pretreatment conditions. *Int. J. Emerg. Technol. Adv. Eng.* 3, 42-44.

Balasundram V., Ibrahim N., Kasmani R.M., Hamid M.K.A., Isha R., Hasbullah H., Ali R.R., 2017. Thermogravimetric catalytic pyrolysis and kinetic studies of coconut copra and rice husk for possible maximum production of pyrolysis oil. *J. Clean.Product.* 167, 218–228.

Bakrim W.B., Ezzariai A. Karouach F., Sobeh M., Kibret M., Hafidi M., YasriA., 2022. ichhornia crassipes (Mart.) Solms: A Comprehensive Review of Its Chemical Composition, Traditional Use, and Value-Added Products. *Front. Pharmacol*. 13, 842511-842531.

Banghokok Post, (Veryfied on April, 2023). https://www.bangkokpost.com/life/social-and-lifestyle/1068024/war-on-weed

Barrett E. P., Joyner L. G., Halenda, P. P., 1951. The determination of pore volume and area distributions in porous substances. I Computations from nitrogen isotherms. *J. Am. Chem. Soc*. 73, 373–380.

Bayuo, J., Pelig-Ba, K.B., Abukari, M.A., 2019. Optimization of adsorption parameters for effective removal of lead (II) from aqueous solution. *Phys. Chem. Indian J*. 14, 1–25.

Benetoli L.O.B., Santana H., Dimas C. E. A. C., Zaia A.M., 2010. Adsorption of glyphosate in a forest soil: a study using Mössbauer and FT-IR spectroscopy, *Quim. Nova* 33, 855-859.

Benhammou A., Yaacoubi A., Nibou L., Tanouti B., 2005. Adsorption of metal ions onto Moroccan stevensite: kinetic and isotherm studies. *J. Coll. Interf. Sci.* 282, 320–326.

Belhachemi M., Addoun F., 2011.Comparative adsorption isotherms and modeling of methylene blue onto activated carbons. *Appl. Water. Sci.* 1, 111–117.

Bernal V., Giraldo L., Moreno-Piraján J. C., 2018. Physicochemical Properties of Activated Carbon: Their Effect on the Adsorption of Pharmaceutical Compounds and Adsorbate–Adsorbent Interactions. *C* 4, 62.

Boonpoke A., 2015. Study on preparation of water hyacinth-based activated carbon for pulp and paper mill wastewater treatment. *J. Env. Biol.* 36, 1143-1148.

Borrero-López A.M., Fierro V., Jeder A., Ouederni A., Masson E., Celzard A., 2017. High added-value products from the hydrothermal carbonisation of olive stones. *Environ. Sci. Pollut. Res.* 24, 9859-9869.

Bote M.A., Naik V.R., Jagadeeshgouda K.B., 2020. Review on water hyacinth weed as a potential bio fuel crop to meet collective energy needs, *Mater. Sci. Ener. Technol*. 3, 397-406.

Brillas E., 2014. A review on the degradation of organic pollutants in waters by UV photoelectro-Fenton and solar photoelectro-Fenton, *J. Braz. Chem. Soc.* 25, 393-417.

Braghiroli F.L., Fierro V., Izquierdo M.T., Parmentier J., Pizzi A., Celzard A., 2012. Nitrogen-doped carbon materials produced from hydrothermally treated tannin. *Carbon* 50, 5411-5420.

Briones R.M., Sarmah A. K., Padhye L.P., 2016. A global perspective on the use, occurrence, fate and effects of anti-diabetic drug metformin in natural and engineered ecosystems. Environ. Poll. 219, 1007-1020.

Cagnon B., Py X., Guillot A., Stoeckli F., Chambat G., 2009. Contributions of hemicellulose, cellulose and lignin to the mass and the porous properties of chars and steam activated carbons from various lignocellulosic precursors. *Biores. Technol.* 100, 292-298.

Cardoso B., Mestre A. S., Carvalho A. P., Pires J., 2008. Activated carbon derived from cork powder waste by KOH activation: preparation, characterization, and VOCs Adsorption. *Ind. Eng. Chem. Res.* 47, 5841-5846.

Castro, J.B., Bonelli P.R., Cerrella E.G., Cukierman, A.L., 2000. Phosphoric acid activation of agricultural residues and bagasse from sugar cane: Influence of the experimental conditions on adsorption. Characteristics of Activated Carbons. *Ind. Eng. Chem. Res.* 39, 4166–4172.

Chen F., Zhou C., Li G., Peng F., 2016. Thermodynamics and kinetics of glyphosate adsorption on resin D301. *Arab. J. Chem.* 9, S1665–S1669.

Chen R., Li L., Liu Z., Lu M., Wang C., Li H., Ma W., Wang S., 2017. Preparation and characterization of activated carbons from tobacco stem by chemical activation. *J. Air Waste Manag. Assoc.* 67, 713-724.

Cheung W. H., Chan C. L. S., Lau K. S. T., Allen S. J., McKay G., 2017. Production of high surface area-activated carbons from waste bamboo scaffolding. *HKIE Transactions* 24, 133 -140.

Choi J.W., Choi N.C., Lee S.J., Kim D.J. 2007. Novel three-stage kinetic model for aqueous benzene adsorption on activated carbon. *J. Coll. Interf. Sci.* 314, 367–372.

Clark B.J., Frost T., Russell M.A., 1993. UV Spectroscopy: Techniques, instrumentation and data handling, Springer Science & Business Media, Published by Chapman & Hall, London.

Corcho-Corral B., Olivares-Marin M., Fernandez-Gonzalez C., Gomez-Serrano V., Marcias-Garcia, A., 2006. Preparation and textural characterization of activated carbon from vine shoots (Vitis vinifera) by H_3PO_4 - chemical activation. *Appl. Surf. Sci.* 252, 5961–5966.

Cusioli L.F., Quesada H.B., Castro A.L., Gomes R.G., Bergamasco R., 2020. Development of a new low-cost adsorbent functionalized with iron nanoparticles for removal of metformin from contaminated water. *Chemosphere* 247, 125852.

Danish M., Hashim R., Ibrahim M.N., Rafatullah M., Sulaiman O., 2012. Surface characterization and comparative adsorption properties of Cr(VI) on pyrolysed adsorbents of Acacia mangium wood and Phoenix dactylifera L. stone carbon. *J. Anal. Appl. Pyrol.* 97, 19–28.

Darwish A.A.A., Rashad M., AL-Aoh H.A., 2019. Methyl orange adsorption comparison on nanoparticles: isotherm, kinetics, and thermodynamic studies. *Dyes Pigments* 160, 563–571.

Deng, H., Zhang, G., Xu, X., Tao, G., Dai, J., 2010. Optimization of preparation of activated carbon from cotton stalk by microwave assisted phosphoric acid-chemical activation. *J. Hazard. Mater.* 182, 217–224.

Diaz E., Sanchis I., Coronella C.J., Mohedano A.F., 2022. Activated Carbons from Hydrothermal Carbonization and Chemical Activation of Olive Stones: Application in Sulfamethoxazole Adsorption. Resources 11, 43.

Dich J, Zahm S.H., Hanberg A., Adami H.O., 1997. Pesticides and cancer. *Cancer Causes & Control.* 8, 420–443.

Din M. I., Ashraf S., Intisar A., 2017. Comparative study of different activation treatments for the preparation of activated carbon: A mini-review. *Sci. Prog.* 100, 299–312.

Dizge N., Aydiner C., Demirbas E., Kobya M., Kara S. 2008. Adsorption of reactive dyes from aqueous solutions by fly ash: kinetic and equilibrium studies. *J. Hazard. Mater.* 150, 737–746.

Dubinin M., 1966. Porous structure and adsorption properties of active carbons. Chemistry and Physics of Carbon, New York, U.S.A.

Duke S. O., 2020. Glyphosate: environmental fate and impact. *Weed Sci.* 68, 201-207.

Elamin, M.R., Abdulkhair, B.Y., Algethami, F.K., Khezami, L.,2021. Linear and nonlinear investigations for the adsorption of paracetamol and metformin from water on acid-treated clay. *Sci. Rep*. 11, 13606.

Echavia G. R. M., Matzusawa F., Negishi N., 2009. Photocatalytic degradation of organophosphate and phosphonoglycine pesticides using TiO_2 immobilized on silica gel, *Chemosphere* 76, 595-600.

El Bakouri H., Usero J., Morillo J., Rojas R., Ouassini A., 2009. Drin pesticides removal from aqueous solutions using acid-treated date stones. *Biores. Technol.*, 100, 2676–2684.

Eleven Carbon[TM] https://elevencarbon.com/activated-carbon/ (25th April 2023).

Elsayed Y., Seredych M., Dallas A., Bandosz T.J., 2009. Desulfurization of air at high and low H_2S concentrations. *Chem. Eng. J.* 155, 594–602.

Fang J., Gao B., Chen J., Zimmerman A.R., 2015. Hydrochars derived from plant biomass under various conditions: characterization and potential applications and impacts. *Chem. Eng. J.* 267, 253-259.

Fillat U., Ibarra D., Eugenio M.E., Moreno A.D., Tomás-Pejó E., Sampedro E.M., 2017. Laccases as a potential tool for the efficient conversion of lignocellulosic biomass: A Review. *Fermentation* 3, 17 (30 pages).

Foo K.Y., Hameed B.H., 2010. Insights into the modeling of adsorption isotherm systems, *Chem. Eng. J.* 156, 2-10.

Freundlich, H.M.F., 1906. Über die adsorption in lösungen. *Z. Phys. Chem.* 57A, 385–470.

Gao X., Wu L., Li Z., Xu Qing, Tain W., Wang R., 2018. Preparation and characterization of high surface area activated carbon from pine wood sawdust by fast activation with H3PO4 in a spouted bed. *J. Mater. Cycles. Waste Manag.* 20, 925–936.

Ghosal P.S., Gupta A.K. 2017. Determination of thermodynamic parameters from Langmuir isotherm constant-revisited. *J. Mol. Liquids* 225, 137-146.

Girisuta B., Danon B., Manurung R., Janssen L.P.B.M., Heeres H.J., 2008. Experimental and kinetic modelling studies on the acid-catalysed hydrolysis of the water hyacinth plant to levulinic acid. *Biores.*

Technol. 99, 8367–8375.

Gomes H. T., Miranda S. M., Sampaio M. J., Silva A.M.T., Faria J.L., 2010. Activated carbons treated with sulphuric acid: Catalysts for catalytic wet peroxide oxidation. *Catal. Today* 151, 153–158.

Gómez-Tamayo M. del Mar, Macías-García A., Díez M.A., Cuerda-Correa E.M., 2008. Adsorption of Zn(II) in aqueous solution by activated carbons prepared from evergreen oak (Quercus rotundifolia L.). *J. Hazard. Mater.* 153, 28–36.

González J.C., Sepúlveda-Escribano A., Molina-Sabio M., Rodrıguez-Reinoso F., 1997. In: B. McEnaney, T.J. Mays, J. Rouquerol, F. Rodrıguez-Reinoso, K.S.W. Sing, K.K. Unger (Eds.), Characterization of Porous Solids, vol. IV, The Royal Society of Chemistry, Cambridge, 9–16.

Gonzalez-Garcıa P., 2018. Activated carbon from lignocellulosics precursors: A review of the synthesis methods, characterization techniques and applications. *Renew. Sust. Ener. Rev*. 82, 1393–1414.

González-García P., Gamboa-González S., Andrade Martínez I., Hernández-Quiroz T., 2019. Preparation of activated carbon from water hyacinth stems by chemical activation with K2CO3 and its performance as adsorbent of sodium naproxen. *Envir. Prog. Sust. Ener.* 39, e13366 (13 pages).

Gregg, S. J., Sing, K. S. W.,1983. Adsorption, Surface Area, and Porosity. (2nd ed.). New York: Academic Press.

Groen, J.C., Peffer, L.A.A., Pérez-Ramírez, J., 2003. Pore size determination in modified mi-cro- and mesoporous materials. Pitfalls and limitations in gas adsorption data analysis. *Microp. Mesopor. Mater.* 60, 1–3.

Gupta G.S., Prasad G., Singh V.N., 1990. Removal of chrome dye from aqueous solutions by mixed adsorbents fly ash and coal. *Water Res.* 24, 45–50.

Hafizuddin M.S., Lee C.L., Chin K.L., Hong P.S., Khoo P.S., Rashid U., 2021. Fabrication of Highly Microporous Structure Activated Carbon via Surface Modification with Sodium Hydroxide. *Polymers* 13, 3954.

Hameed B.H., Krishni R.R., Sata S.A., 2009. A novel agricultural waste adsorbent for the removal of cationic dye from aqueous solutions. *J.Hazard. Mater*. 162, 305–311.

Hanke I., Wittmer I., Bischofberger S., Stamm C., Singer H., 2010. Relevance of urban glyphosate use for surface water quality. *Chemosphere* 81, 422–429.

Herath I., Kumarathilaka P., Al-Wabel M.I., Abduljabbar A., Ahmad M., Usman A.R.A., Vithanage M., 2016. Mechanistic modeling of glyphosate interaction with rice husk derived engineered biochar. *Micropor. Mesopor. Mat*. 225, 280–288.

Ho Y. S., Ng J. C. Y., McKay G., 2000. Kinetics of pollutant sorption by biosorbents: Review. *Sep. Purif. Methods* 29, 189–232.

Honlah E., Segbefia A.Y., Appiah D.O., Mensah M., Atakora P.O., Sabater A., 2019. Effects of water hyacinth invasion on the health of the communities, and the education of children along River Tano and Abby-Tano Lagoon in Ghana. *Cogent. Soc. Sci.*, 5, 1619652 (18 pages).

Hu Z., M.P. Srinivasan M.P., 2001. Mesoporous high-surface-area activated carbon. *Micropor. Mesopor. Mater.* 43, 267–275.

Huang Y., Li S., Chen J., Zhang X., Chen Y., 2014. Adsorption of Pb(II) on mesoporous activated carbons fabricated from water hyacinth using H_3PO_4 activation: Adsorption capacity, kinetic and isotherm studies. *Appl. Surf. Sci.* 293, 160 - 168.

Huang X., Liu Y., Liu S., Li Z., Tan X., Ding Y., Zeng G., Xu Y., Zeng W., Zheng B., 2016. Removal of metformin hydrochloride by Alternanthera philoxeroides biomass derived porous carbon materials treated with hydrogen peroxide. *RSC Adv.* 6, 79275-79284.

Hui T.S., Zaini M.A.A., 2015. Potassium hydroxide activation of activated carbon: A commentary. *Carb. Lett.* 16, 275–280.

Ioannidou O., A. Zabaniotou A., 2007. Agricultural residues as precursors for activated carbon production – a review, *Renew. Sust. Ener. Rev*. 11, 1966–2005.

Infrared Spectroscopy Absorption Table. Available online: https://chem.libretexts.org/Ancillary_Materials/Reference/Reference_Tables/Spectroscopic_Reference_Tables/Infrared_Spectroscopy_Absorption_Table (accessed on 16 April 2023)

Kalumpha M., Guyo U., Zinyama N.P., Vakira F.M., Nyamunda B.C., 2020. Adsorptive potential of Zea mays tassel activated carbon towards the removal of metformin hydrochloride from pharmaceutical effluent. *Int. J. Phytoremediation* 22, 148-156.

Kanissery B., Gairhe B., Kadyampakeni D., Batuman O., Alferez F., 2019. Glyphosate: Its Environmental Persistence and Impact on Crop Health and Nutrition, *Plants* 8, 499-510.

Karagöz S., Tay T., Ucar S., Erdem M., 2008. Activated carbons from waste biomass by sulfuric acid activation and their use on methylene blue adsorption. *Bioresour. Technol.* 99, 6214-6222.

Karimian S., Moussavi G., Fanaei F., Mohammadi S., Shekoohiyan S., Giannakis S., 2020. Shedding light on the catalytic synergies between Fe(II) and PMS in vacuum UV (VUV/Fe/PMS) photoreactors for accelerated elimination of pharmaceuticals: the case of metformin. *Chem. Eng. J.*, 400, 125896.

Kavitha D., Namasivayam C., 2007. Experimental and kinetic studies on methylene blue adsorption by coir pith carbon. *Biores. Technol.* 98, 14–21.

Kilic, M., Apaydin-Varol E., Putun, A.E., 2010. Preparation and surface characterization of activated carbons from Euphorbia rigida by chemical activation with $ZnCl_2$, K_2CO_3, NaOH and H_3PO_4. Appl. Surf. Sci. 261, 247–254.

Kumar A., Jena H.M., 2016. Preparation and characterization of high surface area activated carbon from Fox nut (Euryale ferox) shell by chemical activation with H_3PO_4. *Res. Phys.* 6, 651-658.

Lagergren, S., 1898. About the theory of so-called adsorption of soluble sub-stances. K.Sven. Vetenskapsakad. *Handlingar Band*, 24, 1–39.

Langmuire, I., 1918. The adsorption of gases on plane surfaces of glass,mica and platinum. *J. Am. Chem. Soc.* 40, 1361–1403.

Largitte, L., Brudey, T., Tant, T., Dumesnil, P. C., Lodewyckx, P., 2016. Comparison of the adsorption of lead by activated carbons from three lignocellulosic precursors. Microporous and Mesoporous Materials, 219, 265-275.

Lay C.H., B. Sen B., C.C. Chen C.C., J.H. Wu J.H., S.C. Lee S.C., C.Y.Lin C.Y., 2013. Co-fermentation of water hyacinth and beverage wastewater in powder and pellet form for hydrogen production. *Biores. Technol.* 135, 610–615.

Lee Y.W., Kim H.J., Park J.W., Choi B.U., Choi D.K., 2003. Adsorption and reaction behaviour for the simultaneous adsorption of $NO–NO_2$ and SO_2 on activated carbon impregnated with KOH, *Carbon* 41,1881–1888.

Li K., Ruan H., Ning P., Wang C., Sun X., Song X., Han S., 2018. Preparation of walnut shell-based activated carbon and its properties for simultaneous removal of H_2S, CoS and CS_2 from yellow phosphorus tail gas at low temperature. *Res. Chem. Intermed.*, 44, 1209–1233.

Liou T. H., 2010. Development of mesoporous structure and high adsorption capacity of biomass-based activated carbon by phosphoric acid and zinc chloride activation. *Chem. Eng. J.* 158, 129–142.

Liu Z., Zhang F.S., Wu J., 2010. Characterization and application of chars produced from pinewood pyrolysis and hydrothermal treatment. *Fuel* 89, 510-514.

Liu Q.X., Zhou Y.R., Wang M., Zhang Q., Ji T., 2019. Adsorption of methylene blue from aqueous solution onto viscose-based activated carbon fiber felts: Kinetics and equilibrium studies, *Ads. Sci. Technol.* 37, 312–332.

Liu X., Renard C. M.G.C., Bureau S., Le Bourvellec C., 2021. Revisiting the contribution of ATR-FTIR spectroscopy to characterize plant cell wall polysaccharides. Carbohydr. Polym. 262, 117935.

Lopičić, Z. R., Stojanović M.D., Marković S.B., Milojković J.V., Mihajlović M.M., Kaluđerović Radoičić T.S., Kijevčanin M.J.L, 2019. Effects of different mechanical treatments on structural changes of lignocellulosic waste biomass and subsequent Cu(II) removal kinetics. Arabian J. Chem. 12, 4091-4103.

Lotfi H., Khoshanabad J.R., Vadi M., 2015. Adsorption of metformin as anti-diabetic drug on carbon nanotube and activated carbon. *RJPBCS* 6, 1442.

Lua A.C., Yang T., 2005. Characteristics of activated carbon prepared from pistachio nut shell by zinc chloride activation under nitrogen and vacuum conditions. *J. Colloid Interface Sci.* 290, 505–513.

Lua A.C., Lau F.Y., Guo J., 2006. Influence of pyrolysis conditions on pore development of oil-palm-shell activated carbons, *J. Anal. Appl. Pyrol.* 76, 96–102.

Maguana Y., Elhadiri E., Bouchdoug N., Benchanaa M., 2018. Study of the in fluence of some factors on the preparation of activated carbon from walnut cake using the fractional factorial design. *J. Envir. Chem. Eng.* 6, 1093–1099.

Mak S., B. Tey B., K. Cheah K., W. Siew W., K. Tan K., 2009. The effect of mechanical grinding on the mesoporosity of steam-activated palm kernel shell activated carbons. *J. Chem. Technol. Biotechnol.* 84, 1405–1411.

Marbawi H., Othman A. R., Halmi M. I. E., Gansau J. A., Sabullah K., Yasid N. A., 2020. Re-evaluation of Thermodynamic Parameters using Dimensionless Langmuir Constants from Published Data on Glyphosate Adsorption onto Activated Carbon Loaded with Manganese and Iron. *J. Environ. Biorem. Toxicol.* 3, 6–10.

Mohammad A. H., 2017. Master thesis: Pregled postupaka za proizvodnju bioetanola iz lignoceluloznih sirovina, Šumarski fakultet, Beograd.

Mohammad A.H., Kijevčanin M., 2022. Synthesis of activated carbons from water hyacinth biomass and its application as adsorbents in water pollution control: Scientific paper, *J. Serb. Chem. Soc.* 88, 69–82.

Mohammad A.H., Radovic I., Ivanović M., Kijevčanin M., 2022. Adsorption of metformin on activated carbon produced from the water hyacinth biowaste using H_3PO_4 as a chemical activator. *Sust.* 14, 11144.

Mohanty K., Jha M., Meikap B.C., Biswas M. N., 2005. Preparation and Characterization of Activated Carbons from Terminalia Arjuna Nut with Zinc Chloride Activation for the Removal of Phenol from Wastewater. *Ind. Eng. Chem. Res.* 44, 4128-4138.

Mohanty K., Das D., Biswas M.N., 2006. Preparation and characterization of activated carbons from Sterculia alata nutshell by chemical activation with zinc chloride to remove phenol from wastewater. *Adsorption* 12, 119–132.

Mojoudi N, Mirghaffari N, Soleimani M, Shariatmadari H, Belver C, Bedia J., 2019. Phenol adsorption on high microporous activated carbons prepared from oily sludge: equilibrium, kinetic and thermodynamic studies. *Sci. Rep.* 9, 19352.

Morley W.A., Seneff S., 2014. Diminished brain resilience syndrome: A modern day neurological pathology of increased susceptibility to mild brain trauma, concussion, and downstream neurodegeneration. *Surg. Neurol. Int.* 5, 134731 (24 pages).

Muneer M., Boxall C., 2008. Photocatalyzed degradation of a pesticide derivative glyphosate in aqueous suspensions of titanium dioxide. *Inter. J. Photoener*. 7, 197346 (7 pages).

Niaei H.A., Rostamizadeh M., 2020. Adsorption of metformin from an aqueous solution by Fe-ZSM-5 nano-adsorbent: isotherm, kinetic and thermodynamic studies. *J. Chem. Thermodyn*. 142, 106003

Nor M., Lau N., Lee L. C., Teong L. K., Mohamed, A. R., 2013. Synthesis of activated carbon from lignocellulosic biomass and its applications in air pollution control—a Review. *J. Envir. Chem. Eng*. 1, 658–666.

Nowicki P., Pietrzak R., Wachowska H., 2010. Sorption properties of active carbons obtained from walnut shells by chemical and physical activation. *Catal. Today* 150, 107–114.

Nwosu F. O., Olu-Owolabi B. I., Adebowale K. O., 2012. Kinetics and Thermodynamic Adsorption of Pb(II) and Cd(II) Ions from Used Oil onto Thevetia neriifolia Nutshell Active Carbon. *Current Res. Chem.* 4, 26-40.

Ojediran, J.O., Dada, A.O., Aniyi, S.O. Robinson O.D., Adejoke D. A., 2021. Mechanism and isotherm modeling of effective adsorption of malachite green as endocrine disruptive dye using Acid Functionalized Maize Cob (AFMC). *Sci. Rep.* 11, 21498.

Oluwatimileyin S.J., Asiata Omotayo, I., Olugbenga S.B., 2022. Metformin adsorption onto activated carbon prepared by acid activation and carbonization of orange peel. *Inter. J. Phytorem.* 20, 1–12.

Ozdemir I., Şahin M., Orhan R., Erdem M., 2014. Preparation and characterization of activated

carbon from grape stalk by zinc chloride activation, *Fuel Proc. Technol*. 125, 200-206.

Ozer D., Dursun G., Ozer A. 2007. Methylene blue adsorption from aqueous solution by dehydrated peanut hull, *J. Hazard. Mater.* 144 (2007) 171–179.

Pap S., Shearer L., Gibb S.W., 2023. Effective removal of metformin from water using an iron-biochar composite: Mechanistic studies and performance optimisation. *J. Env. Chem. Eng*. 11, 110360.

Perez G.L., Vera M.S., Miranda L.A., 2011. Effects of herbicide glyphosate and glyphosate-based formula-tions on aquatic ecosystems. Herbicides and Environment; Kortekamp, A., Ed.; InTech: Rijeka, Croatia.

Plazinski W., Rudzinski W., Plazinska A., 2009. Theoretical models of sorption kinetics including a surface reaction mechanism: A review. *Adv. Coll. Interf. Sci.* 152, 2–13.

Pouretedal H. R., Sadegh N., 2014. Effective Removal of Amoxicillin, Cephalexin, Tetracycline and Penicillin G From Aqueous Solutions Using Activated Carbon Nanoparticles Prepared From Vine Wood. *J. Water Process. Eng.* 1, 64 -73.

Prahas D., Kartika Y., Indraswati N., Ismadji, S., 2008. Activated carbon from jackfruit peel waste by H3PO4 chemical activation: Pore structure and surface chemistry characterization. *Chem. Eng. J.* 140, 32–42.

Prashanth V., Priyanka K., Remya N., 2021. Solar photocatalytic degradation of metformin by TiO$_2$ synthesized using Calotropis gigantea leaf extract. *Water Sci. Technol*. 83, 1072-1084.

Priya E. S, Selvan P. S., 2014. Water hyacinth (Eichhornia crassipes) – An efficient and economic adsorbent for textile effluent treatment – A review. *Arab. J. Chem.* 10, S3548-S3558.

Qian Q., Machida M., Tatsumoto H., 2007. Preparation of activated carbons from cattle-manure compost by zinc chloride activation. *Biores. Technol.* 98, 353–360.

Raja S. A., Lee C. L. R., 2019. Biomethanation of Water hyacinth using additives under forced mixing in a bio reactor. *Inter. J. Chem. Sci. Res.* 2, 15-24.

Raji, F.; Pakizeh, 2014. M. Kinetic and thermodynamic studies of Hg(II) adsorption onto MCM-41 modified by ZnCl$_2$. *Appl. Surf. Sci.* 301, 568–575.

Redlich O., Peterson D.L., 1959. A useful adsorption isotherm. *J. Phys. Chem.* 63, 1024-1026.

Regti A., Laamari M.R., Stiriba S.E., El Haddad M., 2017. Potential use of activated carbon derived from Persea species under alkaline conditions for removing cationic dye from wastewaters. *J. Ass. Arab Univer. Bas. Appl. Sci.* 24, 10–18.

Riyanto C. A., Prabalaras E., 2019. The adsorption kinetics and isoterm of activated carbon from Water Hyacinth Leaves (Eichhornia crassipes) on Co(II). *J. Phys.: Conf. Ser.* 1307, 012002.

Rodriguesa P.V., Silva F.A. N. G., Pontesa F.V.M., Barbatoc C.N., Teixeira V.G., Assisa T.C., Brandão V. S., Bertolino L.C., 2023. Adsorption of Glyphosate by Palygorskite. *Mater. Res.* 26, 20220335.

Rodriguez-Reinoso F., Molina-Sabio M., 2004. Role of chemical activation in the development of carbon porosity. *Coll. Surf.* A 241, 15–25.

Rouquerol J., Rouquerol F., Sing K. S. W., 1998. Absorption by powders and porous solids. 2nd Eddition Principles, Methodology and Applications. Academic press, San Diego, USA.

Rouquerol J., Llewellyn P., Rouquerol F., 2007. Is the BET equation applicable to microporous adsorbents? Studies in surface science and catalysis? *Surf. Sci. Catal.* 160, 49–56.

Rudzinski W., Plazinski W., 2008. Kinetics of solute adsorption at solid/solution interfaces: On the special features of the initial adsorption kinetics. *Langmuir* 24, 6738–6744.

Sabarinathan G., Karuppasamy P., Vijayakumar C.T., Arumuganathan T., 2019. Development of methylene blue removal methodology by adsorption using molecular polyoxometalate: kinetics, thermodynamics and mechanistic study. *Microchem. J.*146, 315–326.

Saning A., Herou S., Dechtrirat D., Ieosakulrat C., Pakawatpanurut P., Kaowphong S., Thanachayanont C., Titirici M. M., Chuenchom L., 2019. Green and sustainable zero-waste conversion of water hyacinth (Eichhornia crassipes) into superior magnetic carbon composite adsorbents and supercapacitor electrodes. *RSC Adv.* 9, 24248–24258.

Sankar G.P., Ramasamy1 E.V., Gajalakshmi S., Abbasi S.A., 2005. Extraction of volatile fatty acids (VFAs) from water hyacinth using inexpensive contraptions, and the use of the VFAs as feed supplement in conventional biogas digesters with concomitant final disposal of water hyacinth as vermin compost. *Biochem. Eng. J.* 27, 17–23.

Scheurer M., Michel A., Brauch H.J., Ruck W., Sacher F., 2012. Occurrence and fate of the antidiabetic drug metformin and its metabolite guanylurea in the environment and during drinking water treatment. *Water Res.* 46, 4790-4802.

Scholtz M.T., Voldner E., McMillan A.C., Van Heyst B.J., 2002. A pesticide emission model (PEM). Part I: Model development. *Atm. Environ.* 36,5005–5013.

Semerjian, L. Equilibrium and kinetics of cadmium adsorption from aqueous solutions using untreated Pinus halepensis sawdust. *J. Hazard. Mater.* 2010, 173, 236–242.

Sen K., Mondal N., Chattoraj S., Datta J.K., 2017. Statistical optimization study of adsorption parameters for the removal of glyphosate on forest soil using the response surface methodology. *Environ. Earth. Sci.* 76, 22 (15 pages).

Sen K., Kumar J., Naba D., Mondal K., 2019. Glyphosate adsorption by Eucalyptus camaldulensis bark-mediated char and optimization through response surface modelling. *Appl. Water Sci.* 9, 162 (12 pages).

Shendell D.G., 2011.Chapter: Community Outdoor Air Quality: Sources, Exposure Agents and Health Outcomes in Encyclopedia of Environmental Health, pp. 791-805, Elsevier Science, Michigan, USA.

Simonin, J.P., 2016. On the comparison of pseudo-first order and pseudo-second order rate laws in the modeling of adsorption kinetics. *Chem. Eng. J.* 300, 254–263.

Siyal A.A., Shamsuddin M.R., Rabat N.E., Zulfiqar M., Man Z., Low A., 2019. Fly ash based geopolymer for the adsorption of anionic surfactant from aqueous solution. *J. Clean. Prod.* 229, 232–243.

Song X., Zhang Y., Yan C., Jiang W., Chang C., 2013. The Langmuir monolayer adsorption model of organic matter into effective pores in activated carbon. J. Coll. Interf. Sci. 389, 213-219.

Spessato L., Duarte V.A., Viero P., Zanella H., Fonseca J.M., Arroyo P.A., Almeida V.C., 2021. Optimization of Sibipiruna activated carbon preparation by simplex-centroid mixture design for simultaneous adsorption of rhodamine B and metformin. *J. Hazard. Mater.* 411, 125166.

Sulaiman S., Khamis M., Nir S., Scrano L., Bufo S.A., Karaman R., 2016. Diazepam stability in wastewater and removal by advanced membrane technology, activated carbon, and micelle–clay complex. *Desal. Water Treat*. 57, 3098-3106.

Sumathi S., Bhatia S., Lee K.T., Mohamed A.R., 2010. SO_2 and NO simultaneous removal from simulated flue gas over cerium-supported palm shell activated at lower temperatures-role of cerium on NO removal. *Ener. Fuels* 24, 427–431.

Sun R., Fang J. M., Tomkinson J. 2000. Characterization and esterification of hemicelluloses from rye straw. J. Agric. Food Chem. 48, 1247-1252.

Tan K.L., Hameed B.H., 2017. Insight into the adsorption kinetics models for the removal of contaminants from aqueous solutions. J. Taiwan Inst. Chem. Eng. 2017, 74, 25–48.

Tarapitakcheevin P., Weerayutsil P., Khuanmar K., 2013. Adsorption of Acid Dye on activated carbon prepared from water hyacinth by sodium chloride activation. *GMSARN Int. J.* 7, 83 – 90.

Teo C.Y.; Jong J.S.J, Chan Y.Q., 2022. Carbon-Based Materials as Effective Adsorbents for the Removal of Pharmaceutical Compounds from Aqueous Solution. Ads. Sci. Technol. 2022, 3079663.

Tien C., 2019. Introduction to Adsorption. Basics, Analysis, and Applications, Elsevier, Amsterdam, Netherland.

Tseng H.H., Wey M.Y., Fu C.H., 2003. Carbon materials as catalyst supports for SO_2 oxidation: Catalytic activity of CuO-AC. *Carbon* 41, 139–149.

Valizadeh S., Younesi H., Bahramifar N., 2016. Highly mesoporous K2CO3 and KOH/activated carbon for SDBS removal from water samples: Batch and fixed-bed column adsorption process. *Environ. Nanotechnol. Monit. Manag.* 6, 1–13.

Vargas D.P., Giraldo L., Silvestre-Albero J., Moreno-Piraja J.C., 2011. CO2 adsorption on binderless activated carbon monoliths. Adsorption 17, 497–504.

Wang Y., Zhou Y, Liu C., Zhou L., 2008. Comparative studies of CO_2 and CH_4 sorption on activated carbon in presence of water. *Coll. Surf. A: Physicochem. Eng*. Asp. 322, 14–18.

Wang Z. Y., Yu X. D., Pan B., Xing B. S., 2010. Norfloxacin Sorption and Its Thermodynamics on Surface-Modified Carbon Nanotubes. *Env. Sci. Technol.* 44, 978–984.

Wang J., Guo X., 2020. Adsorption kinetic models: Physical meanings, applications, and solving methods. *J. Hazard. Mater.* 390, 122156.

Wazzan N., 2021. Adsorption of non-steroidal anti-inflammatory drugs (NSAIDs) on nanographene surface: Density functional theory study. *Arab. J. Chem.* 14, 103002.

Weber W.J., Morris J.C., 1963. Kinetics of adsorption on carbon from solution. *ASCE Sanit. Eng. Div. J.* 1, 1–2.

Wong S., Ngadi N., Inuwa I.M., Hassan O., 2018. Recent advances in applications of activated carbon from biowaste for wastewater treatment: A short review. *J. Clean. Prod.* 175, 361–375.

Wu F.C., Tseng R.L., Juang, R.S. 1999. Role of pH in Metal Adsorption from Aqueous Solutions Containing Chelating Agents on Chitosan. Ind. Eng. Chem. Res. 38, 270–275.

Wu F.C., Tseng R.L., Juang, R.S. 2009. Initial behaviour of intraparticle diffusion model used in the description of adsorption kinetics. *Chem. Eng. J.* 153, 1–8.

Wu F.C., Liu B.L., Wu K.T., Tseng R.L., 2010. A new linear form analysis of Redlich–Peterson isotherm equation for the adsorptions of dyes. *Chem. Eng. J.* 162, 21–27.

Wu K., Gao B., Su J., Peng X., Zhang X., Fu J.,Chu P. K., 2016. Large and porous carbon sheets derived from water hyacinth for high-performance supercapacitors. *RSC Adv.* 6, 29996–30003.

Xia H., Wu J., Srinivasakannan C., Peng J., Zhang L., 2016. Effect of Activating Agent on the Preparation of Bamboo-Based High Surface Area Activated Carbon by Microwave Heating. High Temper. Mater. Process. 35, 535-541.

Xia Y., Yang T., Zhu N., Li D., Chen Z., Lang Q., Liu Z., Jiao W., 2019. Enhanced adsorption of Pb (II) onto modified hydrochar: modeling and mechanism analysis. *Bioresour. Technol.* 288, 121593.

Yamaguchi N.U., Bergamasco R., Hamoudi S., 2016. Magnetic $MnFe_2O_4$-graphene hybrid composite for efficient removal of glyphosate from water. *Chem. Eng. J.* 295, 391–402.

Yang J., Qiu K., 2011. Development of high surface area mesoporous activated carbons from herb residues. *Chem. Eng. J.* 167, 148–154.

Yang Q., Wang J., Chen X., Yang W., Pei H., Hu N., Li Z., Suo Y., Lic T., Wang J., 2018. The simultaneous detection and removal of organophosphorus pesticides by a novel Zr-MOF based smart adsorbent. *J. Mater. Chem.* 6, 2184–2192.

Yi H., Nakabayashi K., Yoon S. H., Miyawaki J., 2021. Pressurized physical activation: A simple production method for activated carbon with a highly developed pore structure. Carbon, 183, 735-742.

Yorgun S., Vural N., Demiral H., 2009. Preparation of high-surface area activated carbons from Paulownia wood by $ZnCl_2$ activation. *Micropor. Mesopor. Mater.* 122, 189–194.

Yorgun S., Yilidiy D., 2015. Preparation and characterization of activated carbons from Paulownia wood by chemical activation with H_3PO_4. *J. Taiwan Inst. Chem Eng.* 53, 122-132.

Yu F., Sun S., Han S., Zheng J., Ma J., 2016. Adsorption removal of ciprofloxacin by multi-walled carbon nanotubes with different oxygen contents from aqueous solutions. *Chem. Eng. J.* 285, 588–595.

Yue Z., Economy J., 2006. Synthesis of highly mesoporous carbon pellets from carbon black and polymer binder by chemical activation. Micropor.Mesopor. Mater. 96, 314–320.

Zaini M. S., Arshad M., Shatir S., Syed-Hassan A., 2023.Adsorption Isotherm and Kinetic Study of Methane on Palm Kernel Shell-Derived Activated Carbon. *J. Biores. Bioprod.* 8, 66-77.

Zbair M., Ainassaari K., Drif A., Ojala S., Bottlinger M., Pirila M., Brahmi, R., 2018. Toward new benchmark adsorbents: Preparation and characterization of activated carbon from argan nut shell for bisphenol A removal. *Envir. Sci.Poll. Res*. 25, 1869–1882.

Zhai Y., Peng C., Xu B., Wang T., Li C., Zeng G., Zhu Y., 2017. Hydrothermal carbonization of sewage sludge for char production with different waste biomass: effects of reaction temperature and energy recycling. *Energy* 127, 167-174.

Zhang B., Zhang T., Zhang Z., Xie M., 2019. Hydrothermal synthesis of a graphene/magnetite/montmorillonite nanocomposite and its ultrasonically assisted methylene blue adsorption. *J. Mater. Sci.* 54, 11037–11055.

Zhang Q., Wei Y., Han H., Weng, C., 2018. Enhancing bioethanol production from water hyacinth by new combined pretreatment methods. Biores. Technol. 251, 358-363.

Zhu S., Liu Y.G., Liu S.B., Zeng G.M., Jiang L.H., Tan X.F., Zhou L., Zeng W., Li T.T., Yang, C.P., 2017. Adsorption of emerging contaminant metformin using graphene oxide. *Chemosphere* 179, 20–28.

Биографија аутора

Ahmad Hakky Mohammad је рођен 1. маја 1959. године у Багдаду, Ирак, где је завршио гимназију Al Mansour 1977. године. Основне студије завршио је на на Пољопривредном факултету Универзитета у Багдаду, одсек за хортикултуру, 1982. Ahmad Hakky Mohammad је мастер студије завршио на Шумарском факултету Универзитета у Београду 2017. године, где је одбранио мастер рад под називом „Преглед поступака за производњу биоетанола из лигноцелулозних сировина (Overview of procedures for the production of bioethanol from lignocellulosic raw materials)". Докторске студије на Технолошко-металуршком факултету Универзитета у Београду уписује у октобру 2018. године на одсеку Хемијско инжењерство под менторством проф. Мирјане Кијевчанин.

Ahmad Hakky Mohammad има богату професионалну каријеру: од 1982 – 1991. радио је као инжењер у одељењу за развој и истраживање у војној индустрији уз подршку Владе Ирака, а од 1992. године ради у Данској и Швајцарској. 2011. године постаје директор Центра за стратешке студије (Истанбул, Турска), а од 2014. до данас ради као директор Iraqi Intellectuals and Academics са седиштем у Истанбулу, Турска.

Верификација научних доприноса

Ahmad Hakky Mohammad, мастер инж, је своје резултате потврдио објављивањем радова у међународним часописима и презентовањем радова на конференцијама: једног рада у истакнутом међународном часопису, једног рада у међународном часопису и једног саопштења са међународног скупа штампана у целости.

- Рад у истакнутом међународном часопису, M22

1. Mohammad, A.H.; Radović, I.; Ivanović, M.; Kijevčanin, M. Adsorption of metformin on activated carbon produced from the water hyacinth biowaste using H_3PO_4 as a chemical activator. *Sustainability* 2022, *14*, 11144. https://doi.org/10.3390/su141811144, IF(2021)= 3.889; ISSN: 2071-1050

- Рад у међународном часопису, M23

1. Mohammad, A.H.; Kijevčanin, M. Synthesis of activated carbons from water hyacinth biomass and its application as adsorbents in water pollution control. *Journal of the Serbian Chemical Society* 2023, 88(1), 69-82.
https://doi.org/10.2298/JSC212121006M, IF(2021)= 1.100; ISSN: 0352-5139

- Саопштење са међународног скупа штампано у целости, M33

1. Mohammad, A.H.; Kijevčanin, M. Synthesis of activated carbons from water hyacinth biomass and its applications as adsorbents for the herbicide glyphosate. 15th International Conference on Fundamental and Applied Aspects of Physical Chemistry, 20th –24th September 2021, Belgrade, Serbia.

Образац 5.

Изјава о ауторству

Име и презиме аутора **Ahmad Hakky Mohammad**

Број индекса **4031/2018**

Изјављујем

да је докторска дисертација под насловом

Optimization of the adsorption process of pollutants from aqueous solutions using Pontederia crassipes biomass

- резултат сопственог истраживачког рада;
- да дисертација у целини ни у деловима није била предложена за стицање друге дипломе према студијским програмима других високошколских установа;
- да су резултати коректно наведени и
- да нисам кршио/ла ауторска права и користио/ла интелектуалну својину других лица.

Потпис аутора

У Београду, 21/06/2023

Ahmad Hakky Mohammad

Изјава о истоветности штампане и електронске верзије докторског рада

Име и презиме аутора **Ahmad Hakky Mohammad**

Број индекса **4031/2018**

Студијски програм **Хемијско инжењерство**

Наслов рада **Optimization of the adsorption process of pollutants from aqueous solutions using Pontederia crassipes biomass**

Ментор проф. **Др Мирјана Кијевчанин**

Изјављујем да је штампана верзија мог докторског рада истоветна електронској верзији коју сам предао/ла ради похрањена у **Дигиталном репозиторијуму Универзитета у Београду.**

Дозвољавам да се објаве моји лични подаци везани за добијање академског назива доктора наука, као што су име и презиме, година и место рођења и датум одбране рада.

Ови лични подаци могу се објавити на мрежним страницама дигиталне библиотеке, у електронском каталогу и у публикацијама Универзитета у Београду.

Потпис аутора

У Београду, 21/06/2023

Ahmad Hakky Mohammad

Изјава о коришћењу

Овлашћујем Универзитетску библиотеку „Светозар Марковић" да у Дигитални репозиторијум Универзитета у Београду унесе моју докторску дисертацију под насловом:

Optimization of the adsorption process of pollutants from aqueous solutions using Pontederia crassipes biomass

која је моје ауторско дело.

Дисертацију са свим прилозима предао/ла сам у електронском формату погодном за трајно архивирање.

Моју докторску дисертацију похрањену у Дигиталном репозиторијуму Универзитета у Београду и доступну у отвореном приступу могу да користе сви који поштују одредбе садржане у одабраном типу лиценце Креативне заједнице (Creative Commons) за коју сам се одлучио/ла.

1. Ауторство (CC BY)

2. Ауторство – некомерцијално (CC BY-NC)

3. Ауторство – некомерцијално – без прерада (CC BY-NC-ND)

4. Ауторство – некомерцијално – делити под истим условима (CC BY-NC-SA)

5. Ауторство – без прерада (CC BY-ND)

6. Ауторство – делити под истим условима (CC BY-SA)

(Молимо да заокружите само једну од шест понуђених лиценци.
Кратак опис лиценци је саставни део ове изјаве).

Потпис аутора

У Београду, 21/06/2023

Ahmad Hakky Mohammad

1. **Ауторство**. Дозвољавате умножавање, дистрибуцију и јавно саопштавање дела, и прераде, ако се наведе име аутора на начин одређен од стране аутора или даваоца лиценце, чак и у комерцијалне сврхе. Ово је најслободнија од свих лиценци.

2. **Ауторство – некомерцијално**. Дозвољавате умножавање, дистрибуцију и јавно саопштавање дела, и прераде, ако се наведе име аутора на начин одређен од стране аутора или даваоца лиценце. Ова лиценца не дозвољава комерцијалну употребу дела.

3. **Ауторство – некомерцијално – без прерада**. Дозвољавате умножавање, дистрибуцију и јавно саопштавање дела, без промена, преобликовања или употребе дела у свом делу, ако се наведе име аутора на начин одређен од стране аутора или даваоца лиценце. Ова лиценца не дозвољава комерцијалну употребу дела. У односу на све остале лиценце, овом лиценцом се ограничава највећи обим права коришћења дела.

4. **Ауторство – некомерцијално – делити под истим условима**. Дозвољавате умножавање, дистрибуцију и јавно саопштавање дела, и прераде, ако се наведе име аутора на начин одређен од стране аутора или даваоца лиценце и ако се прерада дистрибуира под истом или сличном лиценцом. Ова лиценца не дозвољава комерцијалну употребу дела и прерада.

5. **Ауторство – без прерада**. Дозвољавате умножавање, дистрибуцију и јавно саопштавање дела, без промена, преобликовања или употребе дела у свом делу, ако се наведе име аутора на начин одређен од стране аутора или даваоца лиценце. Ова лиценца дозвољава комерцијалну употребу дела.

6. **Ауторство – делити под истим условима**. Дозвољавате умножавање, дистрибуцију и јавно саопштавање дела, и прераде, ако се наведе име аутора на начин одређен од стране аутора или даваоца лиценце и ако се прерада дистрибуира под истом или сличном лиценцом. Ова лиценца дозвољава комерцијалну употребу дела и прерада. Слична је софтверским лиценцама, односно лиценцама отвореног кода.